A study of the steady-state and transient characteristics of inhomogeneously pumped lasers

Perkins, Michael C. J.

Award date:
1988

Awarding institution:
University of Bath

A STUDY OF THE STEADY-STATE AND TRANSIENT CHARACTERISTICS

OF

INHOMOGENEOUSLY PUMPED LASERS.

Submitted by Michael C. J. Perkins
for the degree of Ph.D.
of the University of Bath
1988.

ProQuest LLC
789 East Eisenhower Parkway
P.O. Box 1346
Ann Arbor, MI 48106-1346

Contents.

Summary.

Inhomogeneously pumped lasers contain regions of gain and saturable absorption. Depending on the geometry of the laser, these devices can exhibit optical absorptive bistability. Such lasers may suitable for use as memory elements, for pulse shaping and for signal regeneration.

Bistability can be achieved either by current injection or by optical injection. The thesis considers both forms of injection and analyses the steady-state and the transient characteristics of inhomogeneously pumped lasers. Computer models to predict both the steady-state and transient behaviour of such lasers are described together with some results. The assumptions used in this thesis are shown to be justified and include the use of a uniform carrier density (population inversion), and hence gain, within each pumped and passive segment of the laser and, the discretising of wavelength into wavelength "slots". These assumptions allow the photon conservation equation to be solved analytically for each segment, for light travelling in both directions along the device. The analysis does not require the use of the assumptions of a uniform photon flux within the device nor of a constant photon lifetime. Indeed it is shown that these assumption are erroneous when applied to absorptive bistability.

Acknowledgements.

The author wishes to express his gratitude to Dr. R. F. Ormondroyd for his his help and supervision of this research topic.

Thanks are also given to Dr. J. Sarma for his theoretical discussions, to Mr. Ian Middlemast for his help towards numerical techniques and to Mr. Bill Liddel for the use of his generated gain and spontaneous emission data.

The author would like to thank Prof. T. E. Rozzi for providing laboratory and computer facilities and to the University of Bath for providing personal financial support in the form of a University Research Studentship.

List of Symbols.

A_{21}	Spontaneous emission transition probability.
$\underline{B}$	Magnetic flux density.
B_{12}	Absorption transition probability.
B_{21}	Stimulated emission transition probability.
B_r	Bimolecular spontaneous recombination rate.
c	Speed of light.
d	Thickness of active layer.
$\underline{D}$	Electrostatic field vector
e	Electronic charge.
E	Energy.
E_g	Energy of band gap.
$\underline{E}$	Electric field vector.
E_1, E_v	Energy of a state in the valence band.
E_2, E_c	Energy of a state in the conduction band.
$g(n(z),\lambda)$	Gross optical gain.
g_{rt}	Round trip gain.
f_{cc}	Free carrier absorption coefficient.
F_1	Quasi Fermi level in valence band.
F_2	Quasi Fermi level in conduction band.
$G(n(z),\lambda)$	Net effective gain after taking into account confinement factor and free carrier absorption. $G= \Gamma.(g - f_{cc}.(2n + p_0))$
h	Planc's constant.
$\underline{H}$	Magnetic field vector
I	Current.
J(z)	Current density

J	Conduction current.
k	Boltzmann coefficient.
K	Extinction coefficient.
L	Length of segment (or section) of a device.
m_n	Mass of an electron.
m_h	Mass of a hole.
$n(z)$	Carrier density (Inversion population.)
n	Refractive index.
$\tilde{n}$	Complex refractive index.
N_a	Acceptor doping density.
N_d	Donor doping density.
p	Hole population.
p_o	Thermal equilibrium hole density (if $N_d >> N_a$).
$P(h\nu)$	Density of photons at energy $h\nu$.
$P(z,t,\lambda)$	Photon flux in +ve z direction.
r	Reflectivity.
$Q(z,t,\lambda)$	Photon flux in -ve z direction.
$S(n(z),\lambda)$	Spontaneous emission where; $\int_0^\infty S(N(z),\lambda) = B_r.n.(n + p_0)$
S	Average photon density.
r	Position of vector (in space).
t	Time.
t_{rt}	Round trip time.
T	Temperature (degrees Kelvin).
v	Group velocity of light in GaAs ($\beta/2\pi$).
x	An axis in the cartesian coordinate system.
y	An axis in the cartesian coordinate system.
z	An axis in the cartesian coordinate system.

λ	Wavelength.
Γ	Optical confinement factor.
α	Attenuation (loss).
β	Propagation constant.
$\tilde{\beta}$	Complex propagation constant.
δ	Confinement of spontaneous emission to waveguide.
ε	Pemitivity.
ε_0	Free space permitivity.
ε_r	Relative permitivity.
$\tilde{\varepsilon}_r$	Complex relative permitivity.
k_0	Free space propagation constant.
ω	Angular frequency.
μ	Permeability.
μ_0	Free space Permeability.
ν	Frequency of light.
ρ	Charge density.
ρ_c	Density of states in conduction band.
ρ_v	Density of states in valence band.
γ	Ratio of length of passive segment to the length of whole device (for two segment device).
σ	Conductivity
τ_s	Electron-hole recombination lifetime.
τ_p	Photon lifetime.
ψ	Field component.

Chapter 1

Introduction.

1 Introduction.

There has been a great interest in bistable optical devices since they may be suitable for optical memory elements and for pulse shaping and signal regeneration. These devices are a subset of the devices required to implement the concept of optical logic. In this type of logic, it is not the movement of electrons in the form of an electric current which carries information, but light. For optical communications, optical regeneration may be feasible without recourse to conversion from a light signal into an electrical signal and back again. Perhaps the most daunting possibility is the prospect of the speed and computational power which is associated with optical logic.

Bistability is the property of having two distinct states for the same set of input conditions, the states being dependent on the preceding input conditions. Exceptionally, more than two distinct states may be possible. A characteristic of these bistable devices is that they exhibit a hysteresis loop.

1.1 Bistable Optical Devices.

All types of bistable device rely upon :- i) a non-linear material and ii) a feedback mechanism. These devices on the whole can be placed into two main categories, namely dispersive bistability and absorptive bistability. A third category which should be mentioned is that of bistable beam steering which has been reported in parallel twin stripe lasers [1].

1.1.1 Dispersive Bistable Devices.

This group of devices usually consist of a resonator which contains a material exhibiting a non-linear refractive index, where the refractive index is dependent on the intensity of incident light. A non-linear material, which has been under investigation, is Lithium Niobate ($LiNbO_3$) and figure 1.1.1-1 provides an illustration of a dispersive bistable device. If monochromatic light is incident on one of the partially silvered mirrors of the device shown in figure 1.1.1-1, then some of the light will enter the material in the resonator. The optical intensity, within the resonator, will alter the refractive index of the material and hence alter the effective cavity length. Also, the optical intensity within the resonator is dependent on the refractive index of the material because of the change in reflectivity, through constructive or destructive interference, caused by the change in effective cavity length. Hence the light intensity and refractive index of the medium are interdependent. These properties can turn the transmission of the device on or off in a bistable manner and the mechanisms are more fully described in [2]. However, in lithium niobate the non-linearity is rather small and hence a long optical path in the dispersive medium is required.

Lithium niobate is a passive material and there would be a net loss in such a system. However, an active dispersive device has been shown to be feasible using a semiconductor laser amplifier [3] where the light and carriers interact through stimulated emission. Since the effective cavity length is dependent on the carrier density optical bistability is again possible. Unfortunately the device, when modelled, had a rather slow on and off response which was shown to be consistent with the carrier lifetime associated with the laser

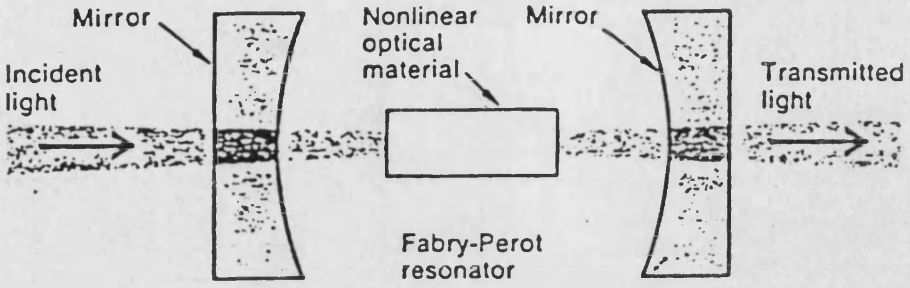

Fig 1.1.1-1 A simple dispersive bistable optical device consisting of a Fabry-Perot resonator containing a non-linear material.

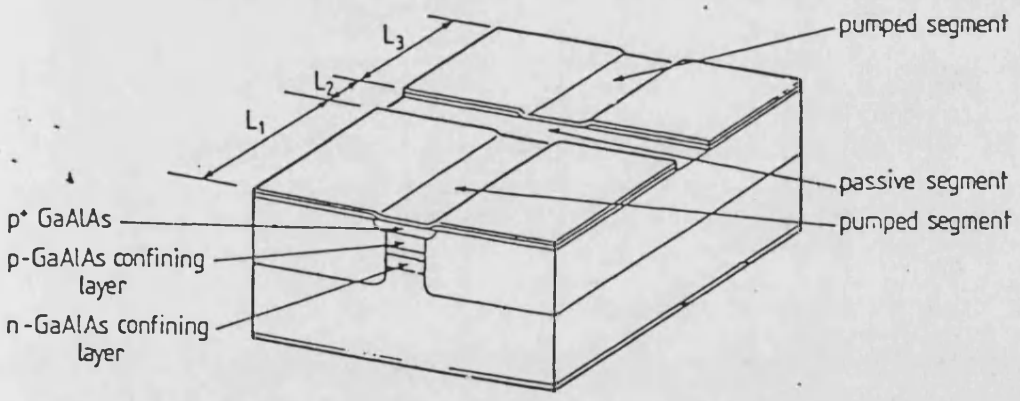

Fig 1.1.2-1 Illustration of a bistable laser containing saturable absorption.

operating below threshold.

1.1.2 Absorptive Bistable Devices.

This is the category of devices which is the subject of this study. An absorptive bistable laser of this type, shown in figure 1.1.2-1, has an optical amplifier and a saturable absorber within a Fabry-Perot resonator. A saturable absorber is one where the incremental loss becomes less for an increasing level of light. The light optically pumps the material to create a population inversion such that the loss is subsequently reduced. Thus the resonator loss is directly dependent on the level of photon intensity. The light, in figure 1.1.2-1, is confined to the active region which is a rectangular dielectric waveguide. Optical amplification is achieved by the injection of carriers into the active region, along a proportion of the length of the device. Saturable absorption is achieved by the absence of the electrical injection of carriers, where transparency is caused by the optical pumping through the passage, and absorption, of incident light in the active region. The gain of the optical amplifier will also saturate since stimulated emission will "use up" the injected carriers thereby reducing the gain. As long as the absorbing segment saturates at a lower photon density than the gain saturates in the pumped segment, the device will exhibit hysteresis, subject to the device remaining dynamically stable.

1.2 Objectives of Thesis.

The aims of this thesis are to present models which characterise absorptive bistable lasers. Both the steady-state characteristics and

transient responses are studied for devices with various geometries. The study also attempts to clarify which of the assumptions, often used in the analysis of absorptive bistability, are valid and those which will introduce errors.

1.3 Review of Previous Work on Absorptive Bistability.

In 1964 Lasher proposed a bistable homojunction laser which had a saturable absorbing section [4]. This can be seen in Figure 1.3-1 . He may have been inspired by Gerritsen's bistable maser which exhibited marked hysteresis [5]. Nathan et. al. implemented Lasher's design and achieved bistable operation [6]. The properties of the homojunction laser, illustrated in chapter 3, require that the device be cooled to liquid nitrogen temperatures (77K) to enable laser operation. In 1968 Basov [7] made some theoretical studies for such a device and obtained good qualitative agreement with fabricated devices. The photon and carrier rate equations, which he formulated, have been the basis of much of the theoretical work in absorptive bistability. As a result of the practical difficulties associated with homojunction lasers very little work on this subject was carried out for ten or so years until double heterojunction lasers succeeded the earlier inferior homojunction lasers. Work on saturable absorption continued in 1978-9, centred on the stability of aged lasers which exhibited self sustained oscillations (SSO) or pulsations. Theories developed by Paoli [8] and by Dixon and Joyce [9] for this behaviour proposed the creation of centres of saturable absorption in the active region of the device which have undergone some form of degradation.

In 1981 much interest was shown for absorptive bistability.

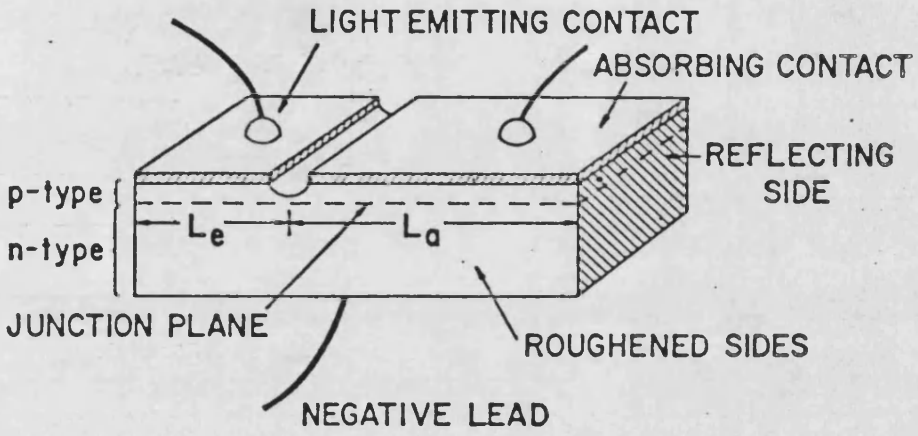

Fig 1.3-1 Schematic drawing of Lasher's proposed device. [4]

Carney and Fonstad constructed a multiple segmented laser [10], shown in figure 1.3-2, which had a rather poor bistable performance because their device had no lateral index guiding. The significance of lateral index guiding will be illustrated in a later chapter.

Harder, Lau and Yariv [11] used a narrow longitudinal twin stripe buried heterostructure laser illustrated in figure 1.3-3. When a current was extracted from the passive segment to deplete the carriers in this segment, hysteresis was observed. The laser also began to produce pulsations where the light output appeared to be modulated at high frequencies. However, neither hysteresis nor were optical pulsations observed for zero current into the absorbing segment. Negative resistance was observed at the absorbing contact [12]. Depending on the source resistance to this contact, this would either lead to a stable light output with a large hysteresis [13] or, a small hysteresis with self pulsations at microwave frequencies. A simple model was used to explain the origin of the negative resistance and to explain the mechanism of the self sustained pulsations [14].

The most prolific worker of recent years on optical bistability has been Kawaguchi. Much of his work has been centred on a novel stripe geometry consisting of many short pumped and passive segments as shown in figure 1.3-4. He reported bistable operation with this laser structure [15] and also analysed the static and dynamic characteristics of the device [16]. He was also the first to achieve bistable operation by means of optical injection [17, 18]. More recently, Kawaguchi has investigated, on a theoretical basis, the effect of non-radiative recombination on bistability and pulsations [19]. Non radiative recombination occurs at impurity or lattice defect centres. It was proposed to control the rate of non-radiative

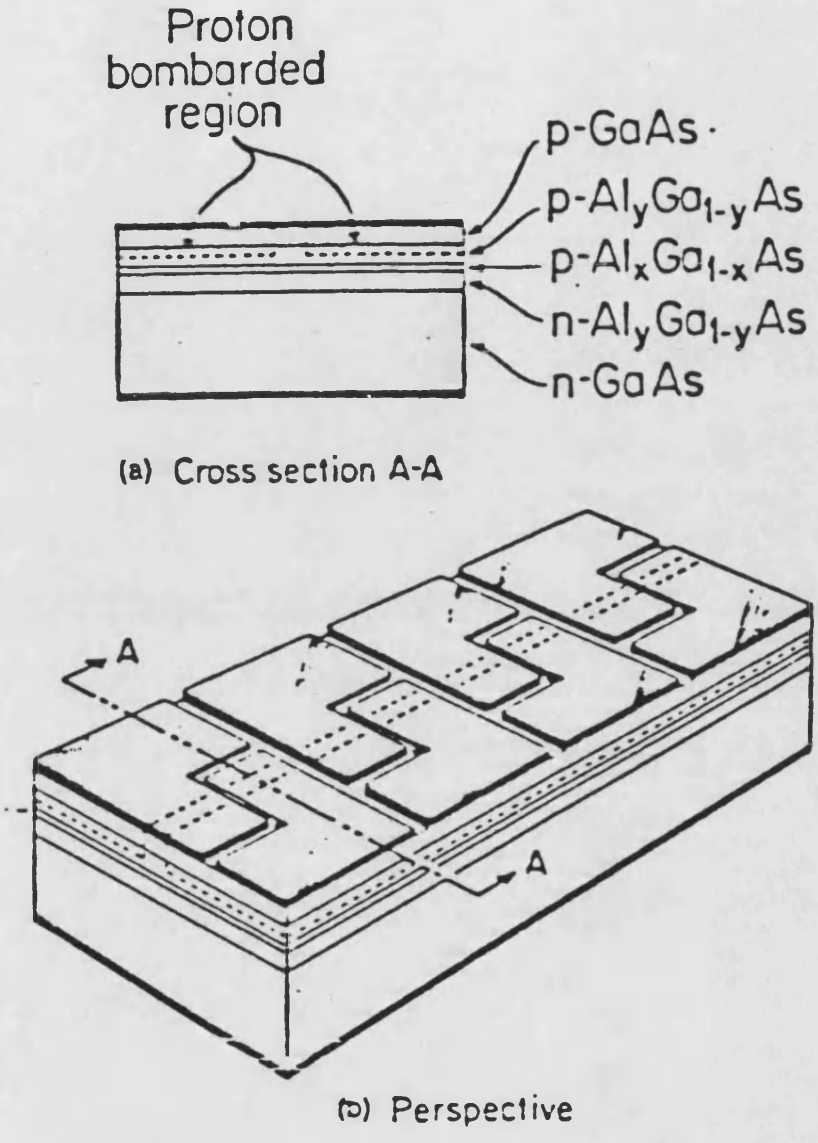

Fig 1.3-2 Drawing of the multiple segment contact laser used in the study by Carney and Fonstad; (a) a cross-sectional view indicating the layer compositions; (b) a perspective view illustrating the contact pattern. [10]

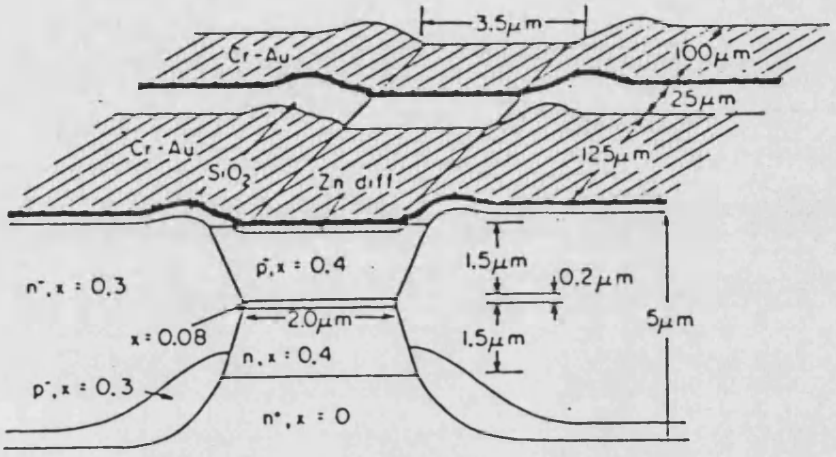

Fig 1.3-3 A view of the tandem twin stripe B-H laser as used by Harder Lau and Yariv. [11 - 14]

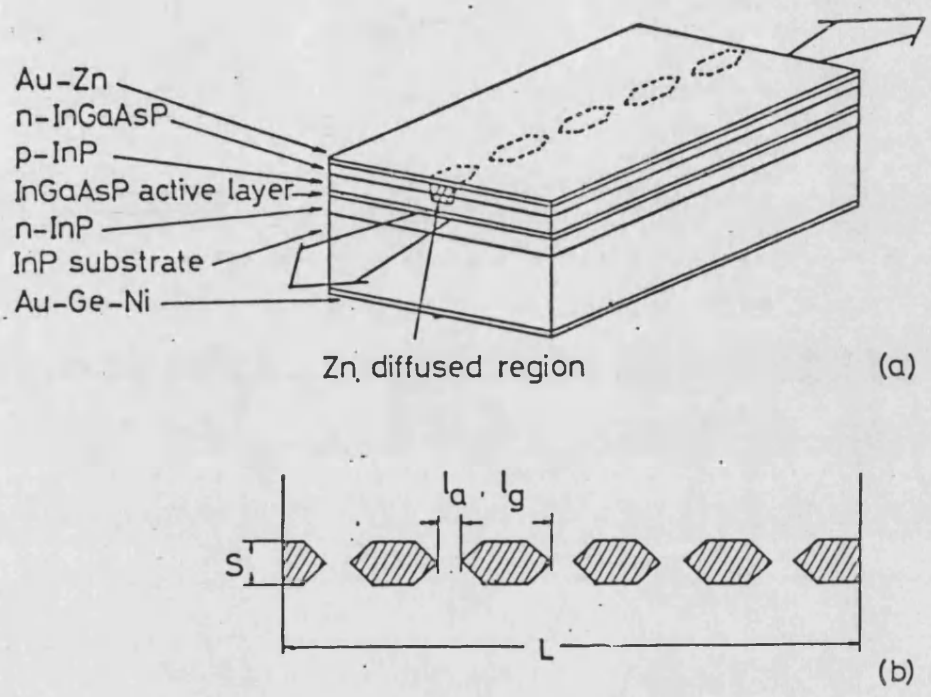

Fig 1.3-4 Schematic diagram of the bistable injection laser used by Kawaguchi. l_a and l_g are the gain and absorbing section lengths respectively. [15 - 18]

recombination by known doses of proton bombardment.

Most recently Kuznetsov has used a much simplified approach of pulsations for lasers with a proton bombarded segment [20]. His rudimentary analyses have even neglected spontaneous emission. However, he has formulated analytical expressions for the form of the pulse shape. Kuznetsov has also studied optical bistability in two segment diodes [21]. Here, he finds an analytical solution of the rate equations, again neglecting spontaneous emission, to give a simple bistability condition.

1.4 Outline of thesis.

Chapter two introduces waveguiding mechanisms in a laser and gives a comprehensive analysis of the slab waveguide. It also gives an indication whether or not a structure can support a stable propagating mode for a slab waveguide structure which has layers composed of a combination of different refractive indices and gain (or loss). The application of the analysis of the slab waveguide to a rectangular dielectric waveguide is outlined using the effective index method. The rectangular waveguide is present in the buried heterostructure laser which is shown, in chapter three, to be the most suitable structure for absorptive bistability. Chapter three also gives a very brief outline of gain and spontaneous emission processes which are fundamental to the operation of the semiconductor laser.

Chapters two and three are essentially the background chapters whereas chapters four, five and six give a description of predominantly original work. In chapter four the accuracy of assumptions often used in the theoretical analysis of absorptively bistable semiconductor lasers are brought into question, and some

errors in using these assumptions are shown graphically. The models used in this chapter are wavelength independent where the gain and spontaneous emission are a simple function of the carrier density (inversion population). Although these models are only for a single wavelength model they are sufficient to illustrate the errors in the commonly used assumptions. However one assumption is clearly verified concerning the longitudinal variation of carriers where it is shown that they may be assumed uniform within a segment. This assumption is verified again in chapter five which uses a more complex model, taking into account the wavelength dependency of gain and spontaneous emission. In a bistable laser structure the light output may contain spontaneous emission, superluminescence or lasing light output or a combination of these. Since these processes have spectral peaks at different wavelengths the wavelength dependency of the gain and spontaneous emission ought to be taken into account.

Chapter six outlines a time dependent model which uses an alternative technique to generate transient responses to changes in electrical injection and optical injection. These models imitate the path of the light, including its generation through spontaneous emission, and the subsequent growth and decay of light along the length of the device. The models also include the wavelength dependency of gain and spontaneous emission, and in particular do not rely upon the erroneous assumptions which are normally used in the analysis of absorptive bistability.

In chapter seven conclusions are drawn up from the results of models outlined in this thesis and some recommendations are suggested for further work.

References.

1) I. H. White and J. E. Carrol. "Room Temperature Optically Triggered Bistability in Twin Stripe Lasers"; Electronic Letters; Vol. 19; 1983; p 547-8.

2) P. W. Smith and W. J. Tomlinson. "Bistable Optical Devices Promise Subpicosecond Switching"; IEEE Spectrum (USA); Vol. 18; No. 6; 1981; p26-33.

3) M. J. Adams. "Time-dependent analysis of active and passive optical bistability in semiconductors"; IEE Proceedings; Vol. 132; Pt. J; No. 6; 1985; p343-8.

4) G. J. Lasher. "Analysis of a Proposed Bistable Injection Laser"; Solid State Electronics; Vol. 7; 1964; p 707-16.

5) H. J. Gerritsen. "Operation of a Memory Element Based on the Maser Principle"; Proc. Inst. Elec. Electron. Engrs.; Vol. 51; 1963; p934-5.

6) M. I. Nathan, J. C. Marinace, R. F. Rutz, A. E. Michel and G. J. Lasher. "GaAs Injection Laser with Novel Mode Control and Switching Properties"; J. of Applied Physics; Vol. 36;No. 2; 1965; p 473-80.

7) N. G. Basov. "O-l-Dynamics of Injection Lasers"; IEEE Journal of Quantum Electronics; Vol. QE-4; No. 11; 1968; p855-64.

8) T. L. Paoli. "Saturable absorption effects in the self-pulsing (AlGa)As Junction Laser"; Applied Physics Letters; Vol. 34; No. 10; 1979; p652-5.

9) R. W. Dixon and W. B. Joyce. "A Possible Model for Sustained Oscillations (pulsations) in (AlGa)As Double-Heterostructure Lasers"; IEEE Journal of Quantum Electronics; Vol. QE-15; No. 6; 1979; p470-4.

10) J. K. Carney and C. G. Fonstad. "Double-Heterojunction Laser Diodes with Multiply Segmented Contacts"; Applied Physics Letters; Vol. 38; No. 5; 1981; p 303-5.

11) Ch. Harder, K. Y. Lau and A. Yariv. "Bistability and Pulsations in C.W. Semiconductor Lasers with a Controlled Amount of Saturable absorption"; Applied Physics Letters; Vol. 39; No. 5; 1981; p 382-4.

12) Ch. Harder, K. Y. Lau and A. Yariv. "Bistability and Negative Resistance in Semiconductor Lasers"; Applied Physics Letters; Vol. 40; No. 3; 1982; p 124-6.

13) K. Y. Lau, Ch. Harder and A. Yariv. "Dynamical Switching of a Bistable Injection Laser"; Applied Physics Letters; Vol. 40; No. 3; 1982; p 198-200.

14) Ch. Harder, K. Y. Lau and A. Yariv. "Bistability and Pulsations in Semiconductor Lasers with Inhomogeneous Current Injection"; IEEE Journal of Quantum Electronics; Vol. QE-18; No. 9; 1982; p 1351-61.

15) H. Kawaguchi and G. Iwane. "Bistable Operation in Semiconductor Laser with Inhomogeneous Excitation"; Electronics Letters; Vol. 17; No. 4; 1981; p 167-8.

16) H. Kawaguchi. "Optical Bistable-Switching Operation in Semiconductor Lasers with Inhomogeneous Excitation"; IEE Proceedings; Vol. 129; pt. 1; 1982; p 141-7.

17) H. Kawaguchi. "Bistable Operation of Semiconductor Lasers by Optical Injection"; Electronic Letters; Vol. 17; No. 20; 1981; p 741-2.

18) H. Kawaguchi. "Optical Input and Output Characteristics for Bistable Semiconductor Lasers"; Applied Physics Letters; Vol. 41; No. 8; 1982; p 702-4

19) H. Kawaguchi. "Optical Bistability and Chaos in a Semiconductor Laser with a Saturable absorber"; Applied Physics Letters; Vol. 45; No. 12; 1984; p1264-6.

20) M. Kuznetsov. "Pulsations of Semiconductor Lasers with a Proton Bombarded Segment: Well-Developed Pulsations"; IEEE Journal of Quantum Electronics; Vol. QE-21; No. 6; 1985; p 587-92.

21) M. Kuznetsov. "Theory of Bistability in Two Segment Diode Lasers"; Optics Letters; Vol. 10; No. 8; 1985; p 399-401.

Chapter 2.

Optical waveguides.

2 Introduction.

The purpose of this chapter is to introduce wave-guiding mechanisms in a laser. The theory is presented from fundamental principles for the dielectric slab waveguide. A necessary but not sufficient condition for a stable mode is given for the combination of gain, or loss, and refractive indices in each layer of the slab waveguide. This result is used in the next chapter when the centre layer of the slab waveguide, illustrated in figure 2-1, has a lower absorption coefficient and a lower refractive index than the surrounding layers. Under these conditions the structure will not support a stable guided mode. Finally, theory associated with the two dimensional problem of a rectangular dielectric waveguide is presented. The method which is considered in more detail, namely the effective dielectric constant (EDC) method is a quite a powerful and gives accurate results to this type of problem.

2.1 Maxwell's Equations.

These are the equations which are fundamental to any problem associated with electromagnetic propagation and are the starting point from which the wave equations are derived. The Maxwell's equations are revised below [1] ;

$$\nabla \times \underline{H} = \frac{\partial \underline{D}}{\partial t} + J \qquad (2.1\text{-}1)$$

$$\nabla \times \underline{E} = -\frac{\partial \underline{B}}{\partial t} \qquad (2.1\text{-}2)$$

$$\nabla \cdot \underline{D} = \rho \qquad (2.1\text{-}3)$$

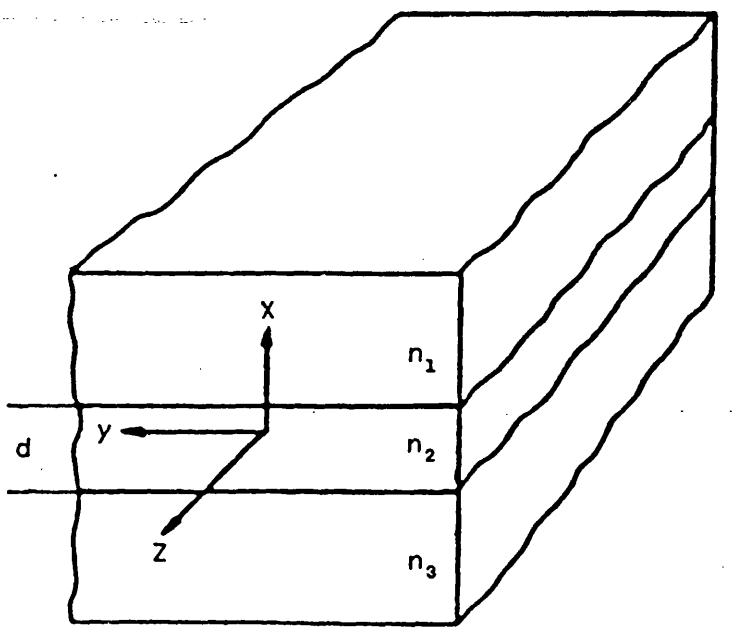

Figure 2-1 A view of the slab waveguide.

$$\nabla \cdot \underline{B} = 0 \qquad (2.1\text{-}4)$$

where;

$$\underline{D} = \varepsilon \underline{E} \qquad (2.1\text{-}5)$$

$$\underline{B} = \mu \underline{H} \qquad (2.1\text{-}6)$$

$$J = \sigma \underline{E} \qquad (2.1\text{-}7)$$

The dielectric media considered in this chapter are non-magnetic such that $\mu = \mu_0$. The wave equation can be derived using the above equations and a vector identity to obtain;

$$\nabla^2 \underline{E} - \mu \varepsilon \frac{\partial^2 \underline{E}}{\partial t^2} - \sigma \mu \frac{\partial \underline{E}}{\partial t} = 0 \qquad (2.1\text{-}8)$$

Equation 2.1-8 is applicable to a homogeneous, source free medium and is also applicable whether the medium is conducting or non conducting. A similar equation can be derived for $\underline{H}$.

It is usual to assume that $\underline{E}$ is of a sinusoidal waveform;

$$\underline{E}(r,t) = \underline{E}(r) \exp(jwt) \qquad (2.1\text{-}9)$$

When equation 2.1-9 is substituted into 2.1-8 the following is obtained.

$$\nabla^2 \underline{E}(r) + \mu \varepsilon \omega^2 \underline{E}(r) - j \sigma \omega \mu \underline{E}(r) = 0 \qquad (2.1\text{-}10)$$

2.2 Free space propagation.

It is useful to consider the simplest form of propagation before the more complex aspect of waveguiding. If a field, uniform in the x

and y direction, is travelling in the z direction and polarised in the y direction, then Ey and Hx are the only non zero components of the field. Equation 2.1-10 gives;

$$\frac{\partial^2 Ey}{\partial z^2} + \tilde{\varepsilon}_r k_0^2 Ey = 0 \qquad (2.2\text{-}1)$$

where;

$$\tilde{\varepsilon}_r = \varepsilon_r + j\frac{\sigma}{\varepsilon_0 \omega} \qquad (2.2\text{-}2)$$

is the complex dielectric constant which takes into account conduction (loss) or gain in the medium. Also;

$$k_0^2 = \mu_0 \varepsilon_0 \omega^2 \qquad (2.2\text{-}3)$$

where k_0 is the free space propagation constant.

A solution for Ey in equation 2.2-1 is;

$$Ey = A \exp[\, j(\omega t - \tilde{\beta} z) \,] \qquad (2.2\text{-}4)$$

where $\tilde{\beta}$ is the complex propagation constant in the medium;

$$\tilde{\beta} = \beta - j\frac{\alpha}{2} = \tilde{n}_r k_0 \qquad (2.2\text{-}5)$$

$\alpha/2$ is the loss, or gain if negative and β is the real part of the propagation constant. Equation 2.2-4 can be rewritten as;

$$Ey = A \exp(-\frac{\alpha}{2} z) \exp[\, j(\omega t - \beta z) \,] \qquad (2.2\text{-}6)$$

$\alpha/2$ is used since Ey is an amplitude. In terms of intensity and power flow the attenuation would be twice this;

$$P(z) = P(0) \exp(-\alpha z) \qquad (2.2\text{-}7)$$

$$\text{If we define } \tilde{n}^2 = \tilde{\varepsilon}_r \; ; \qquad (2.2\text{-}8)$$

$$\text{and } \tilde{n} = n + jK \qquad (2.2\text{-}9)$$

where n is the real part of the refractive index and K, the

imaginary part, is often called the extinction coefficient. We may obtain the relation between complex refractive index and complex dielectric constant;

$$n^2 - K^2 + 2jnK = \tilde{\varepsilon}_r = \varepsilon_r + \frac{j\sigma}{\varepsilon_0 \omega} \qquad (2.2\text{-}10)$$

It is convenient to determine the components of the complex propagation constant in terms of complex refractive index. Hence;

$$\beta = nk_0 \qquad (2.2\text{-}11)$$

$$\frac{\alpha}{2} = -Kk_0 \qquad (2.2\text{-}12)$$

We next consider Maxwell's equations applied to the slab waveguide.

2.3 Dielectric slab waveguide.

It is useful to derive the propagation coefficient of a dielectric slab waveguide as an insight to the optical properties of the active regions of semiconductor lasers. A diagram of the structure to be analysed, and the coordinate system, is shown in figure 2.3-1 in which the wave is propagating in the z-direction and the waveguide is uniform, and infinitely long in the y-direction. Hence $\partial/\partial y=0$. The assumption of $\partial/\partial y=0$ reduces Maxwell's equations 2.1-1 and 2.1-2 into two orthogonal sets of fields. It can easily be seen that the set Hx, Ey and Hz is independent, and hence orthogonal to the set of fields Ex, Hy and Ez. In the first set of fields Ey is the only electric field and there is no component of electric field in the z-direction. However there is a z-component of the magnetic field resulting from Hz. Hence this set of fields is called the

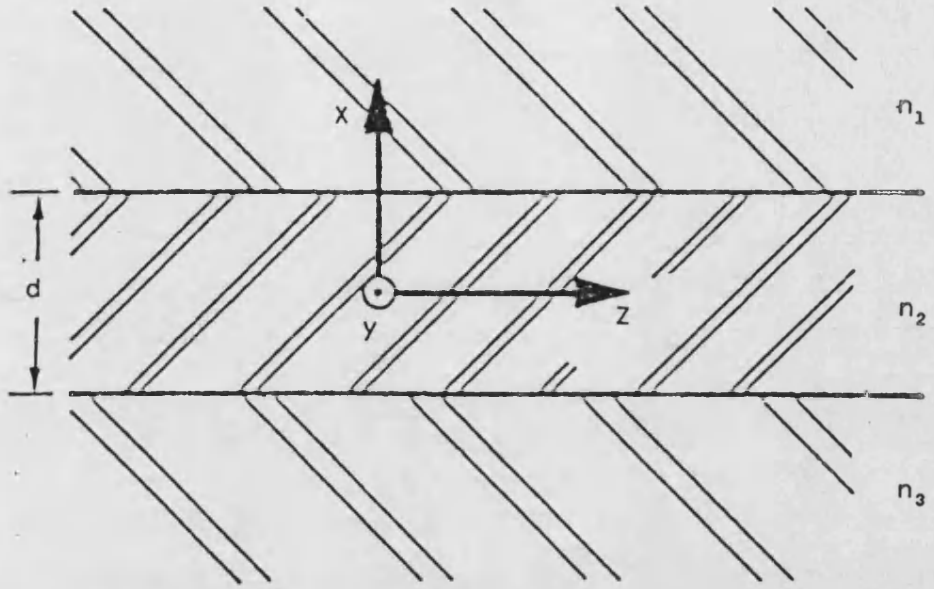

Figure 2.3-1 Representation of slab waveguide and co-ordinate system.

transverse electric (TE) modes. A similar argument can be used for the second set of fields to be called transverse magnetic (TM) modes.

Another result of $\partial/\partial y=0$, is to reduce the three dimensional wave equation;

$$\left[\frac{\partial^2}{\partial x^2} + \frac{\partial^2}{\partial y^2} + \frac{\partial^2}{\partial z^2} + \varepsilon_r k_0^2 \right] \Psi = 0 \qquad (2.3\text{-}1)$$

where Ψ is any field component, into a one dimensional wave equation;

$$\left[\frac{\partial^2}{\partial x^2} + (\varepsilon_r k_0^2 - \beta^2) \right] \Psi = 0 \qquad (2.3\text{-}2)$$

Equation 2.3-2 is often called the scalar wave equation since it applies to all the field components. Also to simplify analysis the dielectric media is assumed to be without loss or gain so that the propagation constant is purely real such that the fields are of the form;

$$\psi = \Psi \exp[\, j(\omega t - \beta z) \,] \qquad (2.3\text{-}3)$$

In general, if there is loss in the medium then the effect of this can often be superimposed on a solution of a lossless medium, particularly in optical waveguides where the loss per "guide wavelength" is usually small where $\alpha \ll \beta$.

In this chapter only TE modes will be discussed but it should be added that similar methods are used to find solutions for TM modes. Before solving the scalar wave equation it is useful to ensure how the boundary conditions at the interfaces of the slab waveguide can be satisfied. From equations 2.1-2 and 2.1-6 we obtain;

$$\frac{\partial Ey}{\partial z} = \mu_0 \frac{\partial Hx}{\partial t} \qquad (2.3\text{-}4)$$

and;

$$\frac{\partial Ey}{\partial x} = -\mu_0 \frac{\partial Hz}{\partial t} \qquad (2.3\text{-}5)$$

If the field is propagating according to equation 2.3-3 then equation 2.3-4 and 2.3-5 become;

$$Hx = -\left[\frac{\beta}{\omega \mu_0} \right] Ey \qquad (2.3\text{-}6)$$

$$Hz = \left[\frac{j}{\omega \mu_0} \right] \frac{\partial Ey}{\partial x} \qquad (2.3\text{-}7)$$

This pair of equations are particularly useful since it states that if Ey and ∂Ey/dx are continuous across the boundary layers of the slab waveguide then the other fields will also be continuous. The problem now becomes one of solving equation 2.3-2 for Ey in all three regions, then solving for the continuity of Ey and dEy/dx across the boundaries. Analysing equation 2.3-2, the solution of;

$$\left[\frac{\partial^2}{\partial x^2} + kx^2 \right] \Psi = 0 \qquad (2.3\text{-}8)$$

where $kx^2 = \varepsilon_r k_0^2 - \beta^2 \quad ; \quad \varepsilon_r k_0^2 > \beta^2$ (2.3-9)

is;

$$\Psi = A_1 \exp(j.kx.x) + A_2 \exp(-j.kx.x) \qquad (2.3\text{-}10)$$

or

$$\Psi = A \cos(kx.x - \theta) \qquad (2.3\text{-}11)$$

and for;

$$\left[\frac{\partial^2}{\partial x^2} - kx^2 \right] \Psi = 0 \qquad (2.3\text{-}12)$$

where $kx^2 = \beta^2 - \varepsilon_r k_0^2 \quad ; \quad \varepsilon_r k_0^2 < \beta^2$ (2.3-13)

is;

$$\Psi = A_1 \exp(kx.x) + A_2 \exp(-kx.x) \qquad (2.3\text{-}14)$$

The type of solution, in a layer, depends upon the value of β^2, whether it is larger or smaller than $(\varepsilon_r k_0^2)$. Using a simple ray approach, the center layer of the slab waveguide must have a higher refractive index than the surrounding layers to support total internal reflection. This is necessary to confine the light to this layer without any loss to the cladding layers. Thus where n_1, n_2 and n_3 are the refractive indices of the layers illustrated in figure 2.3-1;

$$n_2 > n_1 \; ; \; n_2 > n_3 \qquad (2.3\text{-}15)$$

A similar argument, of the inequalities of n_1, n_2 and n_3, results from the solutions of the scalar wave equation discussed above. For a bound mode (where the fields are concentrated in the centre layer) the field Ey must decay exponentially to zero for x tending to plus or minus infinity. For the power to be confined to the active layer the field must vary sinusoidally, in the x-direction, in the center layer. Hence;

$$kx_2^2 = n_2^2 k_0^2 - \beta^2 \; ; \; n_2^2 k_0^2 > \beta^2 \qquad (2.3\text{-}16)$$

$$kx_1^2 = \beta^2 - n_1^2 k_0^2 \; ; \; n_1^2 k_0^2 < \beta^2 \qquad (2.3\text{-}17)$$

and

$$kx_3^2 = \beta^2 - n_3^2 k_0^2 \; ; \; n_2^2 k_0^2 < \beta^2 \qquad (2.3\text{-}18)$$

From these equations we obtain the same inequalities as in equation 2.3-15 since β must be common to all the layers in the slab wave-guide.

Hence for Ey;

$$Ey = \begin{cases} A.\cos(kx_2.d/2 - \theta).\exp(-kx_1.(x - d/2)) & ; x > d/2 \\ A\cos(kx_2.x - \theta) & ; d/2 > x > -d/2 \\ A.\cos(kx_3.d/2 + \theta).\exp(kx_3.(x + d/2)) & ; x < -d/2 \end{cases} \qquad (2.3\text{-}19)$$

$\partial Ey/\partial x$ must also be continuous to satisfy continuity of Hz across the layers from equation 2.3-5.

$$\frac{\partial Ey}{\partial x} = \begin{cases} -A.kx_1.\cos(kx_2.d/2 - \theta).\exp(-kx_1.(x - d/2)) & ; x > d/2 \\ -A.kx_2.\sin(kx_2.x - \theta) & ; d/2 > x > -d/2 \\ A.kx_3.\cos(kx_3.d/2 + \theta).\exp(kx_3.(x + d/2)) & ; x < -d/2 \end{cases} \qquad (2.3\text{-}20)$$

Satisfying the boundary conditions for at d/2 and -d/2 we obtain expressions for θ;

At $x = d/2$

$$\tan(\theta) = \frac{kx_2.\tan(kx_2.d/2) - kx_1}{kx_2 + kx_1.\tan(kx_2.d/2)} \qquad (2.3\text{-}21)$$

and at $x = -d/2$

$$\tan(\theta) = \frac{kx_3 - kx_2.\tan(kx_2.d/2)}{kx_2 + kx_3.\tan(kx_2.d/2)} \qquad (2.3\text{-}22)$$

Eliminating $\tan(\theta)$ from these equations;

$$\tan(kx_2.d) = \frac{kx_2.(kx_3 + kx_1)}{kx_2^2 - kx_1.kx_3} + n.\pi \qquad (2.3\text{-}23)$$

$(n = 0, 1, 2....)$

β can be found by solving the above transcendental equation by numerical means for the mode number n. Also by eliminating

"$\tan(kx_2.d/2)$" from equations 2.3-21 and 2.3-22 an expression for $\tan(\theta)$ can be found;

$$\tan(2\theta) = \frac{kx_2.(kx_3 - kx_2)}{kx_2^2 + kx_1.kx_3} \qquad (2.3\text{-}24)$$

For a symmetric slab wave-guide where $n_1 = n_3$ then further simplification is possible. From this, $kx_1 = kx_3$ and from equation 2.3-24;

$$\theta = 0^0,\ 90^0,\ \text{etc.} \qquad (2.3\text{-}25)$$

Thus two types of solution are possible. If this result is substituted in equation 2.3-21 or 2.3.22 we find that simpler transcendental equations can be found corresponding to whether $\theta = 0^0$ or 90^0.

For $\theta = 0^0$

$$kx_2.\tan(kx_2.d/2) = kx_1 + m.\pi \qquad (2.3\text{-}26)$$

$$(m = 0, 1, 2...)$$

and for $\theta = 90^0$

$$kx_1.\tan(kx_2.d/2) = -kx_2 + m.\pi \qquad (2.3\text{-}27)$$

$$(m = 0, 1, 2...)$$

Equations 2.3-26 and 2.3-27 correspond to the even and odd modes of the symmetric slab waveguide respectively. Figure 2.3-2 shows graphically the propagation constant of the TE modes in a normalised form, where;

$$b = \frac{\beta^2 - n_1^2.k_0^2}{k_0^2\,(n_2^2 - n_1^2)} \qquad (2.3\text{-}28)$$

and; $$D = d.(n_2^2 - n_1^2) \qquad (2.3\text{-}29)$$

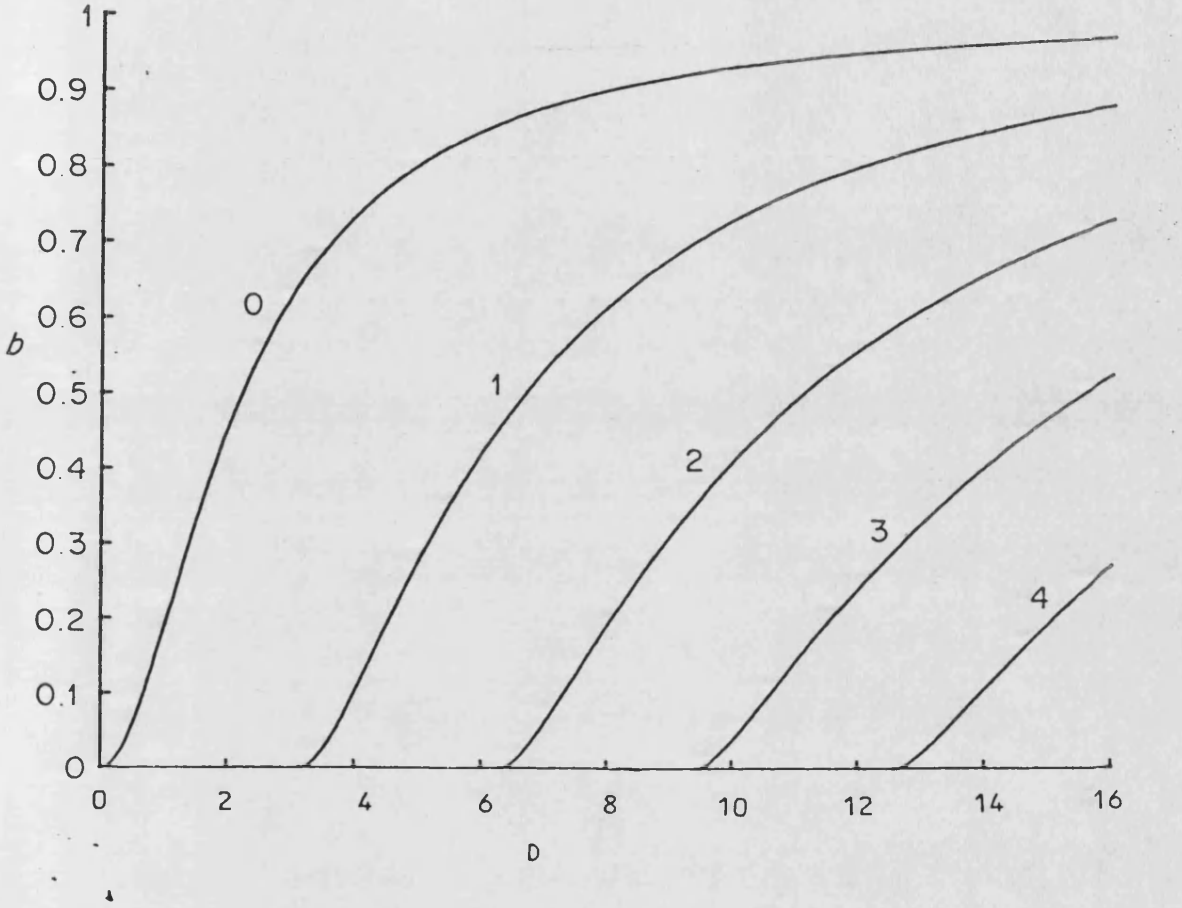

Figure 2.3-2 Normalised propagation constant b (equation 2.3-28) versus normalised thickness of centre layer D (equation 2.3-29) for symmetric three layer slab waveguide. The labelling parameter N indicates the mode number as expressed in equation 2.3-23.

2.4 Confinement factor.

This is the ratio of optical energy in the centre layer to the total optical energy of a mode. It is significant that only this proportion of light will be amplified if the centre layer has optical gain.

Taking $Ey(x)^2$ to be proportional to intensity the confinement factor may be defined as;

$$\Gamma = \frac{\int_{-d/2}^{d/2} Ey(x)^2 \, dx}{\int_{-\infty}^{\infty} Ey(x)^2 \, dx} \qquad (2.4\text{-}1)$$

The confinement factor for the fundamental and higher order modes is illustrated in figure 2.4-1.

2.5 Gain-guiding in a slab waveguide.

In this section the conditions of waveguiding action in a symmetric slab waveguide ($n_1 = n_3$) for layers with complex refractive index are derived. The conditions for gain guided modes for the first TE mode are shown below where the centre layer has gain and the outer layers have either a loss or gain.

It may not be immediately apparent how this analysis is relevant to a stripe laser relying upon the combined gain guiding, to maintain a stable lateral mode, as well as transverse index guiding. However the results in this section are applicable since the weak gain guiding can be superimposed on the strong index guiding by using the effective index method which will be shown later.

Take the lowest mode (even) equation 2.3-26;

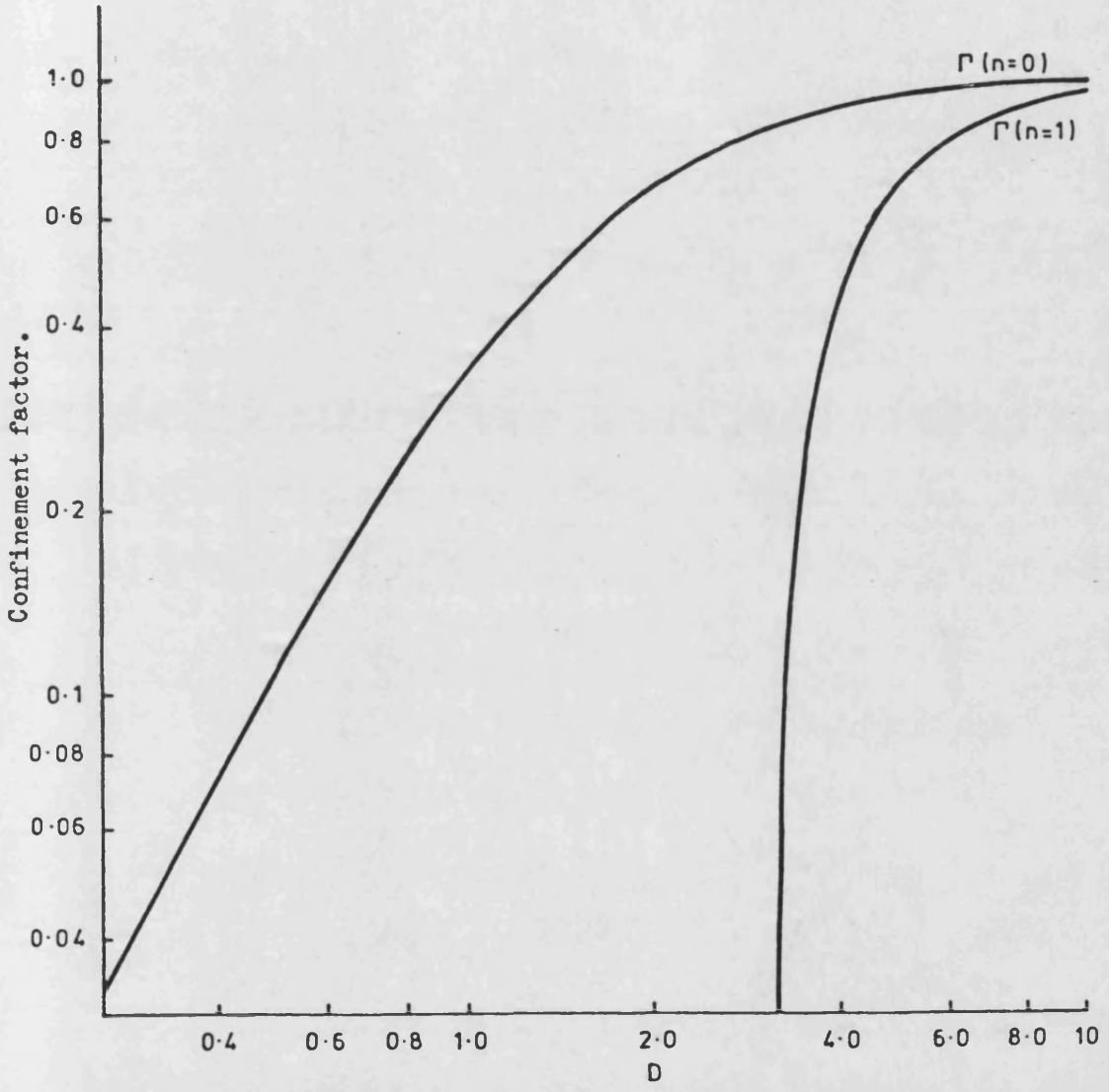

Figure 2.4-1 Confinement factor for lowest and first order modes for the optical distribution in a symmetrical slab waveguide for normalised thickness D (equation 2.3-29)

$$kx_2.\tan(kx_2.d/2) = kx_1$$

where kx_1 and kx_2 are both complex values. In the top cladding layer where the evanescent field is decaying to zero at plus infinity according to;

$$Ey = A_1\exp(-kx_1.x) \qquad (2.5\text{-}1)$$

kx_1 must have a positive real part. In the case of modes which are undergoing gain the curvature of the phase-fronts would indicate that the source is at some distance in the negative direction from the point of analysis. This requires that the imaginary part of kx_1 also be positive so that kx_1 lies in the first quadrant of the complex plane. Thus;

$$kx_2.\tan(kx_2.d/2)$$

must also lie in the first quadrant. Using multiple angle formulae and $kx_2 = kx_{2r} + j.kx_{2i}$ we obtain;

$$(kx_{2r} + j.kx_{2i}).\tan\{ (kx_{2r} + j.kx_{2i}).d/2 \}$$

$$= \frac{\left| \begin{array}{l} kx_{2r}.\sin(2kx_{2r}.d) - kx_{2i}.\sinh(2kx_{2i}.d) \\ \quad +j.[\, kx_{2i}.\sin(2kx_{2r}.d) + kx_{2r}.\sinh(2kx_{2i}.d)\,] \end{array} \right|}{\left| \begin{array}{l} 2\cos^2(kx_{2r}.d/2).\cosh^2(kx_{2i}.d/2) \\ \quad + 2\sin^2(kx_{2r}.d/2).\sinh^2(kx_{2i}.d/2) \end{array} \right|} \qquad (2.5\text{-}2)$$

The denominator of equation 2.5-2 will always be positive. The numerator must then occupy the first quadrant of the complex plane as does kx_1. The imaginary part of equation 2.5-2 must be greater than zero;

$$kx_{2_i}.\sin(2kx_{2_r}.d) + kx_{2_r}.\sinh(2kx_{2_i}.d) > 0 \qquad (2.5\text{-}3)$$

Thus kx_{2_i} and kx_{2_r} must be of the same sign where the product would always be positive. From equations 2.3-16 and 2.3-17 we obtain the relation;

$$kx_2^2 + kx_1^2 = (n_2^2 - n_1^2).k_0^2 \qquad (2.5\text{-}4)$$

since kx_{1_r} and kx_{1_i} are of the same sign, where;

$$kx_1 = kx_{1_r} + j.kx_{1_i} \qquad (2.5\text{-}5)$$

and kx_{2_r} and kx_{2_i} are of the same sign it is useful to equate the imaginary parts of equation 2.5-4.

$$\text{Im}\,(kx_2^2 + kx_1^2) = 2.(kx_{2_r}.kx_{2_i} + kx_{1_r}.kx_{1_i}) > 0 \qquad (2.5\text{-}6)$$

Thus;

$$\text{Im}\,(n_2^2 - n_1^2).k_0^2 = n_2.K_2 - n_1.K_1 > 0 \qquad (2.5\text{-}7)$$

which is the result which Schlosser [2] gives for a necessary but not sufficient condition for stability of a guided mode in a slab waveguide of complex refractive index.

The inequality can be interpreted for some cases;

$K_1 = K_2$, equation 2.5-7 reduces to $n_2 > n_1$ which is the requirement for (refractive) index guiding.

$n_2 = n_1$, this implies $K_2 > K_1$, where the gain is greater in the centre layer than the cladding layers.

If the relative difference between n_1 and n_2 is small, then equation 2.5-7 can rearranged into a more useful expression;

$$\frac{\Delta K}{K_2} + \frac{\Delta n}{n_1} > 0 \qquad (2.5\text{-}9)$$

where $\Delta n = n_2 - n_1$ and $\Delta K = K_2 - K_1$.

Even though there may be one mechanism which may be antiguiding, as long as the other mechanism is dominant the structure will still support a stable mode. Further discussion of gain guiding can be found in [3].

2.6 Guiding in an absorbing slab waveguide.

The above analysis is only applicable where K_2 is positive, where the centre layer has optical gain. If K_2 is assumed to be negative, so that the centre layer has optical loss, then further analysis is required. Again we have the transcendental equation (2.2-26) which must be solved to give the propagating modes.

$$kx_2.\tan(kx_2.d/2) = kx_1$$

In a similar argument as in the previous section kx_1 must have a positive real part for the field to decay in the cladding layers away from the centre layer. We now assume the mode is attenuated as it propagates in the positive z direction. This results in the phase-fronts converging to a point at some distance in the positive z direction from the point of analysis. This implies that the imaginary part of kx_1 is negative. Thus kx_{1_r} and kx_{1_i} are of different sign.

We must now determine the signs of kx_{2_r} and kx_{2_i}. From equation 2.2-26 we find;

$$\mathrm{Im}\ \{\ kx_2.\tan(kx_2.d/2)\ \} < 0 \qquad (2.6\text{-}1)$$

In the same way as before we obtain the inequality;

$$kx_{2_i}.\sin(kx_{2_r}.d) + kx_{2_r}.\sinh(kx_{2_i}.d) < 0 \qquad (2.6\text{-}2)$$

This implies that kx_{2_r} and kx_{2_i} are also of opposite sign and

the imaginary part of equation 2.5-4 must then be negative;

$$\text{Im}\,(kx_1^2 + kx_2^2) = 2.(kx_{2_r}.kx_{2_i} + kx_{1_r}.kx_{1_i}) < 0 \qquad (2.6\text{-}3)$$

From equation 2.5-4 we obtain;

$$\text{Im}\,(n_2^2 - n_1^2).k_0^2 = n_2.K_2 - n_1.K_1 < 0 \qquad (2.6\text{-}4)$$

This a similar equation as derived in the previous section although it should be remembered that k_2 has been assumed negative to represent optical loss in the centre layer. This result can be interpreted for the usual cases;

$K_1 = K_2$, this reduces to $n_2 > n_1$ which, again, is the requirement for index guiding.

$n_2 = n_1$, this implies $kx_2 < kx_1$, where the loss in the centre region is greater than the loss in the cladding layers. It is possible, in this case, to perhaps have gain in the cladding layers though whilst obeying this inequality other reasons may prevent such cases. The assumptions used to obtain this inequality must be observed such as assuming the propagating mode undergoes attenuation.

Equation 2.6-5 may put in a more useful form by making;

$$n_2 = n_1 + \Delta n$$

to obtain;

$$\frac{\Delta K}{K_2} + \frac{\Delta n}{n_1} > 0 \qquad (2.6\text{-}6)$$

where; $\Delta K = K_2 - K_1$

Note the change of sign of the inequality. This is brought about by dividing the expression 2.6-5 by $K_2.n_1$ and remembering that K_2 has been assumed to be negative. This equation is identical to equation 2.5-9 where K_2 has been assumed positive and the mode undergoes gain in the direction of propagation. This result is used in the next chapter for the case of the centre layer having a lower

absorption coefficient and also a lower refractive index than the cladding layers. For this example, equation 2.6-6 clearly shows that this structure is unable to support a stable guided mode.

2.7 Rectangular dielectric waveguide.

Figure 2.7-1 shows the cross-section of a rectangular dielectric waveguide where a central core is surrounded by material. This type of waveguide is more useful than the slab waveguide mentioned earlier since it confines the light in both the x and y directions. However an exact analytic solution for this structure is not possible and either approximation or numerical analysis is necessary. One approximate method is that by Mercatili [4]. He produces results which are most accurate for modes well above cut-off when the optical energy is almost exclusively confined to the region of the core. In particular there is very little energy in the shaded portions of figure 2.7-1 so the field within these regions may be ignored completely. The method then goes on to match the dominant fields at the interfaces. One of the errors in this approximation is it predicts a cut-off frequency for propagation for $n_2 = n_3 = n_4 = n_5 < n_1$. However, for this case it is known to propagate down to DC. For further details of this method see [5].

A significant improvement over the above method is the "effective index" or "effective dielectric constant" (EDC) method [6] which is also illustrated in [3]. This method approximates the problem into two slab waveguides, one in the x direction and the other in the y direction as illustrated in figure 2.7-2. The weaker guiding action in the x direction is solved ignoring any guiding action in the y direction such that $\partial/\partial y$ is assumed zero. For example, for TE modes of the rectangular waveguide in figure 2.7-2

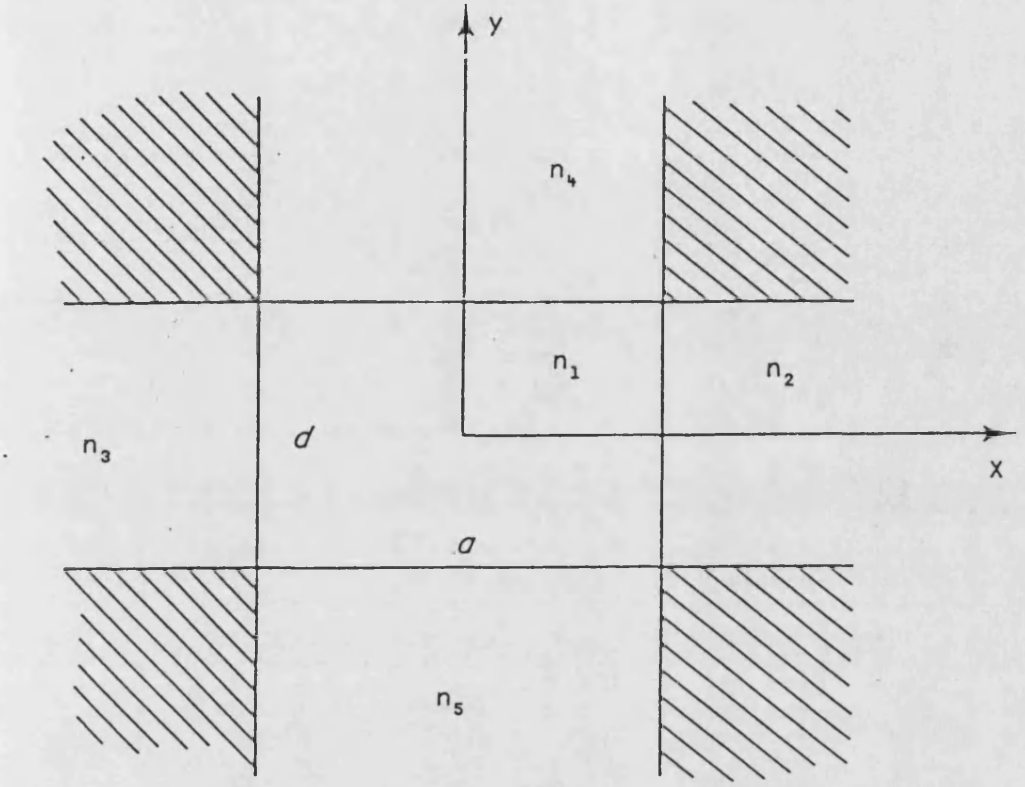

Figure 2.7-1 The rectangular dielectric waveguide. The shaded portions represent the regions where Mercatili's method ignores the fields.

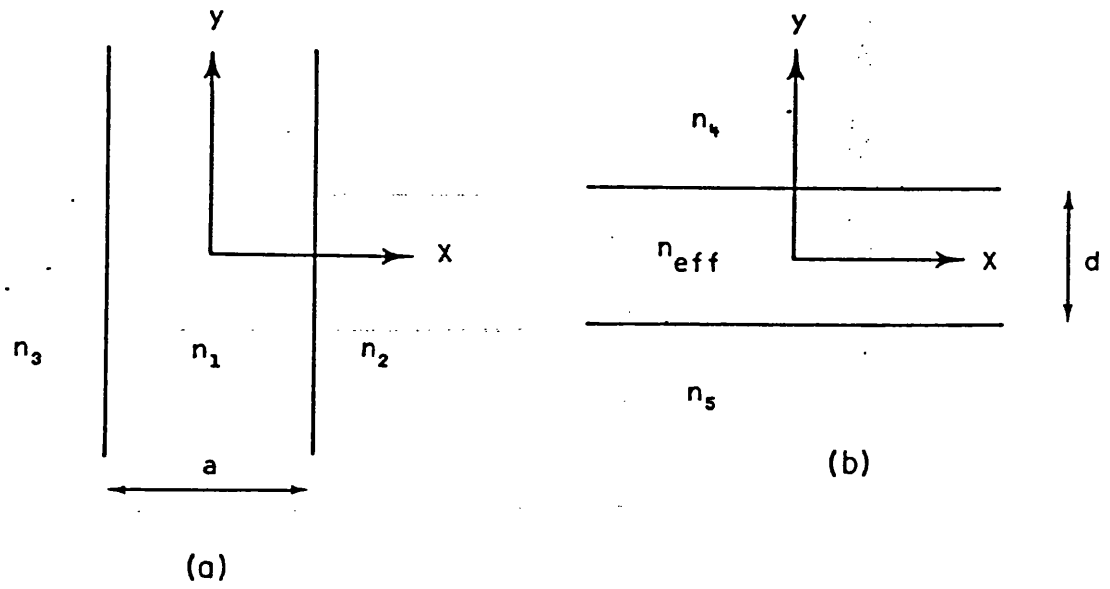

Figure 2.7-2 Illustration of the effective index method applied to the rectangular dielectric waveguide. Problem is reduced from a two dimensional problem to two one dimensional slab waveguide problems in the x-direction (a) and the y-direction (b)

where Ey is the dominant electric field the transcendental equation for TM modes, similar to equation 2.3-23 for TE modes, in the y direction;

$$\tan(ky_1.a) = \frac{n_1^2.ky_1 \;.\; (n_3^2.ky_2 + n_2^2.ky_3)}{n_2^2.n_3^2.ky_1^2 \;-\; n_1^4.ky_2.ky_3} \qquad (2.7\text{-}1)$$

$$\text{where; } ky_1^2 = n_1^2.k_0^2 - \beta y^2$$

$$ky_2^2 = \beta y^2 - n_2^2.k_0^2$$

$$ky_3^2 = \beta y^2 - n_3^2.k_0^2$$

The above equation when solved gives βy (formerly β in the slab waveguide problem of section 2.3).

$$n_{eff}^2 = n_1^2 - \left[\frac{\beta y}{k_0}\right]^2 \qquad (2.7\text{-}2)$$

This is then used to define an effective index n_{eff} for the core region, as in equation 2.7-2, for the other slab waveguide problem in the y direction for which a transcendental equation for TE modes in the x direction, similar to equation 2.3-23, which may then be solved to give β;

$$\tan(kx_1.d) = \frac{kx_1.(kx_4 + kx_5)}{kx_1^2 - kx_4.kx_5} \qquad (2.7\text{-}3)$$

$$\text{where; } kx_1^2 = n_{eff}^2.k_0^2 - \beta^2$$

$$kx_4^2 = \beta^2 - n_4^2.k_0^2$$

$$kx_5^2 = \beta^2 - n_5^2.k_0^2$$

This method gives good results for rectangular waveguides with sizable aspect ratios or with refractive indices such that one direction of guiding dominates another. It is also ideal in combining

lateral gain guiding and transverse index guiding mechanisms for a laser [7, 8] where the refractive indices are complex quantities.

2.8 Conclusion.

This chapter introduces the fundamentals of the confinement of optical energy to waveguides which are present in semiconductor lasers. The slab waveguide is treated in detail and the application of the EDC method is shown. This gives surprisingly good results for a variety of applications where a two dimensional waveguide problem can be reduced into two, one dimensional slab waveguide problems for which analytic equations are possible. Gain guiding is not an important feature of this study except that it shows that a conventional laser without index guiding will not produce hysteresis, at least of the same magnitude of a B-H bistable laser, due to the high loss of light from the resonant cavity. This will be discussed in more detail in the next chapter. It should be noted, however, that some small light jumps have been observed in very wide SLED's with only moderate lengths of passive region [9].

References.

1) J. A. Stratton. "Electromagnetic theory"; McGrawhill; 1941.

2) W. O. Schlosser. "Gain-Induced Modes in Planar Structures"; The Bell System Technical Journal; Vol. 52; No. 6; 1973; p 887-905.

3) M. J. Adams. "An Introduction to optical waveguides"; John Wiley & Sons; 1981.

4) E. A. J. Mercatili. "Dielectric rectangular waveguide and directional coupler for integrated optics"; Bell System Technical Journal; Vol 48; p 2071-2102.

5) D. Marcuse. "Theory of Dielectric Optical Waveguides"; Academic Press; 1974.

6) R. M. Knox and P. P. Toulios. "Integrated circuits for the millimeter through optical frequency range"; In J. Fox (Ed); Proceedings of the MRI Symposium on submillimeter Waves; Polytechnic Press; Brooklyn; p497-516.

7) T. E. Rozzi, T. Itoh and L. Grun. "Two-dimensional analysis of the GaAs double heterostructure stripe-geometry laser"; Radio Science; Vol. 12; 1977; p 543-49.

8) J. Buus. "The effective index method and its application to semiconductor lasers"; IEEE Journal of Quantum Electronics; Vol. QE-18; No. 7; 1982; p1083-9.

9) I. Middlemast. - Private communication.

Chapter 3

Light emission processes and the buried heterojunction laser.

3 Introduction.

This chapter contains the basic principles of gain and spontaneous emission which are fundamental to the operation of a semiconductor laser. The material on which this research is based is GaAs, which allows optically radiative electron-hole transitions to take place readily. Emission or absorption of a photon can cause an electron to change from a higher energy to a lower energy state or vice versa respectively. The Einstein relations [1] are derived which show that absorption and stimulated emission probabilities are equal and related to the spontaneous emission probability. These relations lead to the necessary condition for net positive gain which was derived by Bernard and Duraffong [2]. A hydrogenic model is briefly described to obtain the transition probability between the conduction band and valence band for GaAs and several references on the calculation of the transition probability are given. The effect of impurities in GaAs is discussed and a method of calculating gain and spontaneous emission is outlined. This chapter gives a brief explanation of other absorption mechanisms which are present in laser structures, namely free carrier absorption and scattering losses. Some knowledge of semiconductors will be assumed and can be found in any relevant text book, such as by Sze [3].

Included in this chapter is an explanation as to why the buried heterojunction laser is the most preferable device structure to be used for absorptive bistability.

3.1 Band Structure of GaAs.

GaAs is a "direct" band-gap semiconductor for which the fundamental derivations of the semiconductor band structure can be found in texts such as those by Long [4] and Harrison [5].

The major features of the energy band structure of GaAs are shown in figure 3.1-1. This is a plot of electron energy as a function of the crystal momentum wave vector k. For GaAs, a direct band-gap material, the minimum energy in the conduction band and the maximum energy in the valence band occur for the same value of k, namely k=0. An electron can make a band to band transition directly from the absorption or emission of a photon.

In most photon absorption and emission processes the total momentum or k value must be conserved. In practice the transitions in a doped direct band-gap semiconductor are not so simply determined.

3.2 Emissive and absorption processes.

Figure 3.2-1 illustrates the three processes for an idealised atomic system having two electron energy states. Figure 3.2-1a shows the absorption of a photon which excites an electron to a higher state. The production of a photon by the spontaneous decay of an electron is shown in Figure 3.2-1b. Finally stimulated gain is illustrated where a photon of the correct energy can induce a downward transition, of an electron in the conduction band to the valence band, to give an identical photon which is of the same frequency and is of the same phase. This photon is said to be coherent with the stimulating photon.

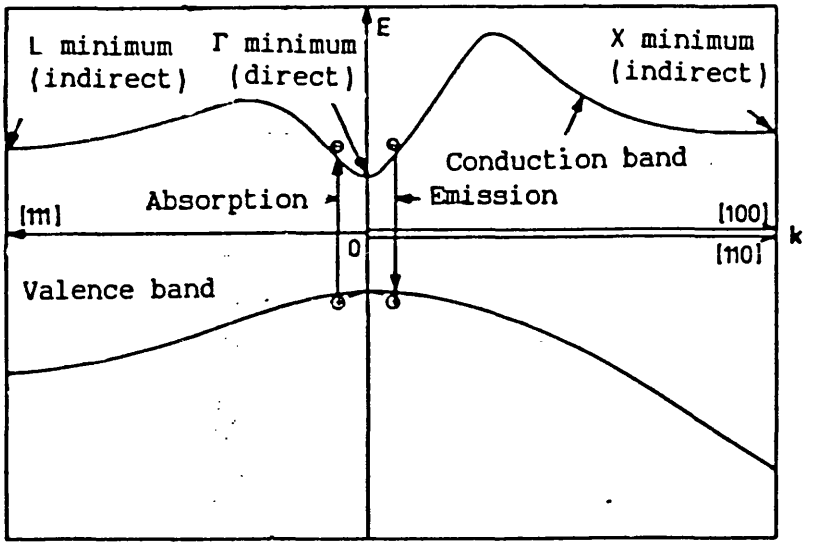

Figure 3.1-1 Band-structure of GaAs.

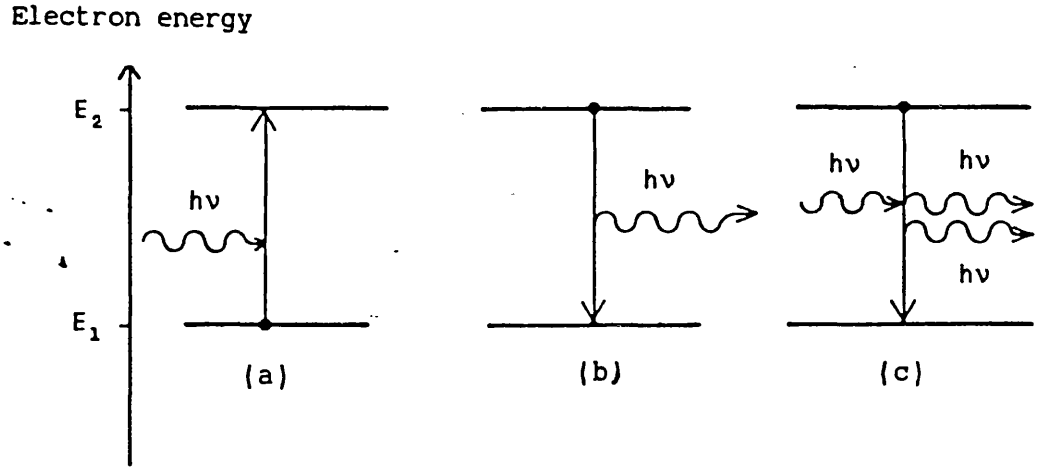

Figure 3.2-1 Schematic representation of absorption emission processes for an idealised atomic system having two allowed electron energy states. (a) represents the absorption of a photon and (b) spontaneous emission by the natural decay of electrons in the higher state to the lower state. (c) represents stimulated emission.

3.2.1 Einstein Relations.

These are the relations between the absorptive, spontaneous and stimulated transition probabilities [1]. In a simplified case, the available states in GaAs is represented by a continuous band of states within the valence and conduction bands as in Figure 3.2.1-1. It should be noted that the Einstein relations hold for any material system. The actual differences between different materials are contained in the transition probabilities, which must be evaluated by either experimental or quantum mechanical means. For this system the rate for the absorptive process depends upon;

1) The probability that the transition can occur, $[B_{12}]$
2) The probability that the state E_1 contains an electron, $[f_1]$
3) The probability that the state E_2 is empty, $[1 - f_2]$
4) The density of photons of energy $h\nu$, $P(h\nu)$; where $h\nu = E_2 - E_1$

The upward transition rate may then be written as;

$$r_{12} = B_{12} \cdot f_1[1 - f_2] \cdot P(h\nu) \qquad (3.2.1\text{-}1)$$

For semiconductor materials the occupation probability f_1 is given by the Fermi-Dirac distribution and is;

$$f_1 = \frac{1}{\exp[(E_1 - F_1)/kT] - 1} \qquad (3.2.1\text{-}2)$$

where F_1 represents the Quasi-Fermi level for the valence band under non-equilibrium conditions. The quasi-Fermi level represents the points where the states would be 50% occupied. Figure 3.2.1-1 shows the case where the valence band is nearly full and the conduction band is nearly empty. The probability of an electron in the conduction band, f_2, is;

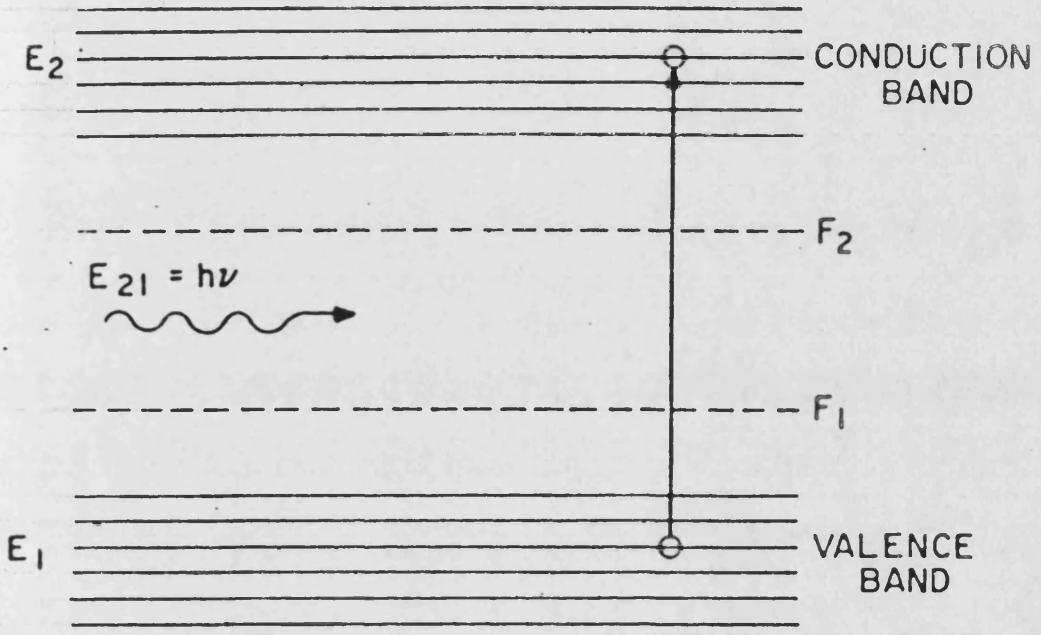

Figure 3.2.1-1 Transition of an electron from E_1 to E_2 by the absorption of a photon where the states are represented by a continuous band of states.

$$f_2 = \frac{1}{\exp[(E_2 - F_2)/kT] - 1} \qquad (3.2.1\text{-}3)$$

The rate of spontaneous emission depends upon;

1) The probability the transition can occur, $[A_{21}]$

2) The probability that the state E_2 contains an electron, $[f_2]$

3) The probability that the state E_1 is empty, $[1 - f_1]$

The spontaneous emission rate is;

$$r_{21}(spon) = A_{21}.f_2.(1 - f_1) \qquad (3.2.1\text{-}4)$$

Using a similar argument for stimulated emission we have;

$$r_{21} = B_{21}.f_2.[1 - f_1].P(h\nu) \qquad (3.2.1\text{-}5)$$

At thermal equilibrium, $F_1 = F_2$ and the upward transition rate must equal the total downward transition rate.

$$r_{12} = r_{21} + r_{21}(spon) \qquad (3.2.1\text{-}6)$$

Combining equations 3.2.1-1, 3.2.1-4 and 3.2.1-5 equation 3.2.1-6 becomes;

$$P(h\nu) = \frac{A_{21}.f_2.[1 - f_1]}{B_{12}.f_1.[1 - f_2] - B_{21}.f_2.[1 - f_1]} \qquad (3.2.1\text{-}7)$$

alternatively;

$$P(h\nu) = \frac{A_{21}}{B_{12}.\exp(h\nu/kT) - B_{21}} \qquad (3.2.1\text{-}8)$$

At thermal equilibrium equation 3.2.1-8 should be the same as the energy distribution as the blackbody radiation distribution;

$$P(h\nu) = \frac{8.\pi.n^3.h\nu^2}{h^3.c^3.[\exp(h\nu/kT) - 1]} \qquad (3.2.1\text{-}9)$$

Hence;

$$B_{12} = B_{21} \qquad (3.2.1\text{-}10)$$

and

$$Z(h\nu) = \frac{A_{21}}{B_{21}} = \frac{8.\pi.n^3.h\nu^2}{h^3.c^3} \qquad (3.2.1\text{-}11)$$

In conclusion, the stimulated and absorption probabilities are equal and related to the spontaneous emission probability. While these relations have been derived for a much simplified system, they still hold for any material system such as the direct band-gap materials used for semiconductor lasers.

3.2.2 Condition for net optical gain.

If stimulated emission is more likely to occur than the process of absorption then there will be a net optical gain, otherwise called a positive net stimulated emission rate. For this to occur r_{21} must exceed r_{12}. The expressions were derived by Bernard and Duraffourg [2]. From equations 3.2.1-1 and 3.2.1-5;

$$B_{21}.f_2.[1 - f_1].P(h\nu) > B_{12}.f_1.[1 - f_2].P(h\nu) \qquad (3.2.2\text{-}1)$$

since $B_{12} = B_{21}$;

$$f_2.[1 - f_1] > f_1.[1 - f_2]$$

$$f_2 > f_1 \qquad (3.2.2\text{-}2)$$

Using equation 3.2.1-2 and 3.2.1-3 for f_1 and f_2 respectively;

$$\exp[(F_1 - F_2)/kT] > \exp[(E_2 - E_1)/kT] \qquad (3.2.2\text{-}3)$$

alternatively;

$$F_2 - F_1 > E_2 - E_1 \; ; \; F_2 - F_1 > h\nu \qquad (3.2.2\text{-}4)$$

Thus the separation of the quasi-Fermi levels must exceed the photon energy for the downward stimulated emission rate to exceed the absorption rate.

The net stimulated rate is a useful quantity and is the difference between r_{21} and r_{12};

$$r_{21}(stim) = B_{21}.f_2.[1 - f_1].P(h\nu) - B_{12}.f_1.[1 - f_2].P(h\nu) \qquad (3.2.2\text{-}5)$$

This reduces to;

$$r_{21}(stim) = B_{21}.[f_2 - f_1].P(h\nu) \qquad (3.2.2\text{-}6)$$

Similarly the net absorption rate is;

$$r_{12}(abs) = B_{21}.[f_1 - f_2].P(h\nu) \qquad (3.2.2\text{-}7)$$

The net absorption rate $r_{12}(abs)$ is the absorption coefficient times the photon flux. The photon flux is simply the photon density distribution times the group velocity v. Hence the attenuation or loss is;

$$\alpha(h\nu) = \frac{B_{21}.[f_1 - f_2]}{v} \qquad (3.2.2\text{-}8)$$

3.2.3 Relation between absorption coefficient and spontaneous emission.

Equation 3.2.1-5 again;

$$r_{21}(spon) = A_{21}.f_2.[1 - f_1]$$

using the relation defined in equation 3.2.1-10 where;

$$A_{12} = Z(h\nu).B_{21}$$

we have

$$r_{21}(spon) = Z(h\nu).B_{21}.f_2.[1 - f_1] \qquad (3.2.3\text{-}1)$$

Combining equations 3.2.2-8 and 3.2.3-1 to eliminate B_{21};

$$r_{21}(spon) = Z(h\nu).\alpha(h\nu).\frac{f_2.[1 - f_1]}{[f_1 - f_2]} \qquad (3.2.3\text{-}2)$$

alternatively;

$$r_{21}(spon) = \frac{Z(h\nu).\alpha(h\nu)}{\exp[\{h\nu - (F_2 - F_1)\}/kT] - 1} \qquad (3.2.3\text{-}3)$$

α, $r_{21}(spon)$, $r_{21}(stim)$ are related and the knowledge of one gives the other two. To evaluate these expressions one quantity such as $\alpha(h\nu)$ must be found by experiment or the transition probabilities B_{21} or A_{21} must be calculated.

3.2.4 Transition probability.

While it is possible to calculate the transition probabilities from measuring the absorption coefficient this discussion would not be complete without a brief explanation how it is possible to calculate the transition probabilities from quantum mechanical means. It is not intended to go deeply into the realms of quantum mechanics and it is assumed sufficient that some results are merely quoted.

The interaction between the electrons in the semiconductor and photons require the techniques of time-dependent perturbation of the Schrodinger equation. With this procedure, the properties of the system are determined in the absence of radiation, and the alteration that occurs in the presence of radiation is then

determined. This gives a transition probability usually referred to as Fermi's Golden Rule:

$$B_{21} = \frac{m}{2.h} \cdot |\langle \Psi_1^*(r,t) \cdot |H^1| \cdot \Psi_2(r,t) \rangle|^2 \qquad (3.2.4\text{-}1)$$

The quantity;

$$\langle \Psi_1^*(r,t) \cdot |H|^1 \cdot \Psi_2(r,t) \rangle$$

is the matrix element of the interaction Hamiltonian between $\Psi_1^*(r,t)$, the complex conjugate of the wave function of the initial state and $\Psi_2(r,t)$, the wave function of the final state. More information on any relevant derivations can be found in most books on basic quantum mechanics [6, 7, 8 and 9].

3.3 Density of states.

Earlier in this chapter, for simplicity, the rates of stimulated emission and spontaneous emission had been given for an atomic system with continuous bands of states. For GaAs the density of states for the valence and conduction band can be approximated to be parabolic with respect to energy in the absence of impurities.

$$\rho_c(E - E_c) = \frac{1}{2\pi^2} \cdot (2m_e/h^2)^{3/2} \cdot (E - E_c)^{1/2} \qquad (3.3\text{-}1)$$

$$\rho_v(E_v - E) = \frac{1}{2\pi^2} \cdot (2m_h/h^2)^{3/2} \cdot (E_v - E)^{1/2} \qquad (3.3\text{-}2)$$

However for GaAs, which has an appreciable impurity concentration, the impurity states merge with the conduction and valence bands to form "band tails" where the bound and free carriers

become virtually indistinguishable. These tails have a significant effect on the emission-wavelength characteristics when compared to pure GaAs.

There are a number of methods which model the shape and the intrusion of the tail into the band gap. Two notable examples are those of Kane [12], and Halperin and Lax [13]. Hwang [14] has compared these methods for particular doping levels and his results are illustrated in Figure 3.3-1. In general the Kane model overestimates the penetration of the tail into the band-gap, particularly that of the conduction band. It should be added that Stern [15] used a crude exponential conduction tail and obtained a good fit between calculated spontaneous line shapes and experimental data.

3.4 K-selection.

It has already been mentioned that in pure GaAs, in photon absorption and emissive processes the k-value or momentum of carriers is conserved. However for a highly doped material, states in the impurity band tails interact with states over a spread of momentum so that the k-selection rule is invalid. As one goes away from the gap into the band, away from the impurity states, a k-selection rule will once again be approximately fulfilled [15].

3.5 Modelling of gain and spontaneous emission.

There are a number of models which attempt to characterise gain and spontaneous emission as a function of wavelength [11 ,15-17]. It is usual to have some band tail model for the density of states and a

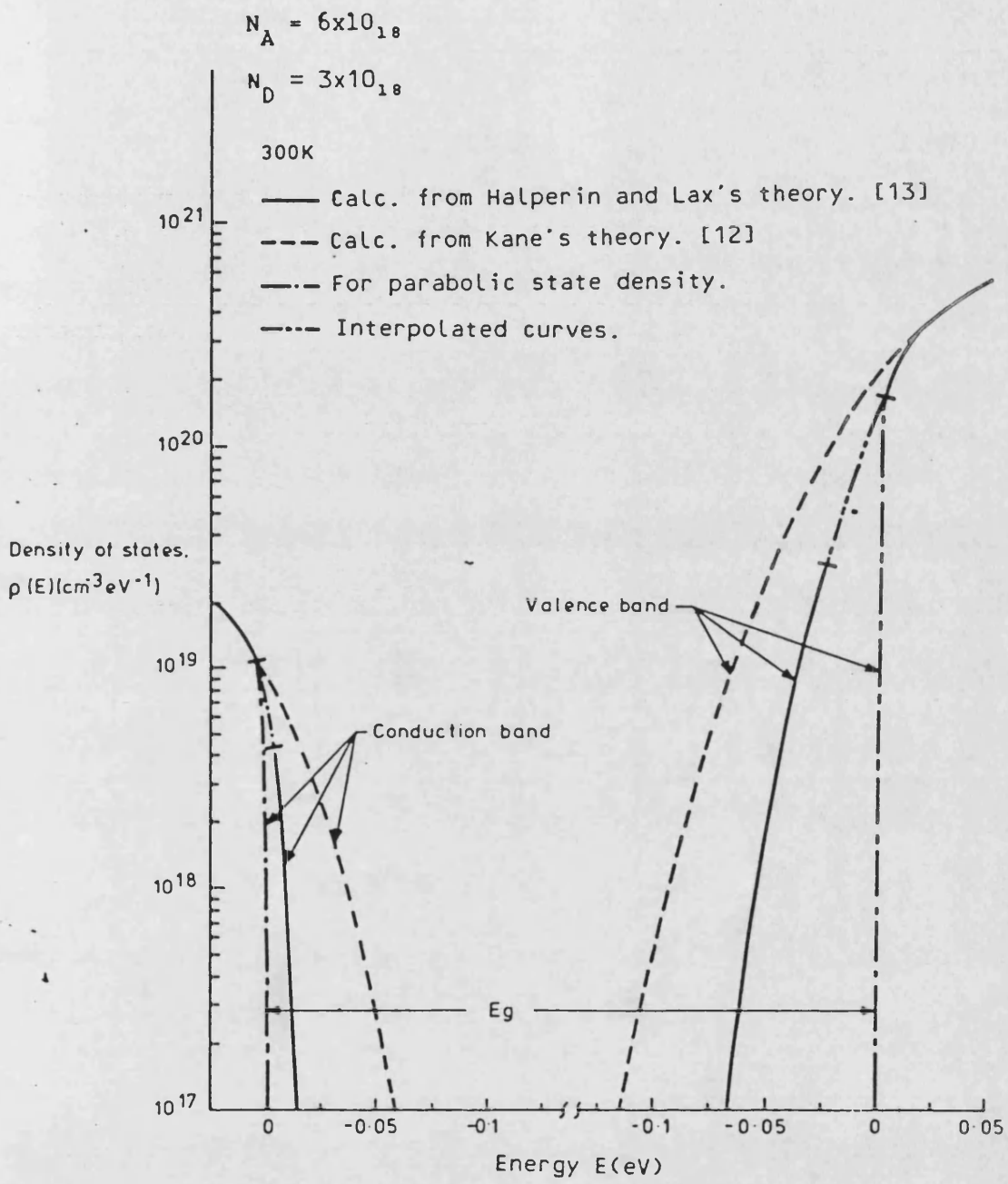

Figure 3.3-1 Comparison of density of states in the band tails of GaAs obtained from different models at 300K for Na = $6x10^{18}/cm^3$ and Nd = $3x10^{18}/cm^3$. The injection level for the calculation is approximately equal to the threshold level at 300K for a typical laser with a total loss of 100/cm. [14]

no k-selection rule. Since momentum should be conserved for states away from the tails further into the bands, the transition probability, B_{21}, would be a function of position. However it is usual to assume that B_{21} is a constant since this simplifies the analysis. This simplification is considered reasonable on the grounds that the characteristics are not particularly sensitive on B_{21}. Also the magnitude of other errors due to the uncertainty of the calculation for B_{21} are comparable with any variation of B_{21}. However, it should be remembered that the transition probability is a function of position (E,k) and photon energy hν.

Using a known transition probability and densities of states it is possible to calculate the rates of spontaneous emission and gain.

For a no k-selection rule we have:

$$r_{sp}(h\nu) = \int_0^\infty Z(h\nu).B_{21}.\rho_c(E).\rho_v(E - h\nu).f_2(E).[1 - f_1(E - h\nu)]\, dE \qquad (3.5\text{-}1)$$

and;

$$g(h\nu) = \frac{1}{v} \int_0^\infty B_{21}.\, \rho_c(E).\rho_v(E - h\nu).[f_2(E) - f_1(E - h\nu)]\, dE \qquad (3.5\text{-}2)$$

The units of $r_{sp}(h\nu)$ are; number of photons per unit volume, per unit time, per unit energy interval, and the units of gain are per unit length.

For the evaluation of equation 3.5-1 and 3.5-2 the electron and hole quasi-Fermi levels F_1 and F_2 are required. These can be evaluated by solving the integral equations:

$$n = \int_0^\infty \rho_c(E).f_2(E)\, dE \qquad (3.5\text{-}3)$$

and

$$p = \int_0^{\infty} \rho_v(E).f_1(E)\, dE \qquad (3.5\text{-}4)$$

where;

$$n + Na = p + Nd \qquad (3.5\text{-}5)$$

to maintain electrical neutrality where Na and Nd are the acceptor and donor doping densities. The values of F_1 and F_2 must then be placed in equations 3.5-1 and 3.5-2 to obtain values of gain and spontaneous emission for the given population inversion.

It is possible to calculate the total spontaneous emission rate:

$$Rsp = \int_0^{\infty} rsp(E)\, dE \qquad (3.5\text{-}6)$$

This would then give the total radiative recombination rate in the absence of any incident photon, which would give rise to absorption or stimulated emission. It can be shown, with some approximation:

$$Rsp = Z(Eg) \cdot B_{21} \cdot (n + n_0) \cdot (p + p_0) \qquad (3.5\text{-}7)$$

$Z(Eg) \cdot B_{21}$ is the bimolecular recombination rate usually denoted by the symbol B_r. n_0 and p_0 are the electron and hole populations for thermal equilibrium. In thermal equilibrium the product of n_0 and p_0 are sufficiently small such it is reasonable to be ignored. Stern [15] uses a net spontaneous emission rate where

$$R_{sp} = R_0 + R_{net} \qquad (3.5\text{-}8)$$

where $$R_0 = B_r.n_0.p_0 \qquad (3.5\text{-}9)$$

and $$R_{net} = B_r.[n.p + n.p_0 + n_0.p] \qquad (3.5\text{-}10)$$

A further simplification can be made if:

$$p_0 >> n_0 \qquad (3.5\text{-}11)$$

Rnet now becomes:

$$R_{net} = B_r.n.(p + p_0) \qquad (3.5\text{-}12)$$

For high rates of injection the injected electron concentration will equal the injected hole concentration where;

$$p = n \qquad (3.5\text{-}13)$$

Hence;

$$R_{net} = B_r.n.(n + p_0) \qquad (3.5\text{-}14)$$

This expression is used in later chapters. It shows that carrier lifetime, without optical interaction, at normal injection rates is dependent on the inversion population namely:

$$\tau_s = \frac{1}{B_r.(n + p_0)} \qquad (3.5\text{-}15)$$

The calculated value of B_r has a wide variation of values depending on the method used. Stern [16] has shown that the bimolecular recombination rate has a small dependence on the population inversion. From experimental data it appears that a value in the vicinity of 10^{-10} cm^{-3}/S is appropriate. [18]

3.6 Result from a hydrogenic model of doped GaAs.

The results from a hydrogenic model [17] are shown graphically in figures 3.6-1 and 3.6-2 of the wavelength dependency of gain and spontaneous emission. These results are used, in chapters five and six, for models which incorporate the wavelength dependence of gain and spontaneous emission.

3.7 Free carrier absorption and scattering losses.

Free carrier absorption results from a direct interaction between light and the carrier concentration. The absorption is directly proportional to the concentration of holes and electrons and to the square of the wavelength.

An expression used for free carrier absorption is;

$$f_{cc}.(2n + p_0) \qquad (3.7\text{-}1)$$

where f_{cc} is the free carrier absorption coefficient, n the carrier density and p_0 the doping density.

Optical scattering occurs as a result of an imperfect waveguide structure of the laser where irregularities allow a certain amount of light to escape the waveguide.

3.8 The buried heterojunction bistable laser.

The buried heterostructure (B-H) laser is introduced in this chapter and it shown to be suitable for absorptive bistability. This type of device, shown in figure 3-1, has been used successfully for bistable operation by Harder, Lau and Yariv [19, 20]. First of all, the double heterojunction laser is shown to be much superior to that of the homojunction laser.

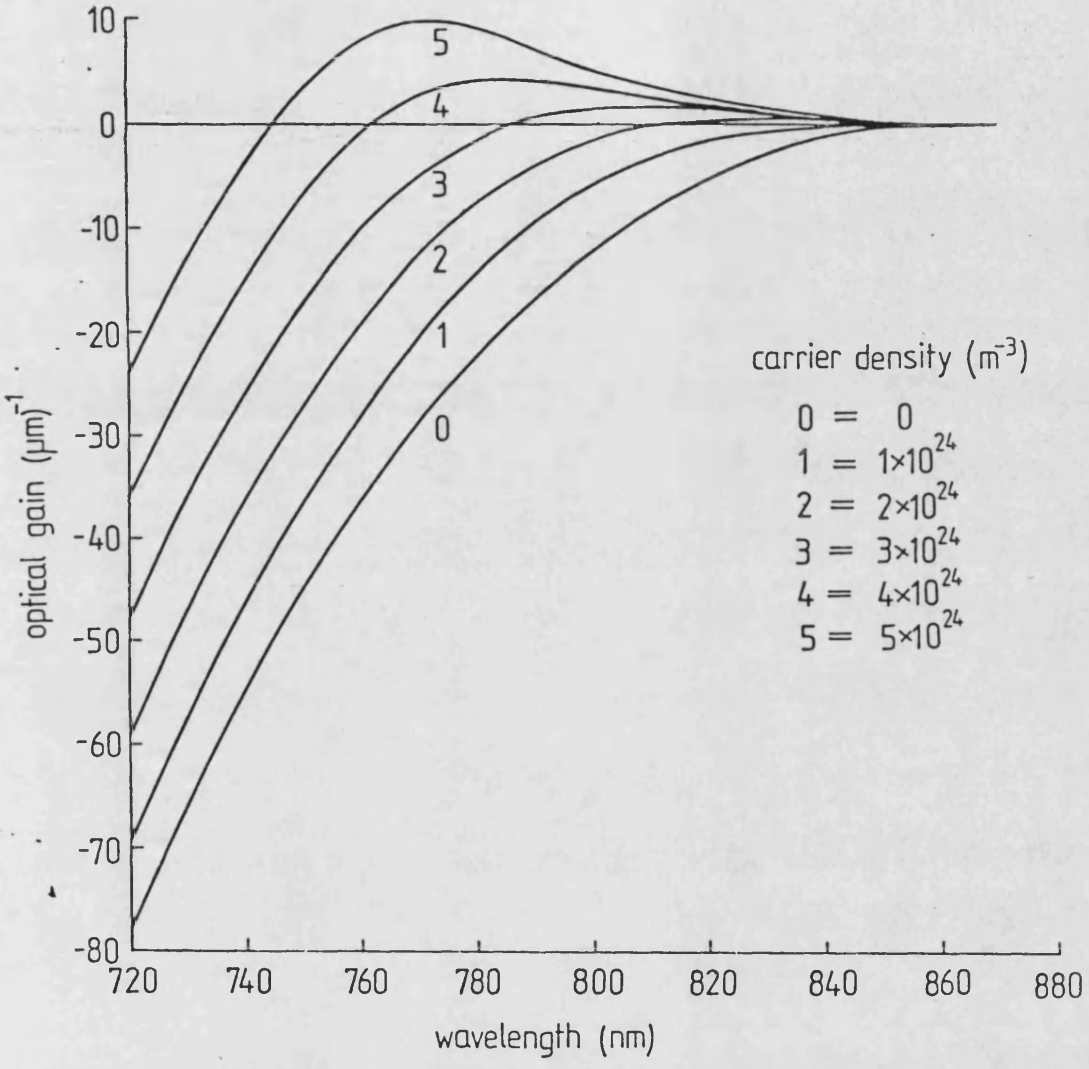

Figure 3.6-1 Graph of the wavelength dependency of gain [17].

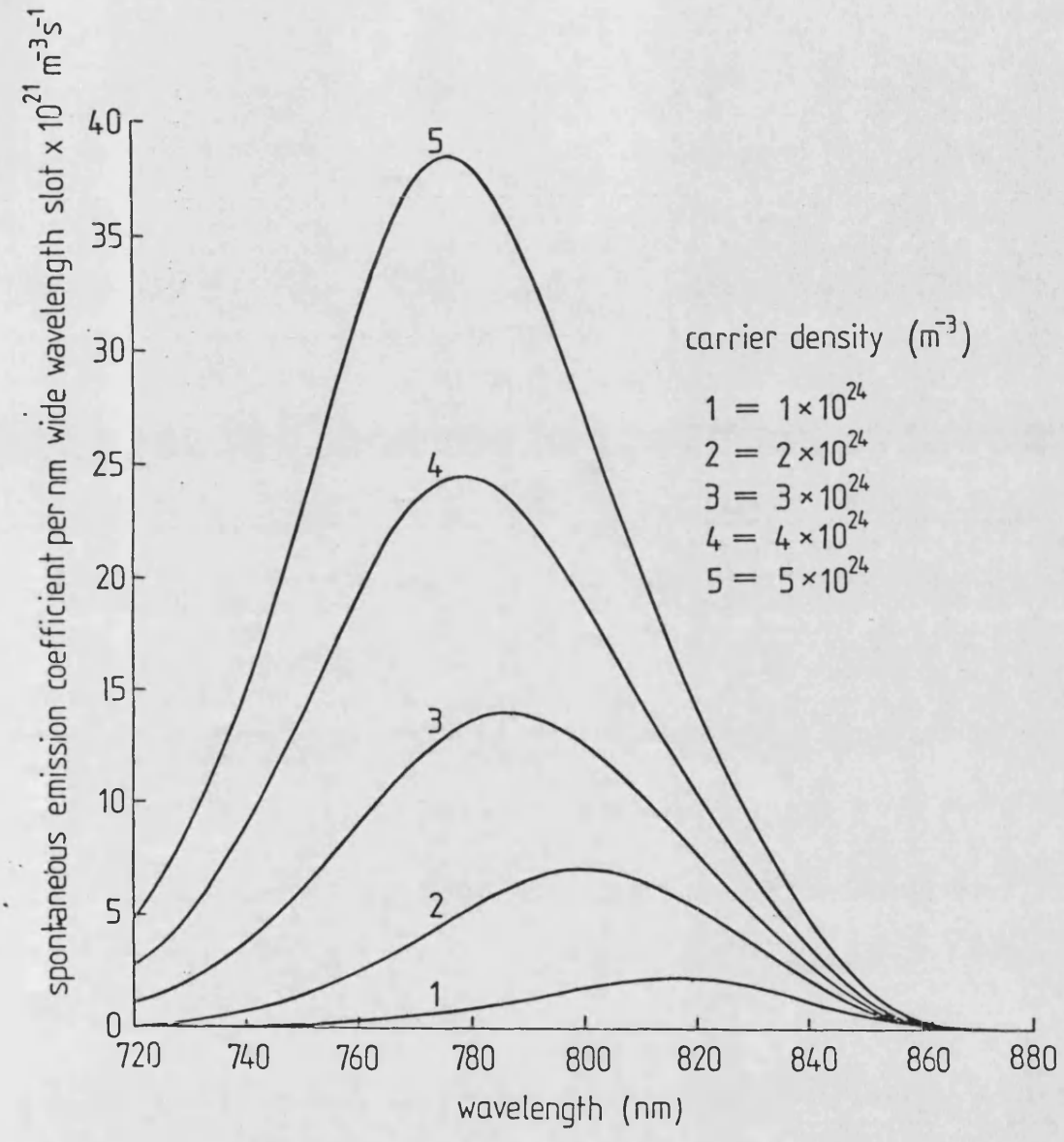

Figure 3.6-2 Graph of the wavelength dependency of spontaneous emission [17].

3.8.1 Heterojunction vs homojunction laser.

The construction of a homojunction laser is illustrated in figure 3.8.1-1. When the junction is forward biased, electrons and holes are injected into the active region. The band energy diagram showing details of the junction is shown in figure 3.8.1-2c. The position and thickness of this active region depends on the doping densities of the n and p GaAs, the corresponding diffusion lengths of holes and electrons and to some extent the current density owing to electric field and hot carrier effects. In total the active region may be a few microns wide so that a large current must be passed through the junction to create a population inversion in the whole of the active region.

The change in refractive index either side of the active layer is very small, also shown in figure 3.8.1-2c, and this produces a low confinement factor as illustrated. The concept of confinement factor has been introduced in section Chapter two. The poor confinement factor has two consequences. Firstly, only the proportion of optical power confined to the active region will undergo any amplification. Secondly, since the material either side of the junction will be heavily absorbing, the proportion of light not confined to the active region will be strongly attenuated. Thus the gain in the active region must be sufficient to overcome these effects in order to achieve lasing. As a result the homojunction laser had a very high threshold current density for lasing at room temperature such that is was common to cool the laser to liquid nitrogen temperatures (77K) or lower.

The double heterostructure laser is a great improvement on the homojunction laser. The construction of this type of laser is shown

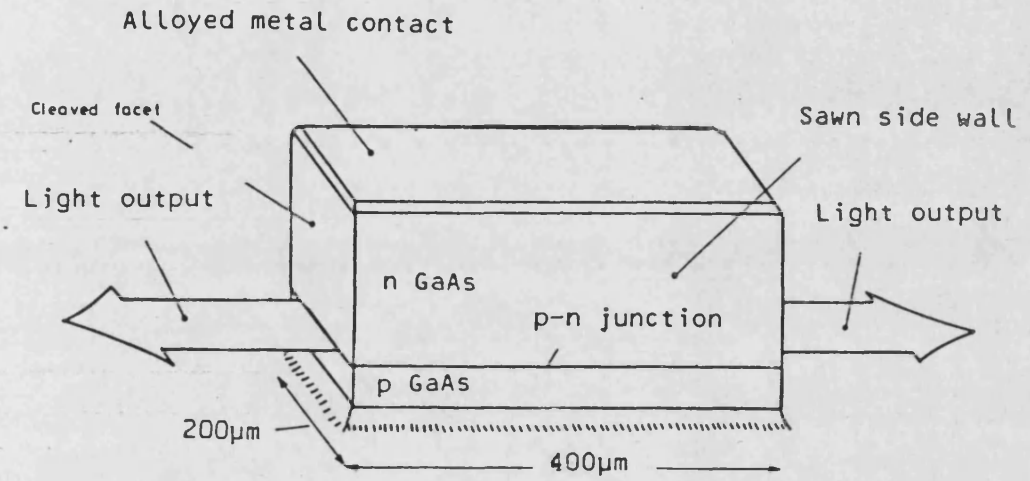

Figure 3.8.1-1 Schematic construction of a homostructure semiconductor laser.

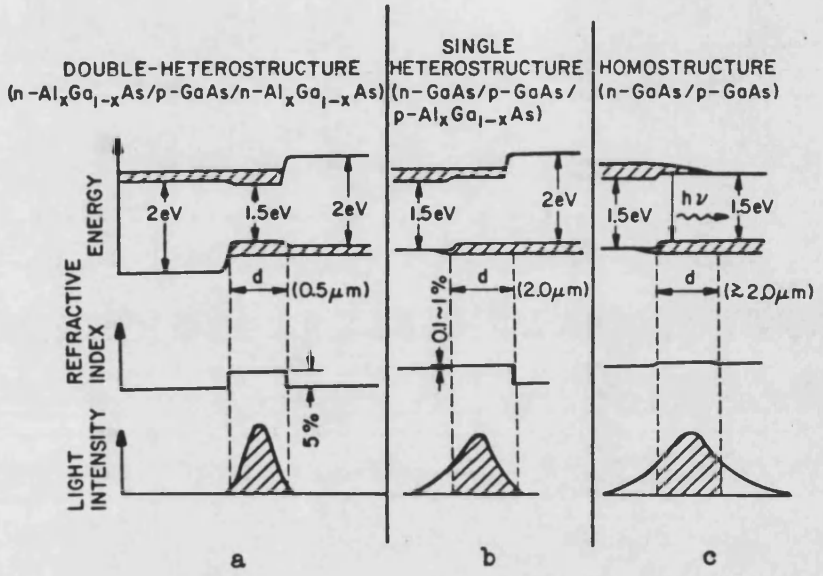

Figure 3.8.1-2 Comparison of some characteristics of (a) double heterostructure, (b) single heterostructure, and (c) homostructure lasers. The top row shows energy band diagrams under forward bias. The refractive index change for GaAs/GaAlAs is about 5%. The change across a homostructure is less than 1%. The confinement of light is shown in the bottom row. [3]

in figure 3.8.1-3 where, for the example shown, the stripe is defined by proton bombarded of the adjacent regions to form a highly resistive material [21]. One of the uses of a narrow stripe is to reduce the injection current to maintain the current density required for lasing. A feature of the double heterostructure is the thin GaAs active layer surrounded by n type and p type GaAlAs and is illustrated in figure 3.8.1-2a. This has two significant aspects. First the potential barrier at the material interfaces provide carrier confinement to the width of the active region. This is illustrated in figure 3.8.1-2a where the active region may be made much thinner than that of the homojunction laser. The current density (J) for the same optical gain is approximately reduced in the ratio of thicknesses of active regions. The carrier injection rate per unit volume is;

$$\frac{J}{e.d} \qquad (3.8.1\text{-}1)$$

where e is the electronic charge and d is the thickness of active layer.

The second aspect is the improved confinement of optical power to the active layer by the greater differences of refractive indices of GaAs and GaAlAs to produce efficient (refractive) index guiding. See figure 3.8.1-4 for details of the dependency of refractive index on aluminium content. Much more of the optical power is amplified in the active region than in the homojunction laser. Also any optical power in the GaAlAs layers is attenuated to a much lesser extent since the band-gap of GaAlAs is larger and will only absorb light of a higher energy than that emitted from GaAs. The combined effects of these improvements allow the double heterostructure laser to operate C.W. (continuously) at room temperature using a moderate injection

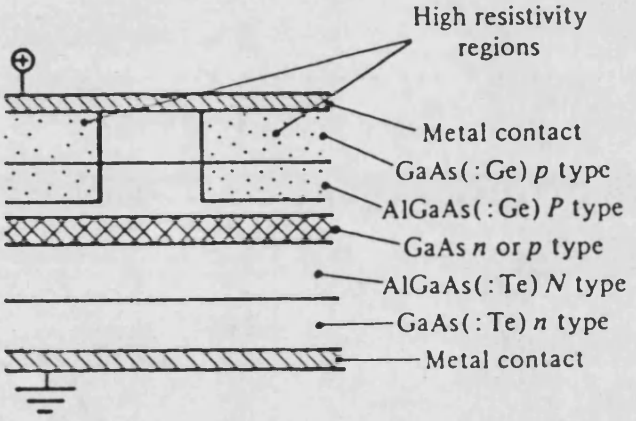

Figure 3.8.1-3 Cross sectional view of a stripe geometry heterojunction laser showing the layer composition.

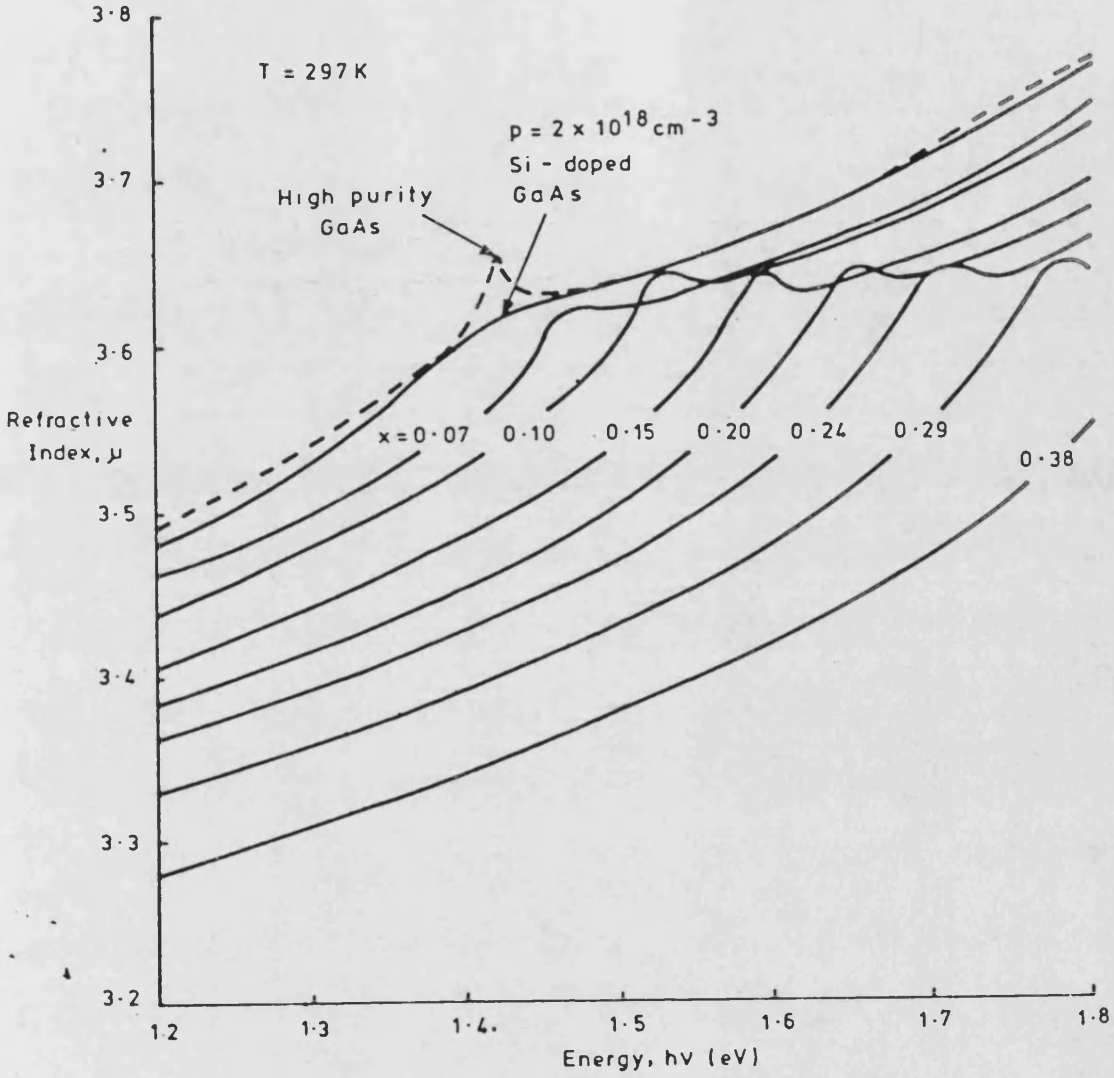

Figure 3.8.1-4 Refractive index of GaAlAs as a function of photon energy with composition as a parameter. [22]

current of a few tens of milliamperes for most narrow stripe heterojunction lasers.

The single heterostructure is illustrated in figure 3.8.1-2b which is an intermediary step between the homojunction and double heterojunction lasers. Figure 3.8.1-5 shows the difference of threshold currents versus temperature for these the three types of laser structures mentioned.

3.8.2 The bistable heterostructure laser.

The laser illustrated in figure 3.8.2-1 with the pumped segment cross-section similar to the view in figure 3.8.1-3 is not suitable for bistable operation.

Within the pumped segment of this device light is produced, from spontaneous emission, and amplified by optical gain. The light is confined in close proximity to the stripe by the gain guiding mechanism outlined earlier in the previous chapter. When the light emerges from the pumped segment, into the passive segment, there is no mechanism to guide the light. There are two reasons; firstly the light, emitted into the passive region, will be absorbed creating hole-electron pairs which will depress the real part of the refractive index [24]. Secondly these carriers will reduce the optical loss, where the passive region is partially optically pumped. Both of these mechanisms cannot support a stable mode such that the power will disperse into the passive region. Furthermore, the curved phase-fronts of the light from the pumped segment, corresponding to a gain-guided mode, serve to disperse the light further. At this point it is not thought significant which of the mechanisms is dominant to produce the dispersion of light which is seen to appear in superluminescing diodes (SLED's). The overall effect is illustrated

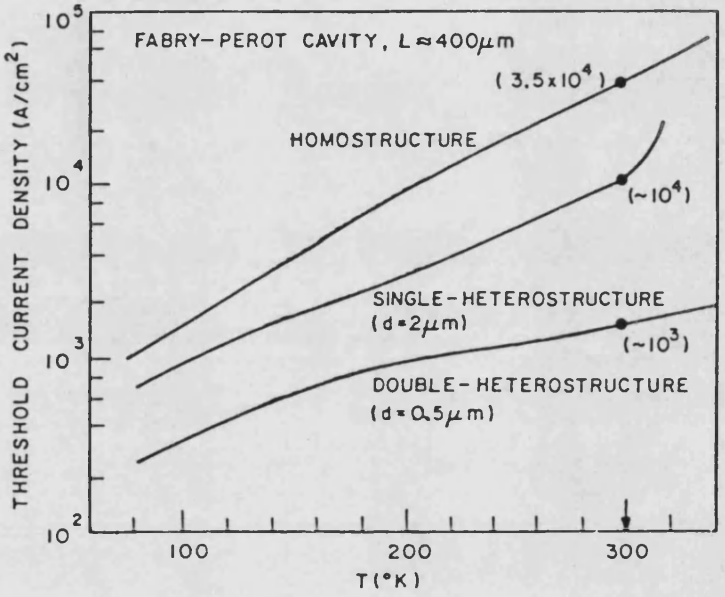

Figure 3.8.1-5 Threshold current density (A/cm^2) versus temperature for three laser structures. [23]

in figure 3.8.2-1 where very little power is reflected back under the stripe. This explanation would appear to explain why Carney and Fonstrad only saw limited hysteresis in their multiply segmented laser which had no lateral index guiding mechanism present.

Figure 3.8.2-2 illustrates a device which is particularly suited to bistable operation. This device, called a buried heterostructure laser, has lateral index guiding where the active layer is a rectangular dielectric waveguide, continuous along the device. This index guiding would be dominant to the antiguiding effects which have just been mentioned. The overall result that light is confined to the buried active layer where it would be absorbed or undergo gain, there being no other major resonator loss apart form loss at the facets.

3.9 Conclusions.

This chapter contains an overview of the mechanisms involved in the absorption and emission processes, and includes an overview of the calculation of gain and spontaneous emission. Much detail has been omitted and for further information the reader is invited to see the literature and text books, referenced in this chapter. However the purpose of this chapter has been to illustrate an approach to calculate the gain and spontaneous emission characteristics which will be necessary in later chapters.

This chapter also introduces the reasons behind the use of index guided structures for bistable lasers. Without index guiding the efficiency of such devices is likely to be impaired so that the magnitude of hysteresis is severely reduced. Also the angle of divergence of light emitted from the active region into the passive region is rather difficult to anticipate with any degree of accuracy.

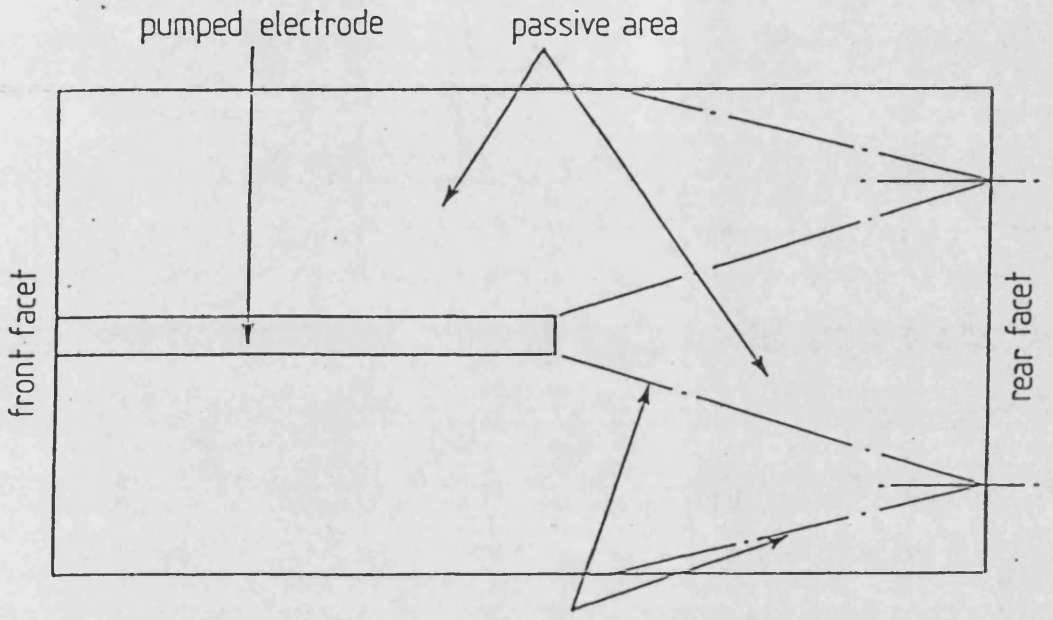

Figure 3.8.2-1 Sketch showing the dispersion of optical power for a device with no lateral index guiding.

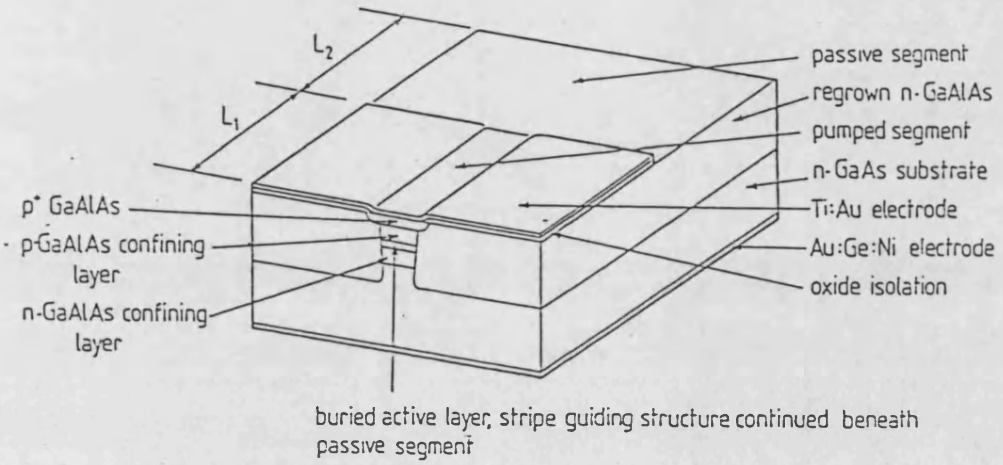

Figure 3.8.2-2 Diagram of bistable buried heterojunction laser.

References.

1) A. Einstein. Phys. Z.; Vol. 18; 1917; p 121.

2) M. G. A. Bernard and G. Duraffong; Phys. Stat. Solidi.; Vol 1; 1961; p 699.

3) S. M. Sze. "Physics of Semiconductor Devices"; Wiley (Interscience); 1969.

4) D. Long. "Energy Bands in semiconductors"; Wiley (Interscience); New york; 1968.

5) W. A. Harrison. "Solid State Theory"; McGraw-Hill; New York; 1970.

6) R. L. White. "Basic Quantum Mechanics"; McGraw-Hill; New York; 1966.

7) J. M. Cassels. "Basic Quantum Mechanics"; McGraw-Hill; New York; 1970.

8) H. G. Unger. "Introduction to Quantum Electronics"; Pergamon Press; 1970.

9) R. Loudon. "The Quantum Theory of Light"; Clarendon Press; 1983.

10) H. C. Casey and M. B. Panish. "Heterostructure Lasers; Part a: Fundamental principles"; Academic Press; 1978.

11) F. Stern. "Effect of Band Tails on Stimulated Emission of Light in Semiconductors"; Physical Review; Vol. 148; No. 1; August 1966; p186-94.

12) E. O. Kane. "Thomas-Fermi Approach to Impure Semiconductor Band Structure"; Physical Review; Vol. 131; No. 1; July 1963; p79-88.

13) B. I. Halperin and M. Lax. "Impurity-Band Tails in the High Density Limit. I. Minimum Counting Methods"; Physical Review; Vol. 148; No. 2; August 1966; p722-40.

14) C. J. Hwang. "Properties of Spontaneous and Stimulated Emission in GaAs Junction Lasers"; Physical Review B; Vol. 2; No. 10; November 1970; p4117-34.

15) G. Lasher and F. Stern. "Spontaneous and Stimulated Radiation in Semiconductors"; Physical Review; Vol. 133; No. 2A; January 1964; p A553-63.

16) F. Stern. "Calculated spectral dependence of gain in excited GaAs"; Physical Review; Vol. 47; No. 12; December 1976; p 5382-6.

17) W. Liddel. Private Communication.

18) H. Kressel and J. K. Butler. "Semiconductor Lasers and Heterojunction LESs"; Academic Press; 1977.

19) Ch. Harder, K. Y. Lau and A. Yariv. "Bistability and pulsations in C.W. Semiconductors with a controlled amount of saturable absorption"; Applied Physics Letters; Vol. 39; No. 5; September 1981; p 382-4.

20) K. Y. lau, Ch. Harder and A Yariv. "Dynamical Switching of a Bistable Laser"; Applied Physics Letters; Vol. 40; No. 3; February 1982; p198-200.

21) D. V. Morgan, F. H. Eisen and A. Ezis. "Prospects for ion bombardment and ion implantation in GaAs and InP device fabrication"; I.E.E. Proc.; Vol. 128; pt. I; No. 4; 1981; p 109-30.

22) H. C. Casey, D. D. Sell and M. B. Panish. "Composition Dependence of the GaAlAs between 1.2 and 1.8 eV"; Applied Physics Letters; Vol. 24; No. 2; 1974; p 63-5.

23) M. B. Panish, I. Hayashi and S. Sumshi. "Double-Heterostructure Injection Lasers with Room-Temperature Thresholds as low as 2300 A/cm^2 Applied Physics Letters; Vol. 16; No. 8; 1970; p 326-7.

24) G. H. B. Thompson. "Physics of Semiconductor Lasers"; John Wiley and Sons; 1980.

Chapter 4.

The rate equations and the validity of some assumptions often used in the analysis of absorptive bistability.

4 Introduction.

This chapter introduces the fundamental rate (or conservation) equations used for analysing the behaviour of laser and bistable laser devices. Various workers have made assumptions for laser structures governing the spatial distribution of photon flux and carrier density to form a set of much simplified rate equations. For laser devices which contain passive segments, Basov [1], Paoli [2], Renner and Carrol [3], Harder, Lau and Yariv [4], Kawaguchi [5, 6] and Kuznetsov [7] have used an adapted set of simplified rate equations. However, in this chapter it is shown that the inclusion of a passive segment introduces gross errors in the static light vs current (I-L) characteristics to an extent where the assumptions can no longer be considered valid. The type of device upon which the following analysis is based is shown in figure 4-1. This shows the simplest bistable laser structure having two segments, one pumped and the other passive. Also shown are the magnitudes of the forward (P) and backward (Q) travelling photon fluxes. A more appropriate model described in this chapter features the inclusion of a representative spatial variation of photon flux along the length of the device. This model has much further capabilities regarding its application to more complex multi-segment laser structures such as the types used by Kawaguchi [8, 9] or Harder, Lau and Yariv [10, 11]. Also, using the same model, it is possible to divide each segment into a number of sections to obtain an accurate profile of the spatial variation of photon densities and carrier density. This capability is used to determine the error in assuming a uniform carrier density along the length of a segment and the results shown in this chapter suggest that this is a good assumption.

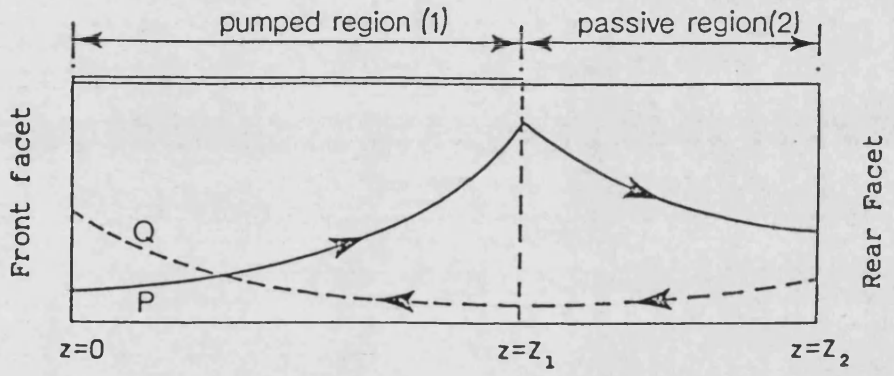

Figure 4-1 Illustration of an inhomogeneously pumped laser showing the variation of flux along the length of the device.

4.1 The photon and carrier conservation equations.

A ray approach is the usual starting point for the analysis of laser devices, where the variation of photon flux in the x and y direction is neglected. This assumption is made on the grounds that the shape of the lateral and transverse fields may be found from the type of analysis of waveguide structures already outlined in chapter two to give the optical confinement factor. This would be constant for a particular guide geometry. Also the dimensions of the active region are small enough such that the diffusion of carriers maintain a near uniform carrier density (inversion population), and hence gain, in the lateral and transverse directions across the guide structure. At any point in a laser device three conservation equations must be consistent with each other, namely the photon conservation equations for P and Q and a carrier conservation equation. The photon conservation equation [12, 13, 14] for the forward travelling flux (in the positive z-direction) of wavelength λ is;

$$\frac{1}{v}\frac{\partial P(z,t,\lambda)}{\partial t} + \frac{\partial P(z,t,\lambda)}{\partial z} = G(n(z,t),\lambda).P(z,t,\lambda) + \delta.S(n(z,t),\lambda) \qquad (4.1\text{-}1)$$

Where;

$$G(n(z,t),\lambda) = \Gamma.[\, g(n(z,t),\lambda) - f_{cc}.(2.n(z,t) + p_0) \,] \qquad (4.1\text{-}2)$$

Similarly the photon conservation equation for photon flux travelling in the reverse direction is;

$$\frac{1}{v}\frac{\partial Q(z,t,\lambda)}{\partial t} - \frac{\partial Q(z,t,\lambda)}{\partial z} = G(n(z,t),\lambda).Q(z,t,\lambda) + \delta.S(n(z,t),\lambda) \qquad (4.1\text{-}3)$$

And the carrier conservation equation;

$$\frac{dn(z,t)}{dt} = \frac{J(z,t)}{e.d} - \int_0^{\infty} \Gamma.g(n(z,t),\lambda).(P(z,t,\lambda) + Q(z,t,\lambda)).d\lambda$$

$$- B_r.n(z,t).(n(z,t) + p_0) \qquad (4.1\text{-}4)$$

The above carrier conservation equation does not have a non-radiative recombination term but this could easily be included. The effect of carrier diffusion is also neglected to simplify the analysis. While it is assumed that the diffusion of carriers maintain a uniform carrier density in the lateral and transverse directions, this is only so because the dimensions of the active region, in these directions, is small when compared to the diffusion length. However, the variation of the carrier density longitudinally (z-direction) would change sufficiently slowly along the majority of the length of the device so that the effect of diffusion in this direction may be ignored. There will be some diffusion of carriers between adjacent segments with different levels of current injection but this is again complicated by current spreading and other related effects such as the forward diode-voltage drop across the active region. In this study, since diffusion and other effects severely complicate the modelling, these effects will be ignored. It is prudent to add that, on the whole, authors of analyses of absorptive bistability in semiconductor lasers do not mention diffusion or current spreading. At this point it should be noted that;

$$B_r.n(z,t).(n(z,t) + p_0) = \int_0^{\infty} S(n(z,t),\lambda.)d\lambda \qquad (4.1\text{-}5)$$

ie. the total spontaneous emission rate over the whole spectral range must be consistent with the bimolecular recombination rate.

4.2 Simplified rate equations.

To enable the solution of equations 4.1-1, 4.1-3 and 4.1-4 to be within reasonable grasp they must be simplified. In most dynamic laser and bistable laser studies [1 - 7] the level of photon flux (S) is assumed uniform throughout the device. Secondly, within a segment of the device the carrier density is assumed uniform having values n_1 in the pumped segment and n_2 in the passive segment. Finally the authors assume that the gain and spontaneous emission are a simple function of carrier density. This approach represents a single wavelength model, in which wavelength is not a variable, for the device illustrated in figure 4-1. The photon conservation equation for this model is;

$$\frac{dS}{dt} = [(1 - \gamma).G_1 + \gamma.G_2].S \qquad (4.2\text{-}1)$$

$$+ \delta.B_r.[(1 - \gamma).n_1.(n_1 + p_0) + \gamma.n_2.(n_2 + p_0)] - \frac{S}{\tau_p}$$

$$\text{where } \gamma = \frac{L_2}{L_1 + L_2} \qquad (4.2\text{-}2)$$

and L_1 and L_2 are the lengths of the pumped and passive segments respectively.

The carrier conservation equations for the pumped and passive segments respectively are;

$$\frac{dn_1}{dt} = \frac{J}{e.d} - g_1.S - B_r.n_1.(n_1 + p_0) \qquad (4.2\text{-}3)$$

and;

$$\frac{dn_2}{dt} = - g_2.S - B_r.n_2.(n_2 + p_0) \qquad (4.2\text{-}4)$$

The photon lifetime term τ_p represents the loss of photon flux from the cavity at the facets, and for an approximate value taken to be [15];

$$\tau_p = \frac{L_1 + L_2}{V_g . \ln(1/r)} \qquad (4.2\text{-}5)$$

In the analyses by the authors [1-7] this is assumed independent of the level of photon flux. Also, the effect of free carrier absorption is usually included in the photon lifetime term. However, in this work it is more applicable to include free carrier absorption in the net gain term (G) such that;

$$G = g - f_{cc} . (2.n + p_0) \qquad (4.2\text{-}6)$$

and using a linear function of gain;

$$g = a.n - b \qquad (4.2\text{-}7)$$

It is not uncommon to have a constant value of the free carrier absorption rate which is independent of carrier density. The choice made here is to consider photon lifetime purely in terms of loss at the facets, due to the reflectance (r), in order to facilitate direct comparison with other models. To simplify the analysis the optical confinement factor (Γ), mentioned in section 4.1, is eliminated from further equations and is included in the coefficients of equation 4.2-6 and 4.2-7 describing the gain (g). Equations 4.2-1 to 4.1-7 may be solved analytically to calculate the static I-L characteristics. It is more usual to use these equations to describe the dynamic behaviour of laser devices using some method of numerical integration.

4.3 Analysis of single wavelength model.

The intention of this section is to show that the assumption of a uniform photon density throughout a bistable device and assuming a constant photon lifetime, introduces gross errors in the steady state I-L characteristics. However, these assumptions are shown to be applicable to the analysis of lasers without any absorbing segments. In the next chapter the analysis is extended to include the effect of wavelength.

The wavelength independent rate equations applicable for this analysis may be written as;

$$\frac{1}{v}\cdot\frac{\partial P(z)}{\partial t} + \frac{\partial P(z)}{\partial z} = G(n).P(z) + \delta.B_r.n.(n + p_0) \qquad (4.3\text{-}1)$$

$$\frac{1}{v}\cdot\frac{\partial Q(z)}{\partial t} - \frac{\partial Q(z)}{\partial z} = G(n).Q(z) + \delta.B_r.n.(n + p_0) \qquad (4.3\text{-}2)$$

and;

$$\frac{dn}{dt} = \frac{J}{e.d} - \Gamma.g.(P + Q) - B_r.n.(n + p_0) \qquad (4.3\text{-}3)$$

To reduce 4.3-1 into a first order differential equation it is chosen that the carrier density, and hence gain, is assumed to be uniform in each segment. Secondly the variation of photon fluxes is averaged out over each segment. This is achieved by integrating the values of flux such that;

$$\bar{P}_1 = \frac{1}{L_1}\int_0^{Z_1} P(z).dz \qquad (4.3\text{-}4)$$

and

$$\bar{Q}_1 = \frac{1}{L_1} \int_0^{Z_1} Q(z).dz \qquad (4.3\text{-}5)$$

We obtain from 4.3-1;

$$\frac{1}{v}.\frac{d\bar{P}_1}{dt} = G_1.\bar{P}_1 + \delta.B_r.n_1.(n_1 + p_0) + \frac{[P(0) - P(Z_1)]}{L_1} \qquad (4.3\text{-}6)$$

and from 4.3-2;

$$\frac{1}{v}.\frac{d\bar{Q}_1}{dt} = G_1.\bar{Q}_1 + \delta.B_r.n_1.(n_1 + p_0) + \frac{[Q(Z_1) - Q(0)]}{L_1} \qquad (4.3\text{-}7)$$

Equations 4.3-6 and 4.3-7 are combined where;

$$S_1 = \bar{P}_1 + \bar{Q}_1 \qquad (4.3\text{-}8)$$

to obtain;

$$\frac{1}{v}.\frac{dS_1}{dt} = G_1.S_1 + 2.\delta.B_r.n_1.(n_1 + p_0) - \frac{[Q(0) - P(0) + P(Z_1) - Q(Z_1)]}{L_1} \qquad (4.3\text{-}9)$$

Equation 4.3-9 is modified by introducing photon lifetimes to obtain;

$$\frac{1}{v}.\frac{dS_1}{dt} = G_1.S_1 + 2.\delta.B_r.n_1.(n_1 + p_0) - \frac{S_1}{v.\tau_{p_1}} - \frac{S_1}{v.\tau_{p_2}} + \frac{\gamma.S_2}{(1 - \gamma).v.\tau_{p_3}} \qquad (4.3\text{-}10)$$

Where;

$$\frac{S_1.L_1}{v.\tau_{p_1}} = Q(0) - P(0) \qquad (4.3\text{-}11)$$

is the photon flux leaving the device at the front facet. It should be noted that Q(0) and P(0) are related by;

$$P(0) = r.Q(0) \qquad (4.3\text{-}12)$$

where, r, is the reflectivity of the facets.

The term;

$$\frac{S_1.L_1}{v.\tau_{p_2}} = P(Z_1) \qquad (4.3\text{-}13)$$

is the flux leaving the pumped segment (at $z = L_1$) to enter the passive segment and;

$$\frac{S_2.L_2}{v.\tau_{p_3}} = Q(L_1) \qquad (4.3\text{-}14)$$

is the flux entering the pumped segment from the passive segment.

The variation of carrier density along the length of the pumped segment has been assumed to be uniform and hence the carrier conservation equation for the pumped segment becomes;

$$\frac{dn_1}{dt} = \frac{J_1}{e.d} - g_1.S_1 - B_r.n_1.(n_1 + p_0) \qquad (4.3\text{-}15)$$

At this point it is prudent to add that the value of n_1 does not necessarily indicate a mean carrier density in the same way as S_1 is the mean photon density in the pumped segment.

Using the same technique for the passive segment we obtain a similar rate equation;

$$\frac{1}{v}.\frac{dS_2}{dt} = G_2.S_2 + 2.\delta.B_r.n_2.(n_2 + p_0) - \frac{S_2}{v.\tau_{p_4}} - \frac{S_2}{v.\tau_{p_3}} + \frac{(1-\gamma).S_1}{\gamma.v.\tau_{p_2}} \qquad (4.3\text{-}16)$$

Where;

$$S_2 = \frac{1}{L_2} \int_{L_1}^{L_2} (P(z) + Q(z))\, dz \qquad (4.3\text{-}17)$$

and;

$$\frac{S_2 . L_2}{v . \tau_{p_4}} = [P(Z_2) - Q(Z_2)] \qquad (4.3\text{-}18)$$

is the flux leaving the device at the rear facet at $z = Z_2$. It should be noted that;

$$Q(Z_2) = r . P(Z_2) \qquad (4.3\text{-}19)$$

It is possible to eliminate τ_{p_2} and τ_{p_3} using;

$$(1 - \gamma) . S_1 + \gamma . S_2 = S \qquad (4.3\text{-}20)$$

$$(1 - \gamma) . S_1 = (1 - \alpha) . S \qquad (4.3\text{-}21)$$

$$\gamma . S_2 = \alpha . S \qquad (4.3\text{-}22)$$

where S is the average flux in the device. We obtain;

$$\frac{1}{v} \cdot \frac{dS}{dt} = [(1 - \alpha) . G_1 + \alpha . G_2] . S$$

$$+ 2 . \delta . B_r . [(1 - \gamma) . n_1 . (n_1 + p_0) + \gamma . n_2 . (n_2 + p_0)]$$

$$- \frac{S}{v} \cdot \left[\frac{(1 - \alpha)}{\tau_{p_1}} + \frac{\alpha}{\tau_{p_4}} \right] \qquad (4.3\text{-}23)$$

The expression in the brackets of the last term of the above equation represents $1/\tau_p$, where τ_p is the overall photon lifetime. Equation 4.3-23 may be compared with equations 4.2-1 to 4.2-4 and

also with equations in refs [1-7] but where $S_1 = S_2 = S$ which leads to, from inspection of equations 4.3-20 to 4.3-22, $\alpha = \gamma$. The assumption in the analysis here, has been only to assume that carrier density is uniform in each segment.

In the next section the above model is compared with a more accurate model, in the steady-state, to find the magnitude of the variations of α/γ and photon lifetime in terms of light output. It is chosen to plot values against light output since these values would be monotonic (single valued) for any value of light output.

From equations 4.3-21 and 4.3-22;

$$\alpha/\gamma = \frac{S_2}{\gamma.S_2 + (1 - \gamma).S_1} \qquad (4.3\text{-}24)$$

From equations 4.3-11, 4.3-18 and 4.3-23;

$$\frac{1}{\tau_p} = \frac{(1 - \alpha).v.[Q(0) - P(0)]}{S_1.L_1} + \frac{\alpha.v.[P(Z_2) - Q(Z_2)]}{S_2.L_2} \qquad (4.3\text{-}25)$$

In the simplified models [1-7] of the bistable laser $\alpha/\gamma = 1$ and τ_p is a constant. This is a consequence of assuming a uniform photon density throughout the device. However when a more accurate model is used, which takes into account the spatial variation of photon density, then the actual forms of α/γ and τ_p are rather more complex. In section 4.4.2 results are shown graphically for α/γ and τ_p against light output for specific geometries of bistable lasers and of a laser with no passive segment. These results illustrate the errors in the assumptions in the model of section 4.2.

4.4 Steady-state model with variation of photon flux along length.

The time invariant photon conservation equation, for the forward travelling flux, may be written as;

$$\frac{dP(z)}{dz} = G.P(z) + \delta.B_r.n.(n + p_0) \qquad (4.4\text{-}1)$$

There is a similar equation for the photon flux travelling in the negative z-direction. An attempt to solve these equations may be to use some numerical integration method such as Eulers Method. This method was originally adopted but this was subsequently made obsolete by a more analytic approach to the problem illustrated below which significantly reduced the computational effort.

Using the same assumptions regarding carrier density as in the previous section 4.3, where the carrier density is assumed uniform throughout a segment, equation 4.4-1 becomes a first order ordinary differential equation which has the solution;

$$P(z) = P(Z_h).\exp[G.(z - Z_h)] + \frac{(\exp[G.(z - Z_h)] - 1)}{G}.\delta.B_r.n.(n + p_0) \qquad (4.4\text{-}2)$$

Where $P(Z_h)$ is a point where the photon flux (travelling in a forward, positive direction) is known. From this point the photon flux can be calculated within the segment. There is a similar equation for Q(z) within the segment;

$$Q(z) = Q(Z_i).\exp\{G.(Z_i - z)\} + \frac{(\exp[G.(Z_i - z)] - 1)}{G}.\delta.B_r.n.(n + p_0) \qquad (4.4\text{-}3)$$

These equations are only applicable within the segment. Outside the segment other equations associated with other segments apply. The

carrier conservation equation for this model is;

$$\frac{J}{e.d} = g.(\bar{P} + \bar{Q}) + B_r.n.(n + p_0) \qquad (4.4\text{-}4)$$

where;

$$\bar{P} = \frac{1}{L_1} \int_0^{Z_1} P(z).dz \qquad (4.4\text{-}5)$$

This integral can be evaluated analytically and can be shown to be;

$$\bar{P} = \frac{1}{G} . \left[\frac{P(Z_1) - P(0)}{L_1} - \delta.B_r.n_1.(n_1 + p_0) \right] \qquad (4.4\text{-}6)$$

The average photon density for the pumped segment (for z = 0 to Z_1) is used in the calculation.

A similar set of equations exist for the passive segment.

4.4.1 Modelling procedure.

The above equations, 4.4-2, 4.4-3 and 4.4-4 must be solved so that they are consistent with each other within a segment. Also the photon fluxes P(z) and Q(z) must be continuous across segment boundaries and satisfy other boundary conditions such as reflectivity where appropriate. To ensure this, an iterative method is used which converges onto the complete solution for the device. In this technique a value for the flux $P_m(z)$ in the positive z direction is solved consistently with n_m, using equations 4.4-2 and 4.4-4, using a previously calculated provisional value of the flux $Q_{m-1}(z)$, where the subscript, m, represents the mth iteration. An efficient quadratic interpolation routine (Muller) is used to solve $P_m(z)$ and n_m consistently to a desired accuracy. The error in the interpolation

of equation 4.4-4 is first normalised by n_m and the interpolation routine is stopped when the normalised error is less than 10^{-5}. This routine is carried out for each segment in turn, by ensuring the continuity of flux in the positive z direction. At the rear facet the boundary condition must be satisfied;

$$Q(Z_2) = r.P(Z_2) \qquad (4.4.1\text{-}1)$$

Also, the light output at the rear facet is;

$$(r - 1).P(Z_2) \qquad (4.4.1\text{-}2)$$

The solution technique proceeds by similarly solving for $Q_m(z)$ and n_m in the negative z-direction using the values of $P_m(z)$. The boundary condition at the front facet allows the value of $P_{m+1}(0)$ to be calculated from $Q_m(0).r$. The iterations are carried out back and forth along the device until the values of flux, at a point, (chosen to be the front facet) meet the following requirement;

$$\frac{Q_m(0) - Q_{m-1}(0)}{Q_m(0)} < 10^{-4} \qquad (4.4.1\text{-}3)$$

for four successive passes to prevent spurious convergence.

Although it is conventional to calculate the light output from the injected current, when the characteristics display hysteresis it is then necessary to calculate the I-L characteristics in two passes. The first pass is to draw the characteristics for increasing current, to some desired value above threshold, and to use this as a starting point from which the light output may be calculated as the current is reduced below threshold. Using this technique the model was able to show hysteresis in the I-L characteristic of the inhomogeneously pumped stripe laser. This is plotted in curve (a) of figure 4.4.1-1.

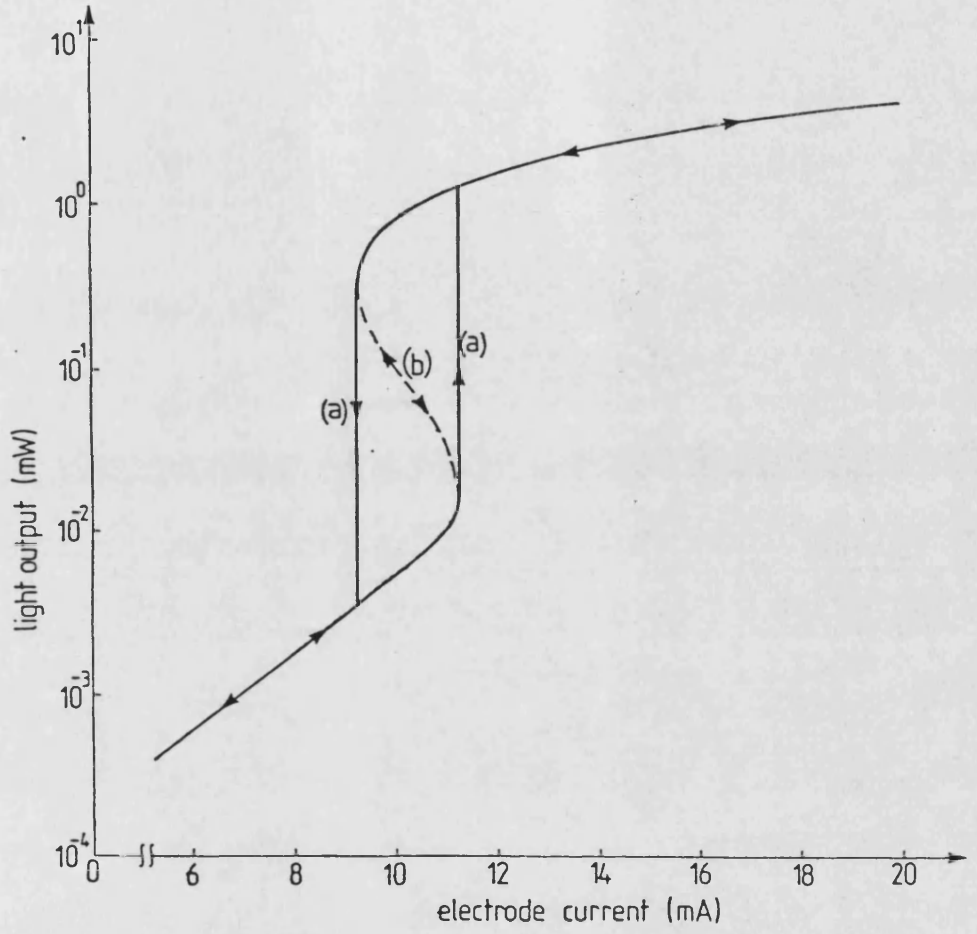

Figure 4.4.1-1 Comparing the results of current being the independent variable and light output being the independent variable.

However, it is more desirable to show hysteresis in a single pass of the injection current instead of two. The technique used here is to make the light output at the front facet the independent variable, from which a single value of current can be calculated. The principle is to force the light output reflected back into the device to be consistent with the desired output. The injected current density and hence the carrier density, gain and spontaneous emission, is made to vary until the light output is consistent with the desired light output.

If the desired light output is X_d, the value of $P_m(0)$ is;

$$P_m(0) = \frac{X_d.r}{(r - 1)} \qquad (4.4.1\text{-}4)$$

and for a particular value of X_d, $P_m(0)$ remains unchanged throughout the iterative process. If the the actual light output after the mth iteration is;

$$X_a = (r - 1).Q_m(0) \qquad (4.4.1\text{-}5)$$

then for X_a to converge to X_d the injection current is made a function of X_d/X_a. The injection current which would be used for the device in the next, m+1th iteration, would be calculated from the light output from the mth iteration.

$$I_{m+1} = I_m.\left[1 + A.\log\left(\frac{X_d}{X_a} \right) \right] \qquad (4.4.1\text{-}6)$$

The exact form of the function for the injection current for the active stripe is not too critical in this procedure, and the iterations are stopped when the condition below has been met for four successive passes;

$$\left| \frac{X_d - X_a}{X_d} \right| < 10^{-4} \qquad (4.4.1\text{-}7)$$

This prevents the condition being met spuriously. Using this technique, hysteresis becomes an "S" shaped curve where the turning points of the curve mark the extent of the hysteresis. By way of comparison curve (b) in figure 4.4.1-1 is a plot of the characteristics of the inhomogeneously pumped stripe laser recalculated using this technique.

A significant advantage of this technique is that if the current into the active segment is the independent variable, the model is on the point of instability before switching. Apart from taking considerable time for the model to settle at this point, the current at which switching occurs is somewhat influenced by the previously calculated point or initial starting conditions of P, Q and n in each segment. However when the light output is made the independent variable no such problem exists.

4.4.2 Results.

The model allows the lengths of the segments to be varied and also allows each segment to be subdivided into many sections without changing the technique. This subdivision of each segment will illustrate the error in assuming a uniform carrier density in each segment. Figure 4.4.2-1 shows the difference between one section per segment and fifty sections per segment for a bistable laser of length 300μm with equal length pumped and passive segments (γ = 1/2). For the case of the laser (γ = 0) the error is not graphically visible. It may be concluded, at this point, that the assumption of uniform

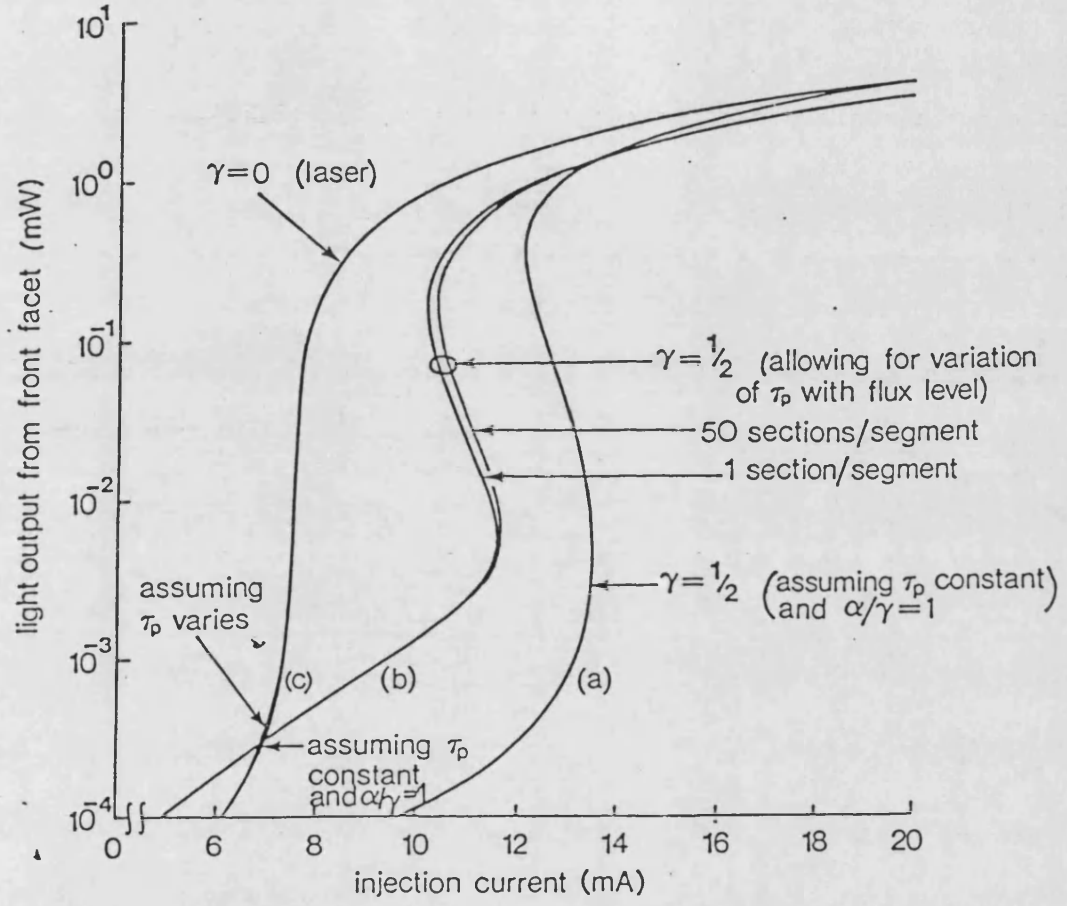

Figure 4.4.2-1 I-L characteristics of a SLED (γ = 1/2) for the case of (a) constant photon lifetime (b) τ_p varying with light output, and (c) laser. For case (b) the effect of using 50 sections per segment and 1 section per segment is shown. (Z_2 = 300μm.)

carrier density within a segment is seen to be entirely reasonable.

The errors in assuming a uniform photon density, along the length of the device, and in assuming a constant photon lifetime now receive attention. From the above model, for a particular value of light output, X_d, then P(z), Q(z), n_1 and n_2 can be solved by the above technique and these values can be used to evaluate α/γ and τ_p from equations 4.3-24 and 4.3-25. Figures 4.4.2-2 and 4.4.2-3 show the results of α/γ and τ_p in terms of light output. Figure 4.4.2-1 also includes the characteristics for a laser ($\gamma = 0$) and for a device where $\gamma = 1/2$ assuming constant photon lifetime and a uniform photon density. This is to illustrate the error of these assumptions when compared with characteristics representing a more accurate spatial solution.

These results clearly show that the assumptions of uniform photon density and of a constant photon lifetime are not reasonable, except for a laser device with no passive region. For this latter type of device the ratio of α/γ is obviously meaningless but the use of a constant photon lifetime is a good approximation, even below threshold. Thus the rate equations, 4.4.2-1 and 4.4.2-2, are often used for a laser;

$$\frac{dS}{dt} = G.S + 2.\delta.B_r.n.(n + p_0) - \frac{S}{\tau_p} \qquad (4.4.2\text{-}1)$$

$$\frac{dn}{dt} = \frac{J}{e.d} - g.S - B_r.n.(n + p_0) \qquad (4.4.2\text{-}2)$$

4.5 Laser characteristics.

Whilst this section is not directly applicable to the study of absorptive bistability, since we have justified the use of simplified rate equations when applied to a laser some analysis of laser

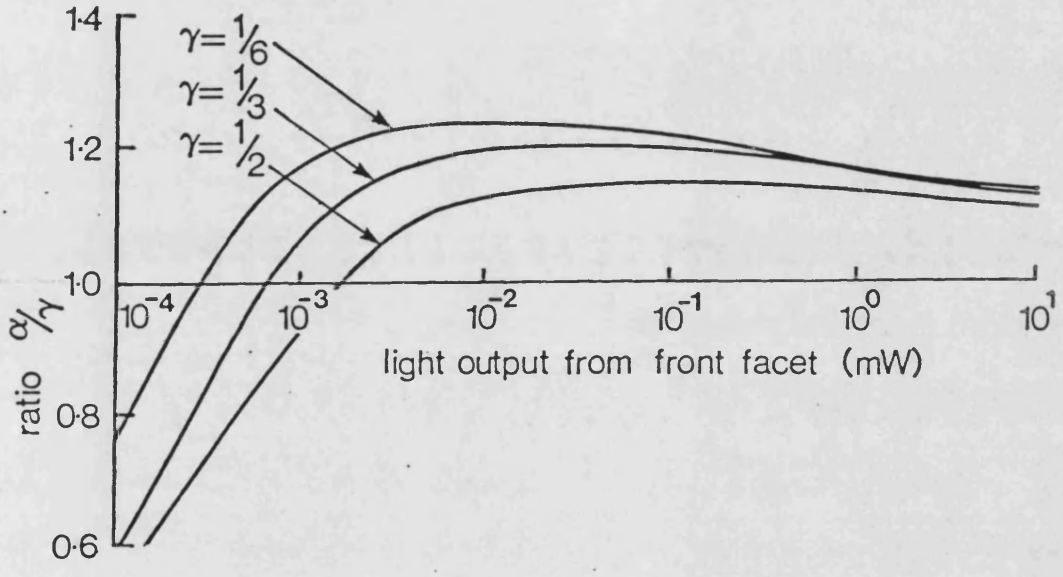

Figure 4.4.2-2 Effect of light output and geometry on the ratio α/γ for a SLED. (Z_2 = 300μm.)

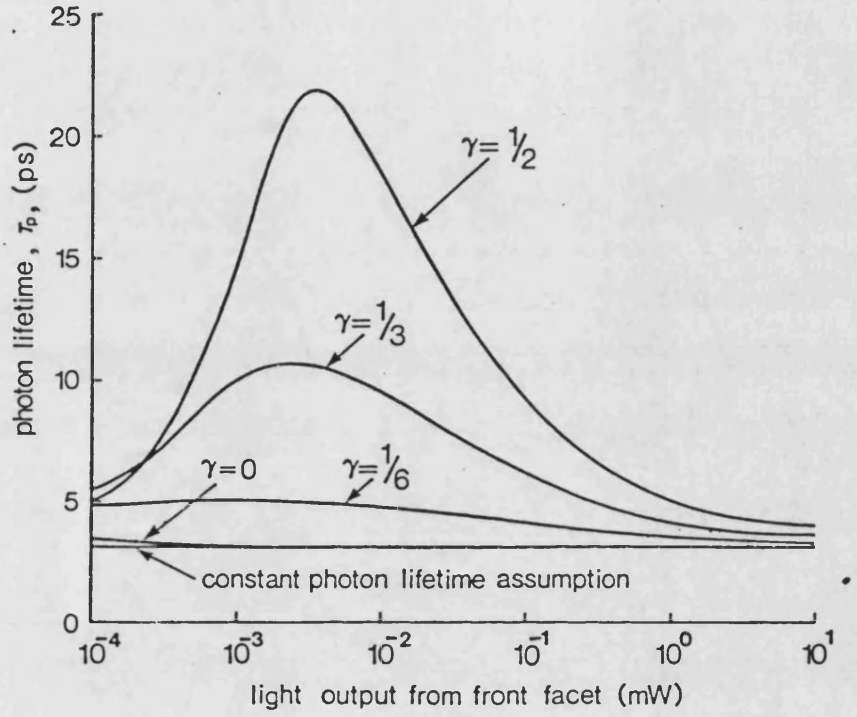

Figure 4.4.2-3 Effect of light output and geometry on the photon lifetime of a sled. (Z_2 = 300μm.)

characteristics is appropriate.

The threshold current density is usually defined where;

$$G_{th} = \frac{1}{\tau_p} \qquad (4.5\text{-}1)$$

"G_{th}" is the threshold net optical gain, in equation 4.4.2-1, which overcomes the losses at the facets. The carrier density "n_{th}" required to produce this gain is then placed in equation 4.4.2-2, but where the "g.S" term is omitted, to find the threshold current density "J_{th}". The definition of threshold current, illustrated in figure 4.5-1, may be considered rather arbitrary but marks the point below which spontaneous emission would dominate, and above which stimulated emission (lasing) would dominate. It should be added that "G_{th}" is never quite reached, except in transient conditions. Also as the level of injection is increased so the light output increases but the optical gain only approaches the value of "G_{th}". Equations 4.4.2-1 and 4.4.2-2 are often rewritten replacing the bimolecular recombination rate term with a much simpler term;

$$\frac{dS}{dt} = G.S + 2.\delta.\frac{n}{\tau_s} - \frac{S}{\tau_p} \qquad (4.5\text{-}1)$$

$$\frac{dn}{dt} = \frac{J}{e.d} - g.S - \frac{n}{\tau_s} \qquad (4.5\text{-}2)$$

where;

$$\tau_s = \frac{1}{B_r.(n_{th} + p_0)} \qquad (4.5\text{-}3)$$

These equations are valid from just below threshold and throughout lasing. This results from the carrier density, in this

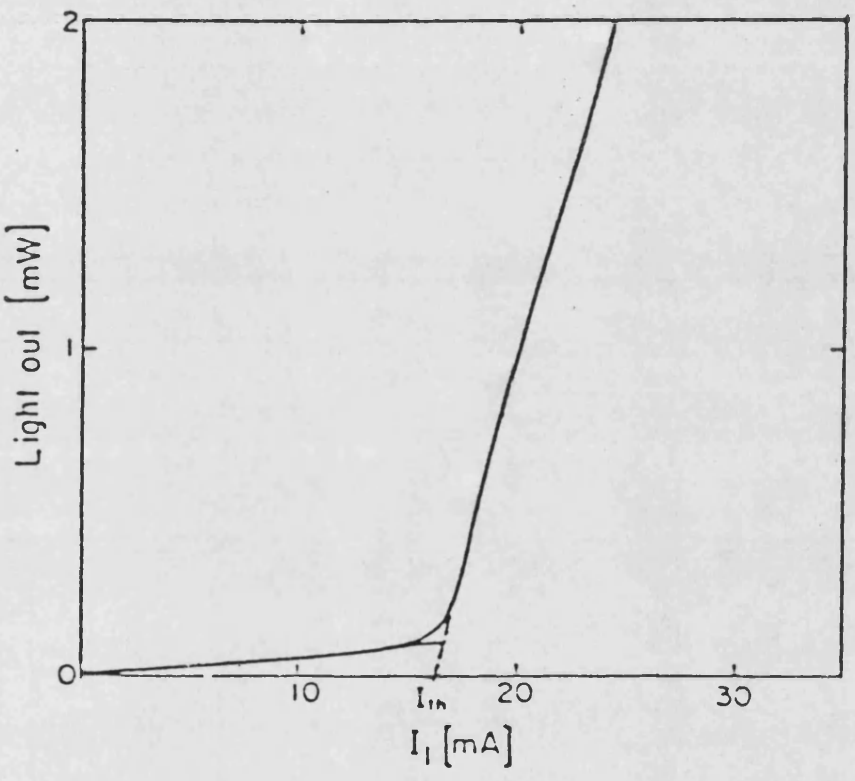

Figure 4.5-1 Light output vs current for a laser indicating threshold current.

range, remaining essentially constant.

The sensitivity of gain on photon density can be determined from a steady state version of equation 4.5-1 to obtain;

$$S = \frac{2.\delta.n}{\tau_s} \cdot \frac{1}{(G - 1/\tau_p)} \qquad (4.5\text{-}4)$$

where as gain tends to $1/\tau_p$ the spontaneous emission in the lasing mode becomes effectively magnified by;

$$\frac{1}{(G - 1/\tau_p)}$$

Hence it can be seen that above threshold the gain and hence carrier density are clamped to just below "G_{th}" and "n_{th}" respectively. Only during a transient may these values be exceeded and then usually only marginally. For further discussion on the steady-state characteristics see [15] and for transient and turn on effects in lasers see [16, 17].

4.6 Conclusions.

In this chapter it is shown that the simplified rate equations are only suitable for the analysis of laser devices without passive regions. When an adapted set of simplified rate equations are applied to a laser containing saturable absorption then gross errors are introduced to an extent where the assumptions can no longer be justified. However the results uphold the very useful assumption of a uniform carrier density within a segment.

References.

1) N. G. Basov; "O-1 Dynamics of injection lasers"; IEEE J. Quantum Electronics; Vol. QE-4; No. 11; 1968; p855-64.

2) T. L. Paoli. "Saturable absorption effects in the self-pulsing (AlGa)As junction laser"; Applied Physics Letters; Vol. 34; No. 10; 1979; p652-655.

3) D. Renner and J. E. Carrol. "Transients in injection lasers - phase-plane analysis and effects on absorbing sections"; Solid-State and Electron. Devices; Vol. 3; No. 6; 1979; p 224-32.

4) Ch. Harder, K. Y. Lau and A Yariv. "Bistability and Pulsations in Semiconductor Lasers with Inhomogeneous Current Injection"; IEEE Journal of Quantum Electronics; Vol. QE-18; No. 9; 1982; p 1351-61.

5) H. Kawaguchi. "Optical bistable-switching operation in semiconductor lasers with inhomogeneous excitation"; IEE Proc.; Vol. 129; No. 4; 1982; pl41-8.

6) H. Kawaguchi. "Optical bistability and chaos in a semiconductor laser with a saturable absorber"; Applied Physics Letters; Vol. 45; No. 12; 1984; p 1264-6.

7) M. Kuznetsov. "Theory of bistability in two-segment diode lasers"; Optics Letters; Vol. 10; No. 8; p 399-401.

8) H. Kawaguchi and G. Iwane. "Bistable operation in semiconductor lasers with inhomogeneous excitation"; Electronic Letters; Vol. 17; No. 4; 1981; p 167-8.

9) H. Kawaguchi. "Bistable operation of semiconductor lasers by optical injection"; Electronics Letters; Vol. 17; No. 20; 1981; p 741-2.

10) Ch. Harder, K. Y. Lau and A. Yariv. "Bistability and Pulsations in C.W. Semiconductor Lasers with a Controlled Amount of Saturable absorption"; Applied Physics Letters; Vol. 39; No. 5; 1981; p 382-4.

11) K. Y. Lau, Ch. Harder and A. Yariv. "Dynamical Switching of a Bistable Injection Laser"; Applied Physics Letters; Vol. 40; No. 3; 1982; p 198-200.

12) R. H. Pantell and H. E. Putoff. "Fundamentals of Quantum electronics"; John Wiley and Sons Inc.; New York; 1969.

13) S. Hasuo and T. Ohmi. "Spatial distribution of the light intensity in the injection laser"; Jap. J. Appl. Phys.; Vol. 13; No. 9; September 1974; p1429-34.

14) J. E. A. Whiteaway and G. H. B. Thompson. "Optimisation of power efficiency of (GaAl)As injection lasers operating at high power levels"; IEE J. Solid-state and Electron Devices; Vol. 1; No. 3; 1977; p81-8.

15) G. H. B. Thompson. "Physics of Semiconductor Laser Devices"; John Wiley and Sons, Ltd.; 1980.

16) H. Kressel and J. K. Butler. "Semiconductor lasers and heterojunction LEDs"; Academic Press; 1977.

17) M. J. Adams. "Rate equations and transient phenomena in semiconductor lasers"; Opto-electronics; Vol. 5; 1973; p201-15.

Chapter 5.

Multi-wavelength model of bistable laser.

5 Introduction.

The model outlined in this chapter embodies much of the analysis of the previous chapter, such as the spatial variation of photon density, but also includes the spectral dependence of gain and spontaneous emission. It is shown how the relative lengths of the pumped and passive segments of the simple inhomogeneously pumped bistable laser affects the threshold current and magnitude of hysteresis. It is seen that there is an optimum geometry in terms of the relative lengths of the two segments.

This chapter extends the simple bistable structure to a laser with two separate electrodes in tandem separated by a passive segment as shown in figure 5-1. The effect of a small current into, and out of, the second electrode of a split-stripe laser on the threshold current and hysteresis is shown.

The analysis is further extended to include the effect of external optical injection into an inhomogeneously pumped laser. In particular the light "input-output" characteristics are plotted for a range of optical wavelengths of injected light for the same below threshold pre-bias injection current. It will be apparent that the ability of the model to accept input light of any wavelength is vital to examine the effect of external optical pumping on the light "input-output" characteristics. The effect of injecting light through either facet into the pumped or and passive segment of the inhomogeneously pumped laser is also considered. This is a feature of this model, where, for any model which ignores the spatial variation of photon density this would not be possible.

Figure 5-1 shows the inhomogeneously injected (split-stripe)

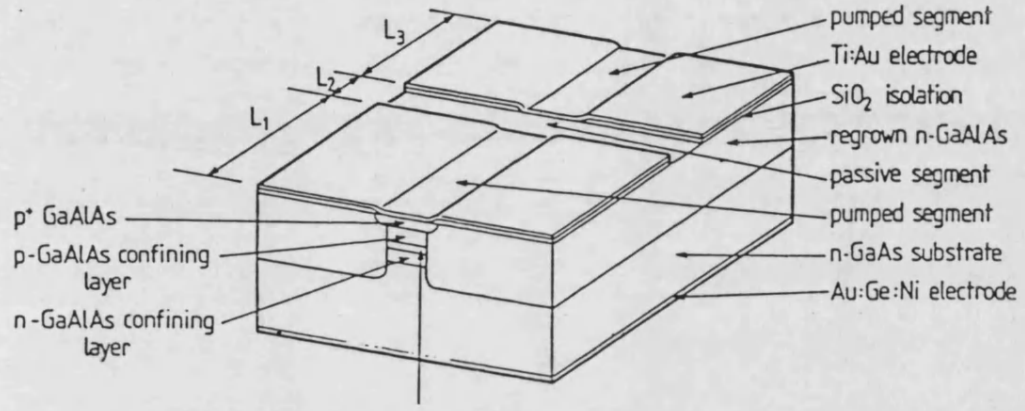

Figure 5-1 Schematic diagram of the multisegment laser modelled. A buried heterostructure is assumed to provide (lateral index) waveguiding.

laser considered in this chapter. This type of device has been analysed theoretically by some workers in the field of bistability [1-7] as already mentioned in the previous chapter. The assumptions used by these workers have been outlined using a single wavelength model. However, neglecting wavelength and using simple functions of carrier density for gain and spontaneous emission is not satisfactory for an absorptively bistable device. For this type of device there are great differences in the carrier densities between the pumped and passive segments, and as a consequence the wavelength corresponding to the gain maximum will be different in each segment [3]. This is illustrated in figure 5-2.

5.1 Analysis of multi-wavelength model.

A ray approach is used, for the same reasons as given in the previous chapter, where the variation of flux is ignored in the x and y direction. The general photon conservation equations are repeated here. For the positive z-direction;

$$\frac{1}{v}\frac{\partial P(z,t,\lambda)}{\partial t} + \frac{\partial P(z,t,\lambda)}{\partial z} = G(n(z),\lambda).P(z,t,\lambda) + \delta.B_r.S(n(z),\lambda) \qquad (5.1\text{-}1)$$

And for the negative z-direction;

$$\frac{1}{v}\frac{\partial Q(z,t,\lambda)}{\partial t} - \frac{\partial Q(z,t,\lambda)}{\partial z} = G(n(z),\lambda).P(z,t,\lambda) + \delta.B_r.S(n(z),\lambda) \qquad (5.1\text{-}2)$$

Again, the carrier conservation equation;

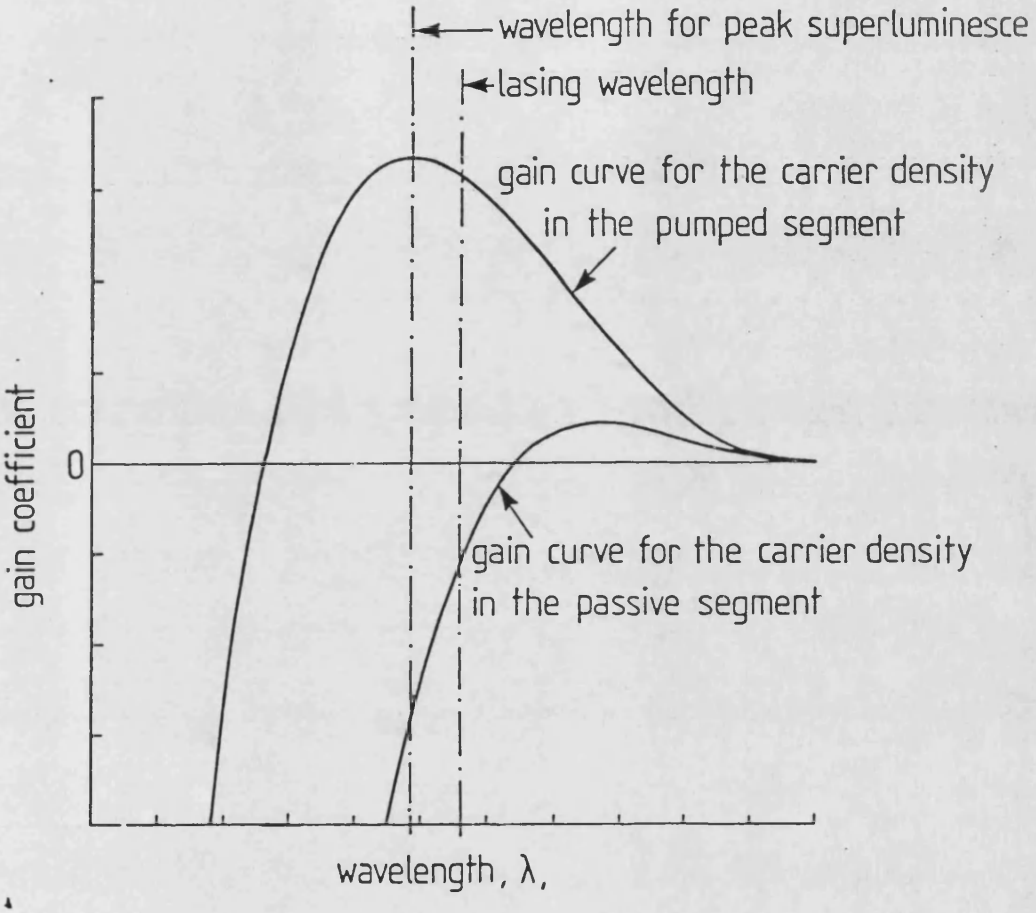

Figure 5-2 Typical stimulated gain coefficient-wavelength characteristics of the material illustrating the shift in wavelength due to the effects of differences of carrier density in each segment.

$$\frac{dn(z)}{dt} = \frac{J}{e.d} - \int_0^{\infty} g(n(z),\lambda).\{ P(z,t,\lambda) + Q(z,t,\lambda) \}.dn$$

$$- B_r.n(z).(n(z) + p_0) \qquad (5.1\text{-}3)$$

The same simplifications are used as in the previous chapter where the derivatives with respect to time are set to zero and the carrier density is assumed constant within a section. Each segment may be made up of any number of sections. In order to reproduce the spectral dependence of gain and spontaneous emission the spectrum is discretised into a number of wavelength slots, rather than continuous functions of wavelength. This results in the photon conservation equation being discretised into a "photon conservation equation" for each wavelength slot. For each slot, solutions to equations 5.1-1 and 5.1-2 may then be found. The photon flux travelling in the positive z-direction, in the "i"th wavelength slot is;

$$P(z,\lambda_i) = P(Z_h,\lambda_i).\exp\{G(n,\lambda_i).(z - Z_h)\}$$

$$+ (\exp\{G(n,\lambda_i).(z - Z_h)\} - 1).\frac{\delta.S(n,\lambda_i)}{G(n,\lambda_i)} \qquad (5.1\text{-}4)$$

This can be compared to the solution for the single wavelength model found in the previous chapter. $P(Z_h,\lambda_i)$ is the known photon flux in the "i"th wavelength slot at $z = Z_h$. Equation 5.1-4 is only valid over the section where the carrier density has been assumed uniform. A similar equation exists for the photon flux travelling in the negative z-direction. At this point it must be emphasised that the total spontaneous emission in all of the slots must be consistent with the bimolecular recombination rate;

$$\sum_{\lambda_i=\lambda_1}^{\lambda_k} S(n,\lambda_i) = B_r.n.(n + p_0) \qquad (5.1\text{-}5)$$

where λ_1 and λ_k represent the upper and lower wavelength slots considered. The above assumptions also modify the carrier density conservation equation for each section;

$$\frac{J}{e.d} = \sum_{\lambda_i=\lambda_1}^{\lambda_k} \{ g(n,\lambda_i).(\bar{P}(\lambda_i) + \bar{Q}(\lambda_i)) \} + B_r.n.(n + p_0) \qquad (5.1\text{-}6)$$

$$\text{Where;} \quad \bar{P}(\lambda_i) = \frac{1}{L} . \int_0^L P(z,\lambda_i).dz \qquad (5.1\text{-}7)$$

represents the mean photon density, in the "i"th wavelength slot. The integral may be evaluated to obtain;

$$\bar{P}(\lambda_i) = \frac{1}{G} . \left[\frac{P(L,\lambda_i) - P(0,\lambda_i)}{L} - \delta.S(n,\lambda_i) \right] \qquad (5.1\text{-}8)$$

A similar expression may be obtained for $\bar{Q}(\lambda_i)$. Within each section P, Q and n must be solved consistently.

5.2 Modelling procedure.

The solution procedure is essentially the same as in the previous chapter except that the computation becomes more complex. This is because the variation of photon density must be calculated for all the wavelength slots. A direct consequence is that the gain and spontaneous emission characteristics are required for each wavelength slot. In order to speed up the evaluation of gain and spontaneous emission for a wavelength slot in the computer program, for a value of carrier density, it was chosen to use a polynomial fit to the gain and spontaneous emission characteristics shown in chapter 3 in figures 3.6-1 and 3.6-2. It was found that a fourth order

(cubic) polynomial was required to adequately describe the gain data and a eigth order polynomial, with the first coefficient set to zero, was necessary to describe the spontaneous emission. With the first coefficient being zero, it ensured that for zero population inversion there is zero spontaneous emission and also reduces the number of terms required to evaluate the polynomial. For programming purposes this method is preferable in terms of its simplicity and speed of evaluation of gain and spontaneous emission. Another method considered was to use an interpolation procedure between points in a table of values.

In each wavelength slot the fluxes P and Q are made continuous throughout the device, subject to the boundary conditions at the facets;

$$P(0,\lambda_i) = r.Q(0,\lambda_i) \qquad (5.2\text{-}1)$$

$$Q(Z_L,\lambda_i) = r.P(Z_L,\lambda_i) \qquad (5.2\text{-}2)$$

There is one further aspect which is more complex than in the model of the previous chapter. At the front facet, the input photon flux, once again, is made consistent with the desired light output. However, in order to satisfy the boundary condition at the front facet, the light reflected back into the device is made to have the spectral dependence of the light output after an iterative pass.

Hence if X_d is the desired light output, at the front facet, for which the injection current is required, and;

$$X_a = \sum_{\lambda_i=\lambda_1}^{\lambda_k} (1 - r).\ Q(0,\lambda_i) \qquad (5.2\text{-}3)$$

is the light output after an iterative pass then;

$$P(0,\lambda_i) = \frac{X_d}{X_a}.r.Q(0,\lambda_i) \qquad (5.2\text{-}4)$$

The injection current, as previously, is made dependent on X_a and X_d;

$$I_{m+1} = I_m \cdot \left[1 + A.\log\left(\frac{X_d}{X_a}\right) \right] \qquad (5.2\text{-}5)$$

where m represents the m^{th} iterative pass, so that the model converges on the complete and consistent solution. The inclusion of wavelength does not dramatically alter the method of solution but the computer processor time naturally increases with the number of wavelength slots.

For the case of optical injection the device is pumped by an injection current just below the device off-state threshold (ie. the onset of hysteresis). Light in a particular wavelength slot can then be forced to enter the active region of the device through either facet. For a fixed current and a known desired light output at the front facet, the light input is made to vary so that the actual light output after iterations converges to the desired light output. The method is the same as above except the light input is now made to vary;

$$P_{in_{m+1}} = P_{in_m} \cdot \left[1 + A.\log\left(\frac{X_d}{X_a}\right) \right] \qquad (5.2\text{-}6)$$

5.3 Results.

For the following result the values of table 5.3-1 are used, unless otherwise stated.

In the model, 151 equally spaced wavelength slots are normally used covering the range of wavelengths between 780 and 840 nm, which should sufficiently describe the gain and spontaneous emission in the

significant spectral range of a superluminescing diode (SLED) and of a laser. The number of slots is limited by computer time. However the distribution of wavelength slots need not be uniform and a high density of slots can be concentrated near the lasing wavelength.

Γ	=	0.75
f_{cc}	=	10^{-21} m^2
B_r	=	10^{-16} m^3 S^{-1}
p_0	=	4×10^{23} m^{-3}
δ	=	10^{-4}
W	=	1 μm
d	=	0.3 μm

Table 5.3-1

5.3.1 The inhomogeneously pumped laser (SLED).

It is again prudent to verify the assumptions that have been made in this chapter. The vehicle used for these tests is the SLED structure of the geometry shown in figure 5.3.1-1. For the geometry stated, figure 5.3.1-2 shows the computed I-L characteristics of this type of device. Although the characteristics are somewhat distorted by the logarithmic scale on the light output axis, hysteresis is a feature. A point of note is that the light output is measured directly in (mW). If the device is split into a sufficiently large

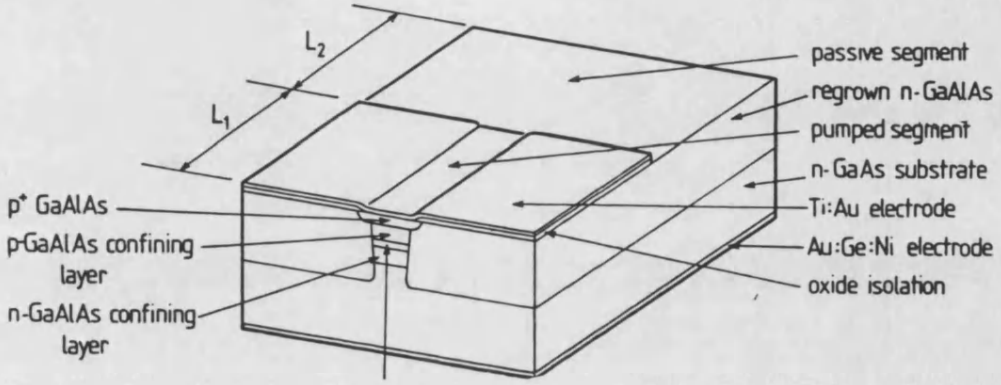

Buried active layer, guiding structure continued beneath passive segment.

Figure 5.3.1-1 Schematic diagram of the SLED type structure modelled.

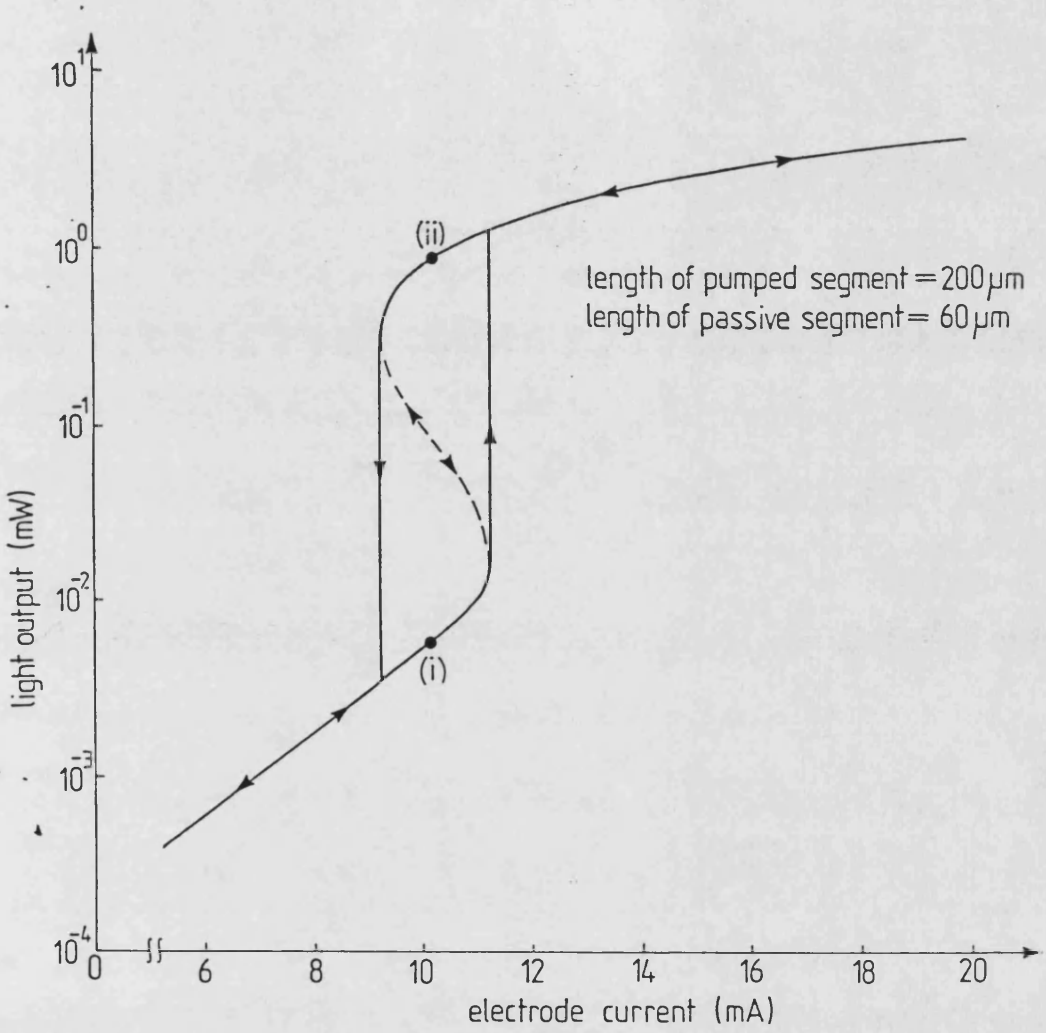

Figure 5.3.1-2 The I-L characteristics of an inhomogeneously pumped laser with a pumped length of 200 μm. and a passive length of 60 μm.

number of sections it is possible to evaluate the longitudinal variation of carrier density n(z) consistently with P(z) and Q(z). This is plotted in figure 5.3.1-3 in the region of hysteresis for the case of the carrier density in (a) the "off state" and (b) the "on state", for the same value of current of 10 mA, ie. points (i) and (ii) on figure 5.3.1-2. Figure 5.3.1-3a shows a near uniform carrier density in the pumped segment while showing a carrier density quickly tailing off to a low value in the passive segment. This is caused by the rapid attenuation of light in this segment and the subsequent rate of absorption diminishing near the rear facet. An interesting point is that the returning wave (Q) in the passive segment is attenuated to such a level that nearing the boundary of the pumped segment spontaneous emission is now becoming dominant. As the backward (Q) wave enters the pumped region, immediately spontaneous emission and then superluminescing become to dominate. In figure 5.3.1-3b the device is now lasing with a single dominant wavelength. It is apparent that the carrier density in the passive segment is now much more uniform. A feature of these longitudinal plots is that there is a discontinuity of carrier density at the boundary between the segments. In practice this would be smeared out by the diffusion of carriers to the passive segment as well as current spreading between the contacts but the effect of these are rather difficult to ascertain. Figure 5.3.1-4 shows the sensitivity of the I-L characteristics of the SLED structure to the number of sections into which each pumped and passive segment is subdivided. The graph is enlarged at its worst point, shown in figure 5.3.1-4b, to illustrate the accuracy of the method. It is found that if the pumped and passive segment are each split into three or more sections there is negligible change in the curves. The error in the characteristic when

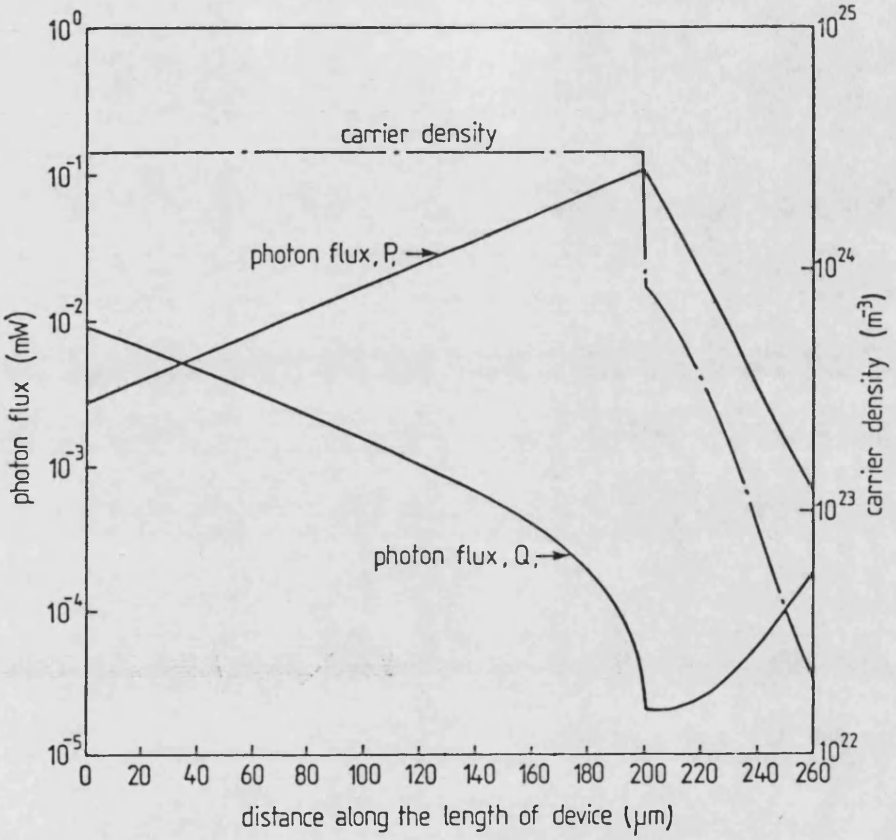

Figure 5.3.1-3a Graphs of the carrier density distribution and the distributions of the photon fluxes P and Q along the length of the device in the "off" state.

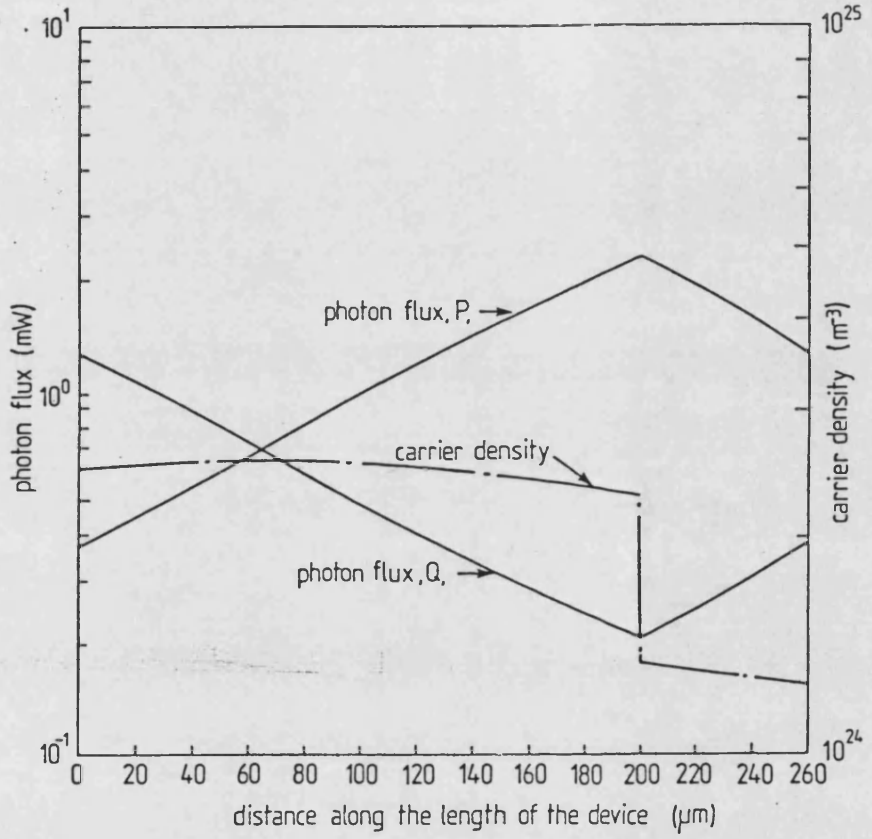

Figure 5.3.1-3b Graphs of the carrier density distribution and the distributions of the photon fluxes P and Q along the length of the device in the "on" state.

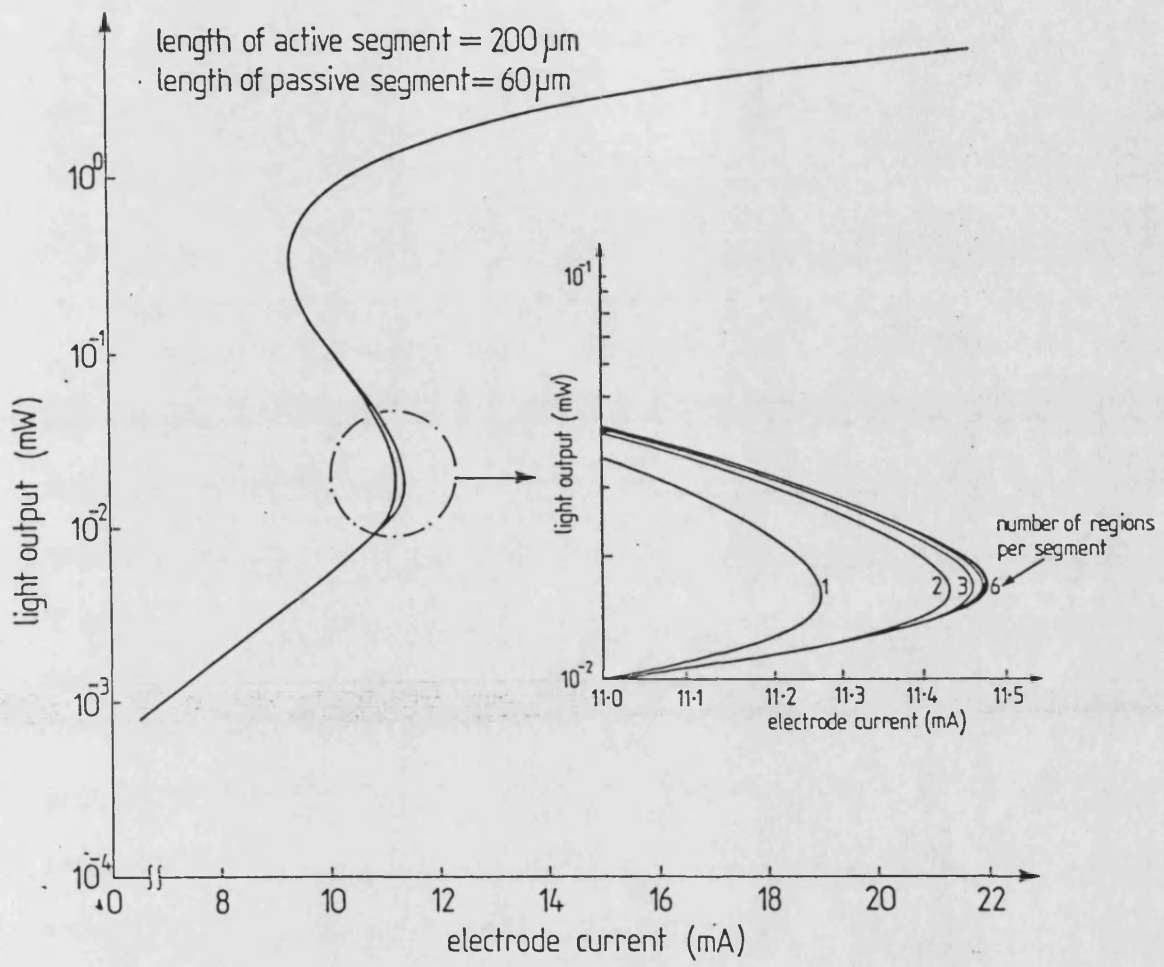

Figure 5.3.1-4 Effect on the accuracy of the I-L characteristics of dividing each segment into several sections.

the pumped and passive segments are not subdivided is still quite small and therefore validates the often used simplification that the carrier density can be assumed to be constant in each pumped or passive segment. As might be expected, the loss of accuracy for assuming a small number of sections per segment is greatest at the point on the characteristic corresponding to the condition where the pumped segment is strongly superluminescing. This is because the photons produced have a relatively short wavelength which are quickly absorbed in the passive segment. Under these conditions, this would produce a high density of carriers in the passive segment, close to the pumped segment which quickly tails off to a low value at the rear facet (as illustrated in figure 5.3.1-3a), rather than a uniform carrier density. All further results have only one section per segment since computer time is roughly proportional to the number of sections within the device.

Figures 5.3.1-5a and 5.3.1-5b shows the spectrum of the light emitted at the front facet of an inhomogeneously pumped laser for two lengths of passive segment, L_p, but with the same length active segment, L_a, for various values of light output. The values of current corresponding to these light outputs are listed. These curves consist of 151 wavelength slots between 720nm and 870nm. All further results use the reduced spectral range from 780nm to 840nm. It is evident that outside of this range any light in the device would be of an insignificant magnitude. The graphs show the expected result that below threshold the spectrum of the emitted light is very broad. As the characteristics proceed around the "S" curve (not possible in practice) the spectrum narrows as lasing behaviour becomes dominant. For the case of the device with the longer the passive segment far more superluminescing is observed before lasing takes place.

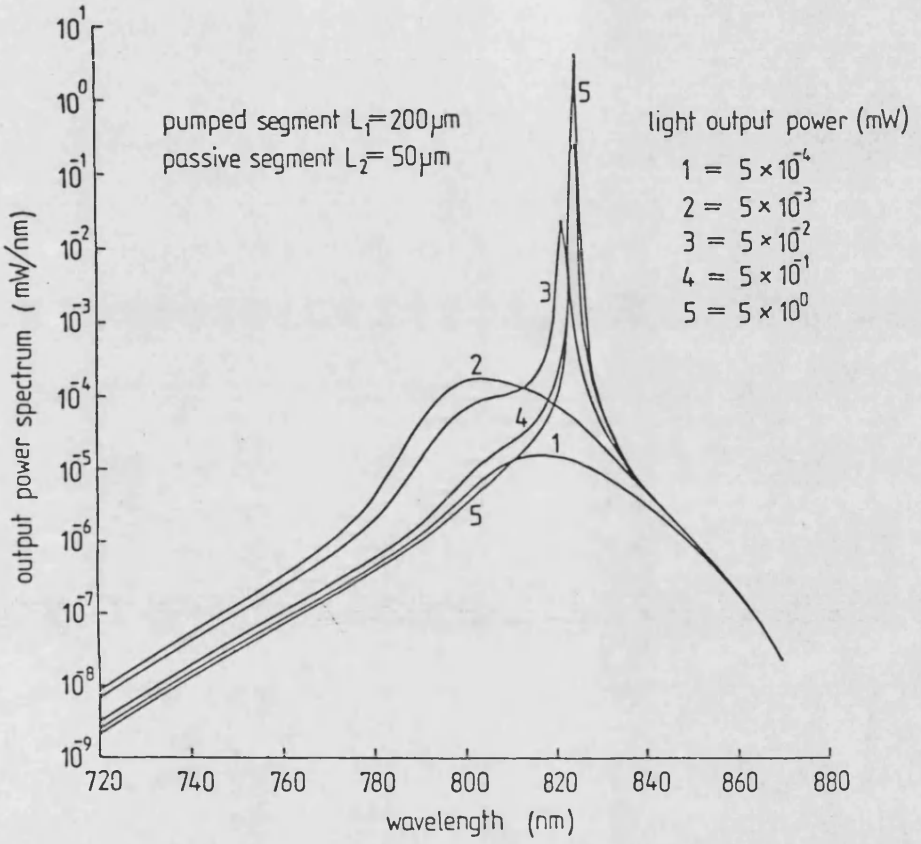

Figure 5.3.1-5a The spectrum of the emitted light at the front facet of an inhomogeneously pumped laser with L_a = 200 μm. and L_p = 50 μm. for different values of light output.

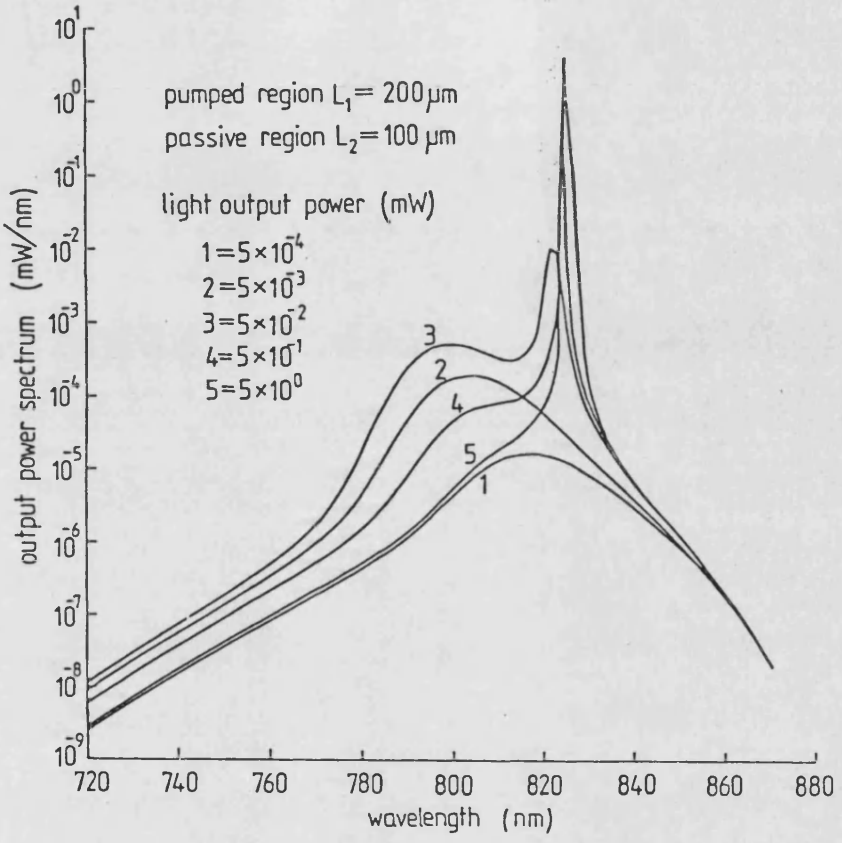

Figure 5.3.1-5b The spectrum of the emitted light at the front facet of an inhomogeneously pumped laser with L_a = 200 µm. and L_p = 100 µm. for different values of light output.

Figures 5.3.1-6 and 5.3.1-7 show the sensitivity of the characteristics on the length of the passive segment and the pumped segment respectively. Simple theory predicts that hysteresis becomes larger for increasing length of passive segment and a decreasing length of pumped segment [8]. However the results from this model suggest that there is a maximum in hysteresis for a particular length of passive and pumped segment, which has not been reported before. This is illustrated in figure 5.3.1-8, which plots the variation of percentage hysteresis with length of passive segment for a fixed length of pumped segment. Here percentage hysteresis is defined as;

$$\left(\frac{I_{smax} - I_{smin}}{I_{smax} + I_{smin}} \right) \times 200\ \% \qquad (5.3.1\text{-}1)$$

Figure 5.3.1-9 plots the variation of the percentage hysteresis of the I-L characteristics as a function of the length of the pumped segment for a fixed length of passive segment. Significantly, both graphs suggest that there is an optimum geometry of the lengths of segments for which maximum hysteresis can be obtained.

Figure 5.3.1-10 shows a contour plot of percentage hysteresis. It is significant that there is an optimum geometry of the lengths of segments for which maximum hysteresis may be obtained. This is around a pumped segment length of 150 to 200μm with a passive segment of 30 to 50μm.

5.3.2 Multisegment laser.

The structure of the multi-segment laser modelled in this paper is shown in figure 5-1. A feature of this model is the ability to pump or extract current from the second electrode whilst passing a current in the first electrode to pump the first segment in the

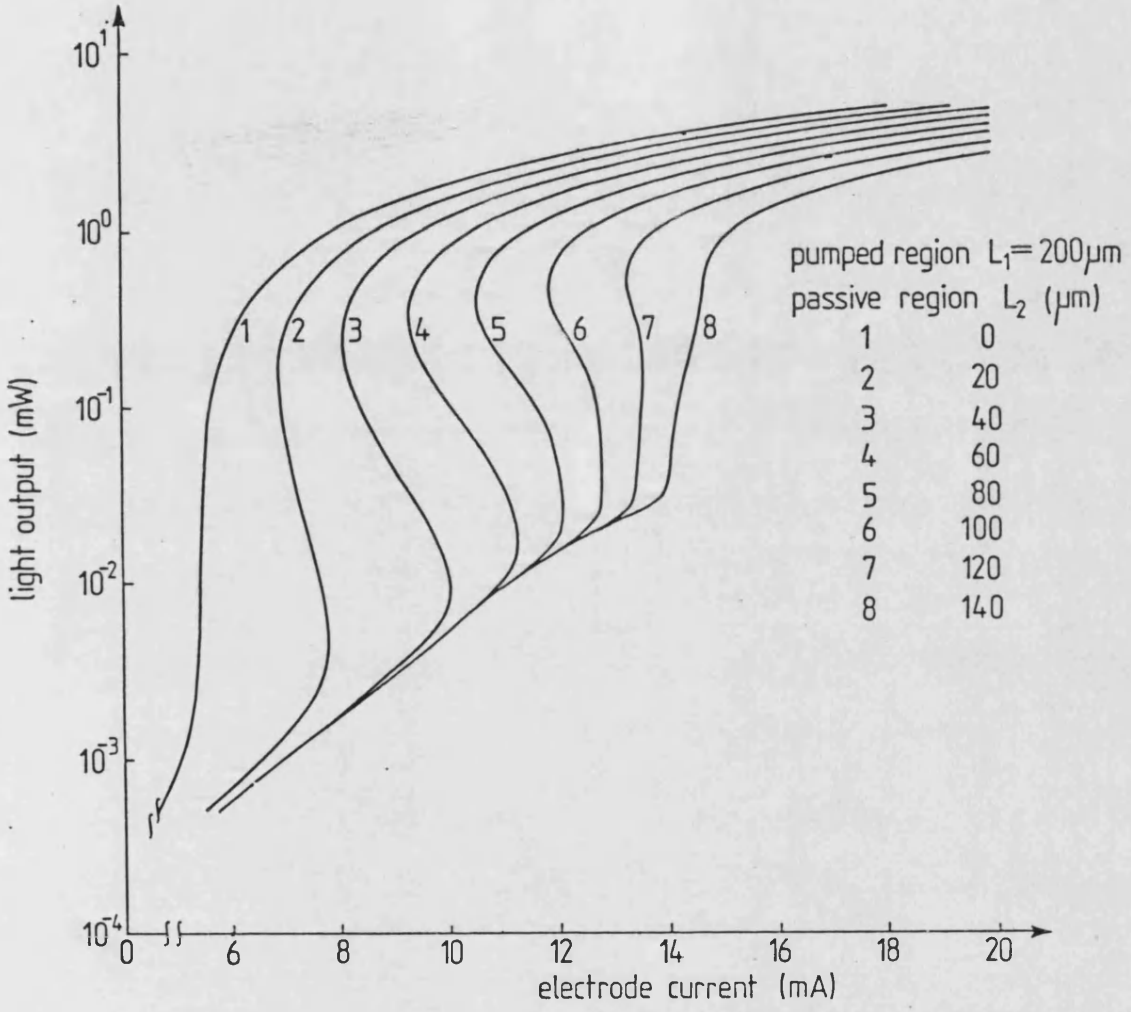

Figure 5.3.1-6 The I-L characteristics of an inhomogeneously pumped laser, with La = 200 μm. as a function of the length of the passive segment, Lp.

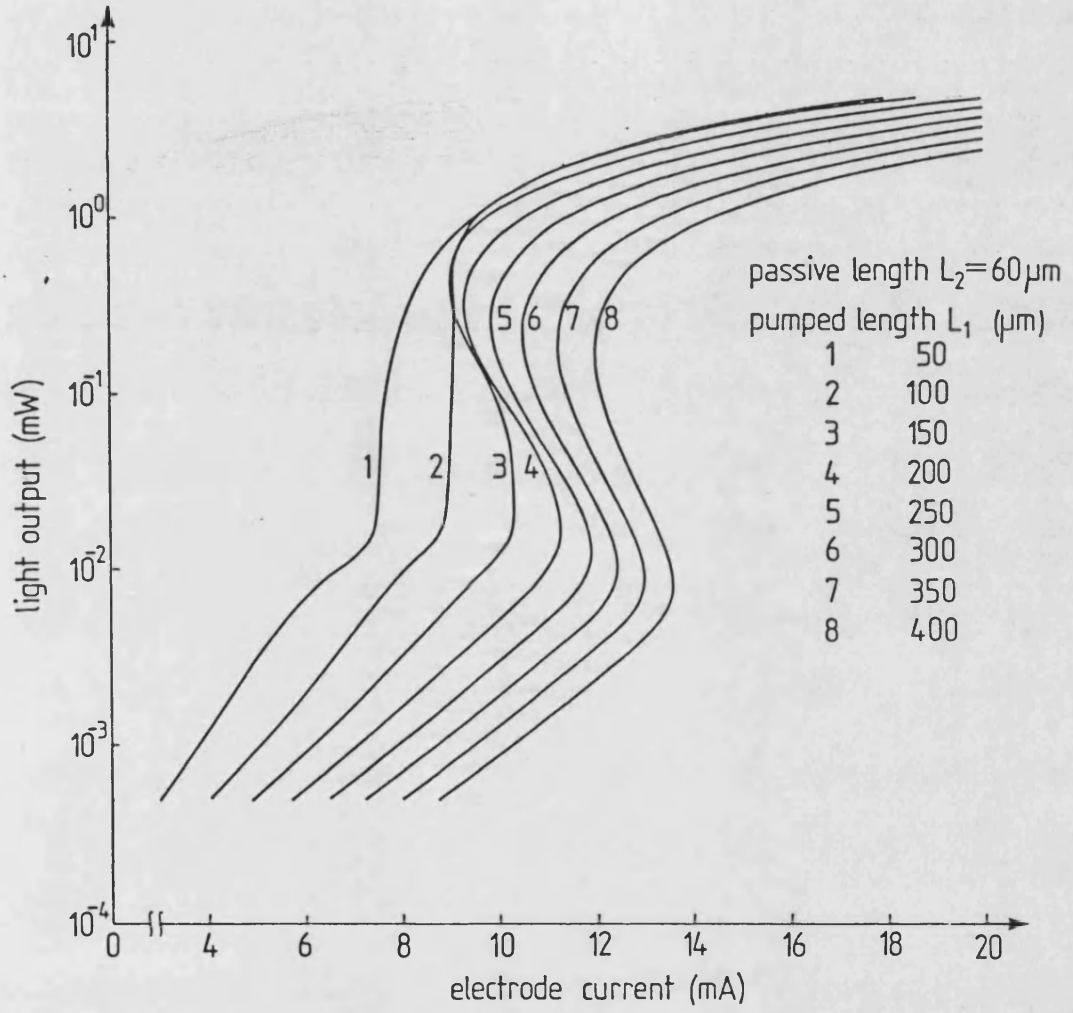

Figure 5.3.1-7 The I-L characteristics of an inhomogeneously pumped laser as a function of the length of the pumped segment for a fixed passive segment length of Lp = 60µm.

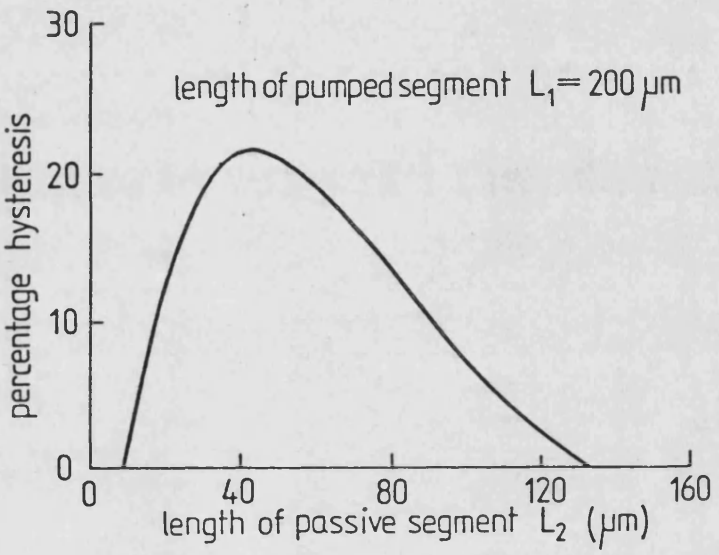

Figure 5.3.1-8 The effect of passive segment length on the percentage hysteresis for La = 200μm.

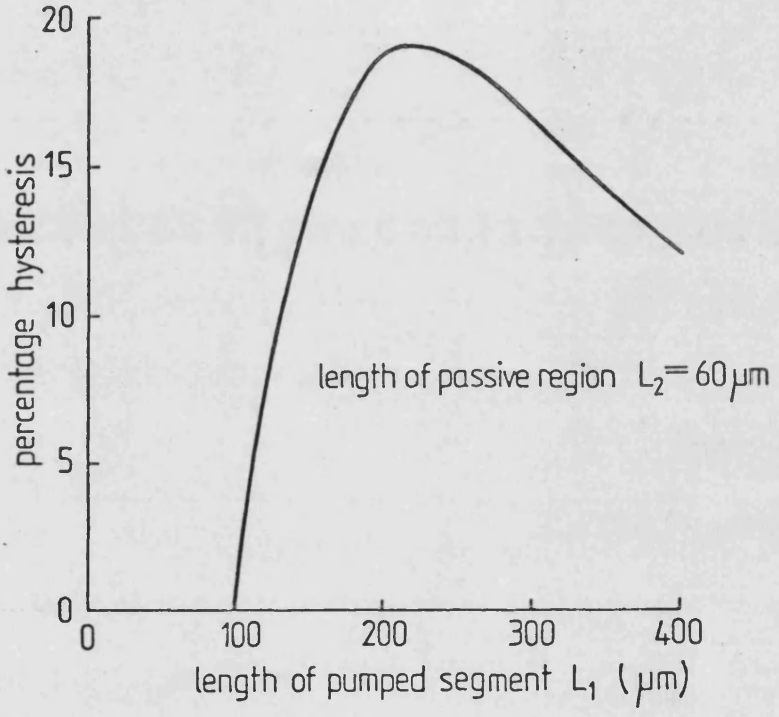

Figure 5.3.1-9 The effect of pumped segment length on the percentage hysteresis for Lp = 60μm.

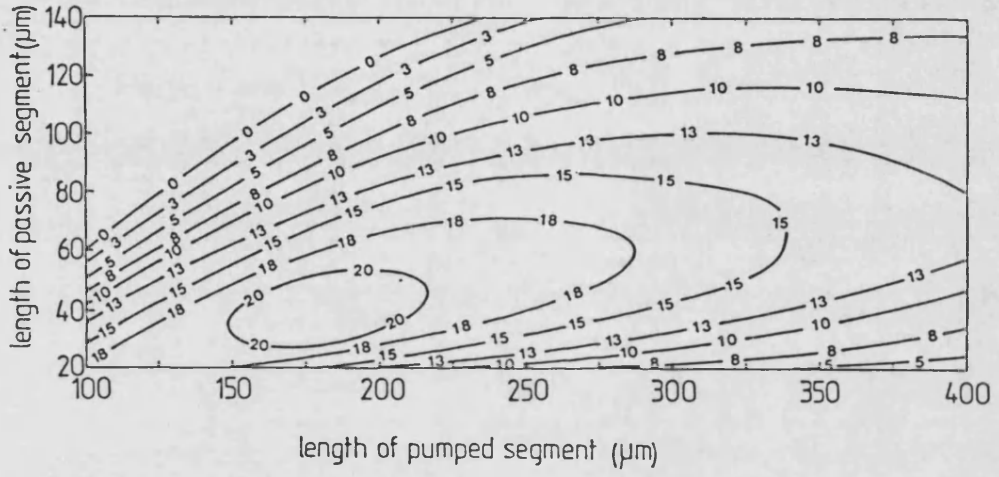

Figure 17

Figure 5.3.1-10 Contour plot of percentage hysteresis for the combination of length of pumped and passive segments.

normal fashion. The second electrode can be used to trigger the device into the "on state". Note that although the current in the second electrode is allowed to go negative the carrier density must not. The effect of extraction of carriers in a multi-segment laser has been demonstrated experimentally by Lau, Harder and Yariv [9, 10]. Figure 5.3.2-1 illustrates the effect of a very small current passed into the second electrode which can control the amount of absorption in the passive segment. The results show, not unexpectedly, that there is a decrease in the threshold current for a positive current into the second electrode and the opposite effect for a negative current. Figure 5.3.2-2 shows the effect of the current I_2 on the hysteresis of the I-L characteristics. It would be expected that extracting current from the passive segment would increase hysteresis but this is not so, beyond a certain point hysteresis is reduced. This behaviour is analogous to the case of a very long passive segment, relative to the pumped segment, except that the absorption is controlled by I_2. For the case of I_2 is zero this corresponds to the SLED structure described earlier, where it will be noted that for a passive segment which is comparable in length to the pumped segment, hysteresis is not observed (shown in figure 5.3.1-8).

5.3.3 Optically induced bistability in an inhomogeneously pumped device.

The effect of optical injection into the active region of a SLED structure device (ie. single pumped segment and a single passive segment) can be seen in figures 5.3.3-1 and 5.3.3-2 as a factor of wavelength of the injected light. These graphs show the optical power in - optical power out characteristics for the given geometry for the

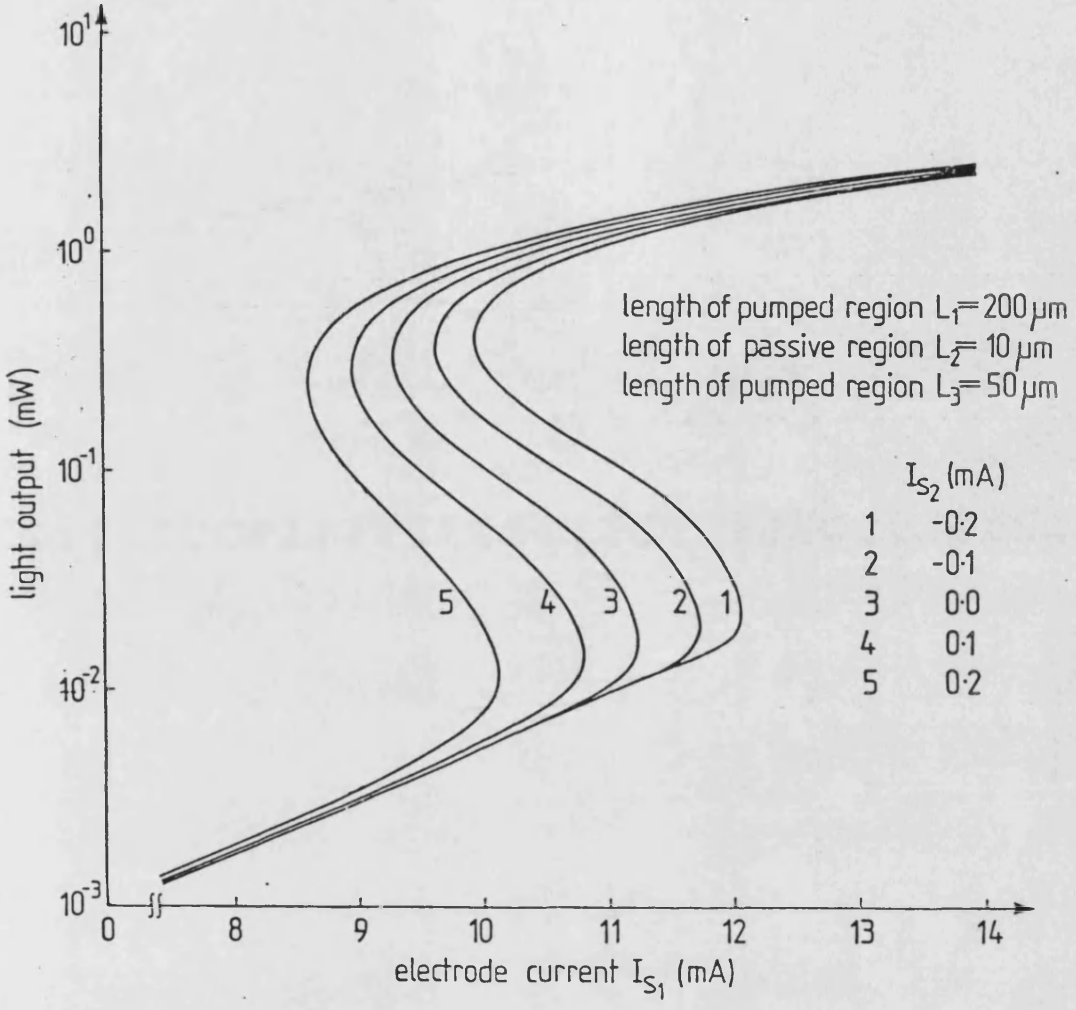

Figure 5.3.2-1 I-L characteristics of a split-stripe laser as a function of the current, Is_2

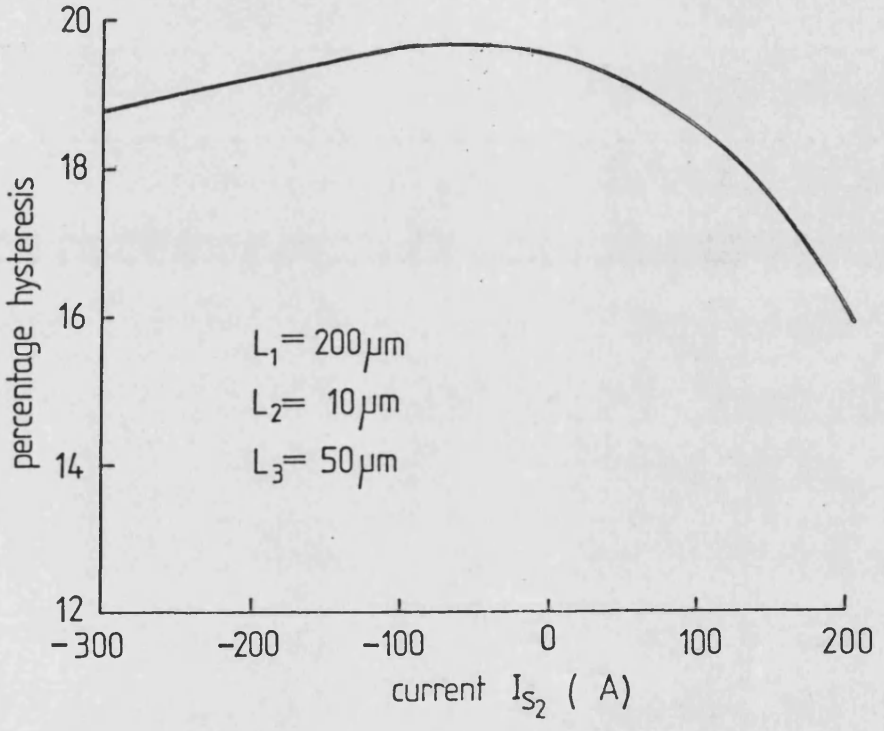

Figure 5.3.2-2 The effect of Is_2 on the percentage hysteresis of a split-stripe laser.

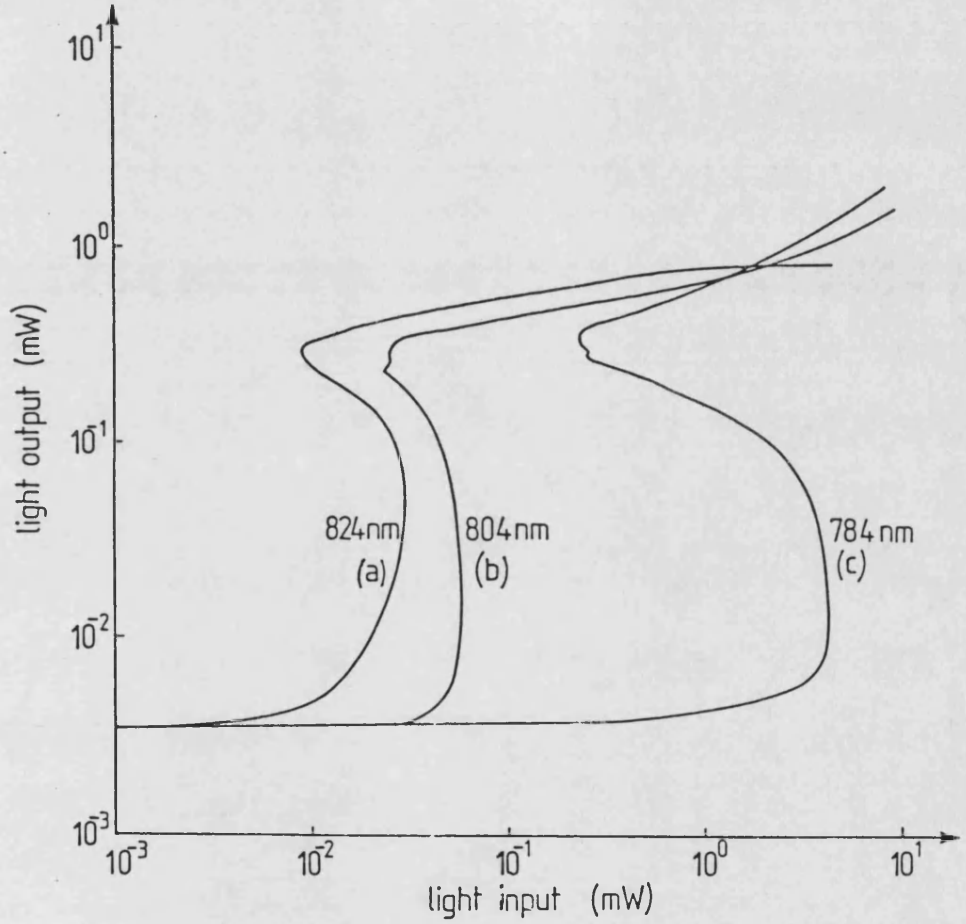

Figure 5.3.3-1 The light input - output characteristics of an inhomogeneously pumped laser as a function of wavelength of the externally injected light into the front facet {ie. into the pumped segment}

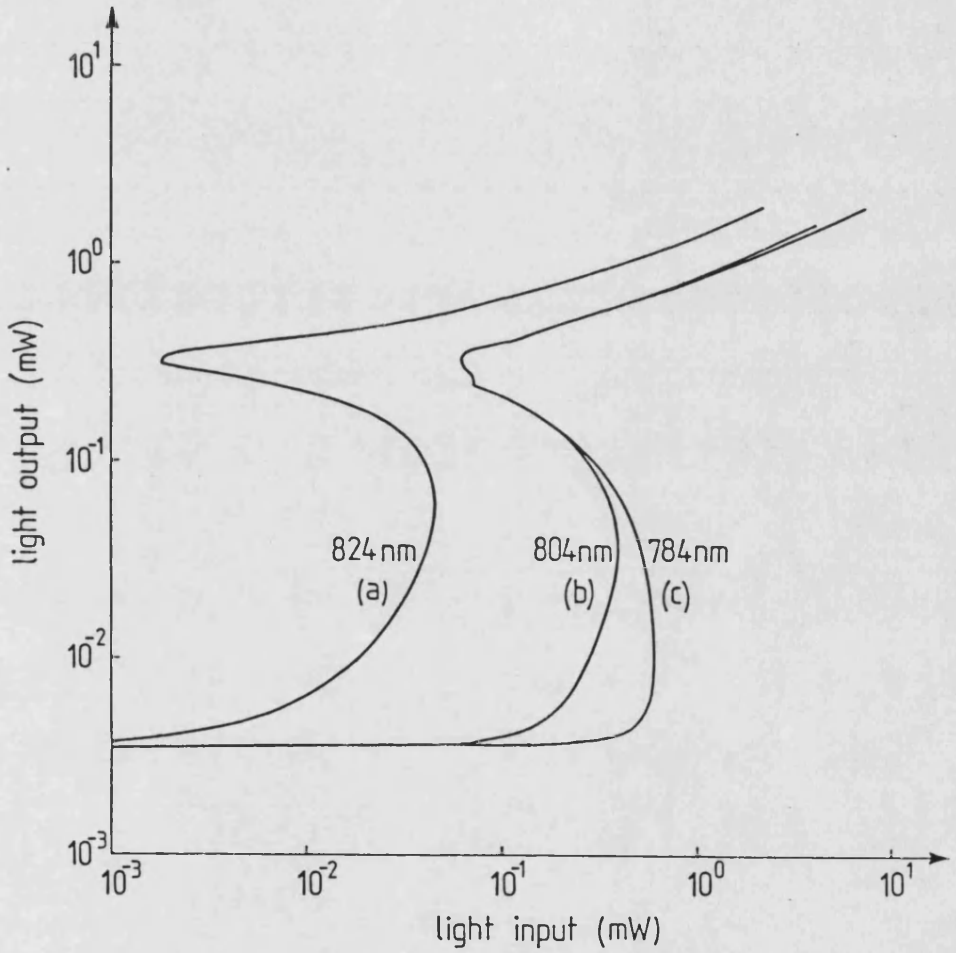

Figure 5.3.3-2 The light input - output characteristics of an inhomogeneously pumped laser as a function of wavelength of the externally injected light into the rear facet {ie. into the passive segment}

cases where the facet at the pumped end of the device is illuminated and the facet at the passive end of the structure is illuminated. To obtain these results the device is biased just below the onset of hysteresis by a suitable injection current. An important feature of these results is the use of wavelength of the external illumination as a variable. The model closely resembles the experiments of Kawaguchi [11, 12]. It will be seen that there are considerable differences in the power in - power out characteristics depending on whether the front (pumped) or rear (passive) facet is illuminated. It should be pointed out that the wavelength of the light output is not necessarily the same as the light input, and in this sense the device is not an optical amplifier.

Any light of short wavelength will be quickly absorbed by the segment into which it is injected and increase the overall gain of the device by optical pumping. Curve "c" in both graphs indicate this. If light of wavelength around the peak of the superluminescence spectrum is injected into the device the result, represented by curve (b) in figures 5.3.3-1 and 5.3.3-2, is dependent into which facet the light is injected. At the rear facet the passive segment will absorb the light, optically pumping this segment into transparency. Thus curves "b" and "c" are very similar in Figure 5.3.3-2, the major difference between the curves is being that, in curve "b", a greater proportion of the input light is passed through the laser and leaves the front facet. However, in curve "b" of Figure 5.3.3-1, the injected light undergoes optical gain in the pumped segment and is then absorbed in the passive segment. Curve "a" in both Figures 5.3.3-1 and 5.3.3-2 are for a wavelength very close to the natural lasing wavelength where the cavity round trip gain would be closest to unity. As a result any light, injected at this wavelength, would

undergo successive gain and absorption as the light would not be strongly absorbed in the passive segment. In this case the light output would be of the same wavelength as the input light.

The sensitivities of the input light on hysteresis can be qualitatively explained by the following discussion. The sensitivity of the input light, which is of a short wavelength and thus would be quickly absorbed, is likely to be lowest. However, where the light experiences gain in the pumped segment and absorption in the passive segment, the sensitivity is increased particularly where the light can experience only moderate loss in the passive segment to allow the light successive gain and absorption. However, at wavelengths much longer than at lasing, the light-in would undergo negligible loss or gain and would pass straight through the device and not produce bistability. Also these characteristics do not take into account any coupling loss of light in, except the loss due to reflectivity, which would be manifest for an experimental device. It should however be mentioned that when the wavelength of the input light is close to the lasing wavelength, but not sufficiently close to the wavelength of a longitudinal mode of the device then curve (a) in figures 5.3.3-1 and 5.3.3-2 will be in error. In this case the input light after it has circulated in the device after reflection by both facets will be out of phase with the incoming light and the results due to the effects of interference would prevail. It is suggested that further work be carried out on this aspect since longitudinal modes are neglected in this analysis. The problem is rather complex since the wavelength of a longitudinal mode depends on the refractive index of the active layer which is dependent on the carrier densities in each segment. This represents a combination of absorptive and dispersive bistability.

5.4 Conclusions.

This chapter has highlighted the effect of geometry on the hysteresis in the I-L characteristics of an inhomogeneously pumped laser due to effects of photon absorption. A technique for analysing the effect of saturable absorption effects has been introduced which includes the effect of the wavelength dependence of gain and spontaneous emission. Once again it has been found that the commonly used assumption of a uniform carrier density in each segment of the device is a reasonable one. It is shown to causes little error, when compared to solutions in which a more accurate carrier density profile is calculated. Although it is commonly assumed that by increasing the length of the passive segment the hysteresis will increase, it has been found that there is an upper bound to this, any further increase in the length of the passive segment actually reduces the hysteresis. This result is a possible explanation to the experimental result of a device by Harder, Lau and Yariv [9] where for the dynamically stable split stripe laser, with only one segment pumped and a long passive segment, no hysteresis was observed.

References.

1) N. G. Basov; "O-1 Dynamics of injection lasers"; IEEE J. Quantum Electronics; Vol. QE-4; No. 11; 1968; p855-64.

2) T. L. Paoli. "Saturable absorption effects in the self-pulsing (AlGa)As junction laser"; Applied Physics Letters; Vol. 34; No. 10; 1979; p652-655.

3) D. Renner and J. E. Carrol. "Transients in injection lasers - phase-plane analysis and effects on absorbing sections"; Solid-State and Electron. Devices; Vol. 3; No. 6; 1979; p 224-32.

4) Ch. Harder, K. Y. Lau and A Yariv. "Bistability and Pulsations in Semiconductor Lasers with Inhomogeneous Current Injection"; IEEE Journal of Quantum Electronics; Vol. QE-18; No. 9; 1982; p 1351-61.

5) H. Kawaguchi. "Optical bistable-switching operation in semiconductor lasers with inhomogeneous excitation"; IEE Proc.; Vol. 129; No. 4; 1982; pl41-8.

6) H. Kawaguchi. "Optical bistability and chaos in a semiconductor laser with a saturable absorber"; Applied Physics Letters; Vol. 45; No. 12; 1984; p 1264-6.

7) M. Kuznetsov. "Theory of bistability in two-segment diode lasers"; Optics Letters; Vol. 10; No. 8; p 399-401.

8) H. Kawaguchi. "Optical bistable-switching in semiconductor lasers with inhomogeneous excitation"; IEE Proc.; Vol. 129; pt. I; No. 4; 1979; p 141-7.

9) Ch. Harder, K. Y. Lau and A. Yariv. "Bistability and pulsations in CW semiconductor lasers with a controlled amount of saturable absorption"; Applied Physics Letters; Vol. 39; No. 5; DATE; p 382-4.

10) K. Y. Lau, Ch. Harder and A. Yariv. "Dynamical switching characteristic of a bistable injection laser"; Applied Physics Letters; Vol. 40; No. 3; DATE; p198-200.

11) H. Kawaguchi. "Bistable operation of semiconductor lasers by optical injection"; Electronics Letters; Vol. 17; No. 20; 1981; p 741-2.

12) H. Kawaguchi. "Optical input-output characteristics for Bistable semiconductor lasers"; Applied Physics Letters; Vol. 41; No. 8; 1982; p 702-4.

Chapter 6

Time dependent analysis of absorptive bistable laser.

6 Introduction.

In this chapter the transient behaviour of bistable lasers is considered. Here a different modelling technique is adopted which relies upon a travelling wave approach rather than that used in [1-7]. Within the device, the light can either grow in magnitude along a segment, or decay. The reflectivity at the facets has the effect of circulating the light in the device, backwards and forwards, and the model in this chapter describe this behaviour. The object of this analysis is to only use the assumptions which have already been verified since in chapter four it has been shown that simplification of the problem by means of some commonly used assumptions, introduce errors. These being the inappropriate use, when applied to absorptive bistability, of a constant photon lifetime and of a uniform photon density within the device. The models proposed in this chapter do not use these assumptions and take into account the spatial variation of photon density along the length of the device and the loss of light at the facets. The accuracy associated with the assumption of a uniform carrier density within a segment has already been shown to be very good in the previous two chapters. This assumption is used to allow an analytic solution to the photon conservation equation and it is an important point to note that the approach does not resort to finite difference techniques [8]. The proposed models include the wavelength dependence of gain and spontaneous emission by discretising any wavelength dependency into a number of wavelength slots in the same way as already described in chapter five for the steady-state model.

The transient model outlined in this chapter relies on the principle that after a "round trip time", t_{rt}, light at a point will

end up from where it started out either amplified, or attenuated, by the "round trip gain" (or loss) together with some spontaneous emission. It should be noted, and is an important observation, that the "round trip gain", $g_{rt}(\lambda_i)$, in a particular wavelength slot is independent of position. This is illustrated in figure 6-1, where the flux at points A, B and C undergo one entire "round trip" and return to their original position having undergone a "round trip gain" in the appropriate wavelength slot. For this device the round trip time is defined as;

$$t_{rt} = \frac{2.Z_L}{v} \qquad (6\text{-}1)$$

where Z_L is the length of the device.

It is rather fortuitous that, within a segment, only the average photon flux is required, merely to satisfy the carrier density equation. Whilst the photon density at the facets must be known in order to calculate the light output from the device, at no other point is the level of photon flux required. This is in contrast to the steady-state model where much of the effort was to ensure that the flux was continuous across the dividing boundaries of sections and had to satisfy the boundary conditions of reflectivity.

6.1 Analysis.

The analysis of this model can be separated into two parts; (i) the equations governing the time dependent behaviour of the carriers in each segment and; (ii) the behaviour of the photon flux within the device. For simplicity, the behaviour of the photon flux can be further broken down into two parts. The first aspect is the photon density at the beginning of the time interval, undergoing gain, and

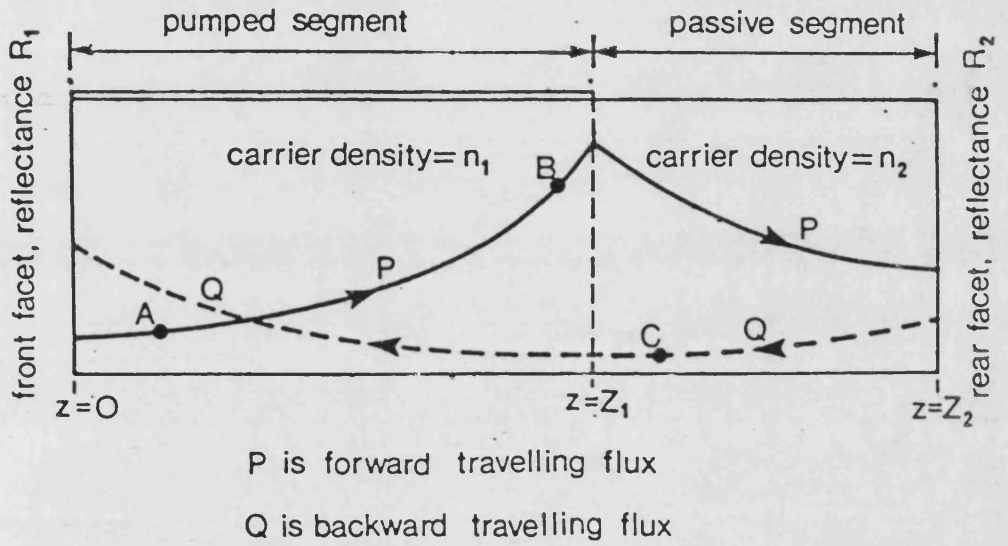

Figure 6-1 Diagram of the two segment laser illustrating the fluxes P and Q in each segment.

the second is spontaneous emission which requires a considerably more complex approach. The following analysis is based on a device having just two segments one pumped and the other passive, as shown in figure 6-1, to illustrate the method. However once the principles are established the analysis may be extended to include any number of segments.

6.1.1 Carrier Conservation Equation.

The average photon density, in a section, must be consistent with the carrier conservation equation which is repeated here;

At any point z, along the length of the device, the carrier conservation equation is;

$$\frac{dn(z)}{dt} = \frac{J}{e.d} - \int_0^{\infty} g(n(z),\lambda).\{ P(z,t,\lambda) + Q(z,t,\lambda) \}.d\lambda$$

$$- B_r.n(z).(n(z) + p_0) \qquad (6.1.1\text{-}1)$$

As in the analysis of the steady-state model in chapter five, the equation does not contain a non-radiative recombination term but this may easily be included. It is assumed that the carrier density distribution is uniform along the length of the pumped and passive segments and that the gain and spontaneous emission curves are discretised into wavelength slots. To aid and to make clearer the analysis;

$$G_1(\lambda_i) = G(n_1,\lambda_i) \qquad (6.1.1\text{-}2)$$

$$G_2(\lambda_i) = G(n_2,\lambda_i) \qquad (6.1.1\text{-}3)$$

where "G" is the net effective optical gain;

$$G = g - f_{cc}.(2n + p_0) \qquad (6.1.1\text{-}4)$$

Equation 6.1.1-1, for the first (pumped) segment, then becomes;

$$\frac{dn_1(t)}{dt} = \frac{J}{e.d} - \sum_{i=1}^{k} \{g_1(\lambda_i).(\bar{P}_1(\lambda_i) + \bar{Q}_1(\lambda_i)) - B_r.n_1.(n_1 + p_0)\} \qquad (6.1.1\text{-}5)$$

where there are k wavelength slots, λ_1 representing the shortest wavelength slot and λ_k the longest wavelength slot and where;

$$\bar{P}_1(t,\lambda_i) = \frac{1}{L_1} \int_0^{Z_1} P(z,t,\lambda_i)\, dz \qquad (6.1.1\text{-}6)$$

is the average photon flux within the first segment. L_1 is the length of the first segment which is bounded by $z = 0$ and Z_1. A similar expression exists for the average flux travelling in the reverse direction.

An approximate solution to equation 6.1.1-5 can be made if the gain and mean photon fluxes change only by a negligible amount in the time interval of m round trip times, $t = m.t_{rt}$;

$$n(t) = n(0).\exp[- B_r.(n(0) + p_0).t] + \{ 1 - \exp[- B_r.(n(0) + p_0).t] \} \cdot \frac{J(t)/ed - \sum_{i=1}^{k} g(\lambda_i).(\bar{P}(0,\lambda_i) + \bar{Q}(0,\lambda_i))}{B_r.(n(0) + p_0)} \qquad (6.1.1\text{-}7)$$

Whilst being only approximate, this equation is chosen for its simplicity. It is used in preference to other, more accurate, methods of numerical integration since in the short time interval "t", the subsequent change in carrier density is likely to be small.

6.1.2 Solution to the photon conservation equation.

The photon conservation equation for the "i"th wavelength slot is;

$$\frac{1}{v}\cdot\frac{\partial P(z,t,\lambda_i)}{\partial t} + \frac{\partial P(z,t,\lambda_i)}{\partial z} = G(n,\lambda_i).P(z,t,\lambda_i) + \delta.S(n,\lambda_i) \qquad (6.1.2\text{-}1)$$

As long as gain and spontaneous emission are independent of time and space then equation 6.1-1 has a solution in a plane;

$$P(z,t,\lambda_i) = f((vt - z),\lambda_i) \cdot \exp(G(n,\lambda_i).z) - \frac{\delta.S(n,\lambda_i)}{G(n,\lambda_i)} \qquad (6.1.2\text{-}2)$$

where $f\{(vt - z),\lambda\}$ is an arbitrary function. Equation 6.1.2-2 is valid as long as the interval in time, over which the solution is considered, is sufficiently short such that the carrier density, and hence gain and spontaneous emission, will have changed only a small amount. The time independent version of 6.1.2-2 can be compared to the solution used in chapter five where $f\{(vt - z),\lambda_i\}$ becomes $f\{\lambda_i\}$, ie. a constant for each wavelength slot. Equation 6.1.2-2 signifies a travelling flux, in the z-direction, which undergoes gain or loss to which spontaneous emission is added. The solution of an inhomogeneous differential equation has two parts, first the complementary function and second the particular integral. The complementary function for an ordinary differential equation involves an arbitrary constant whereas for a solution of a partial differential equation the complementary function now includes an arbitrary function $f\{(vt - z),\lambda_i\}$. The spontaneous emission term is a particular integral of equation 6.1.2-1.

As previously stated earlier the problem is separated into two

parts, one which uses the photon flux at t = 0 as an initial condition for the complememtary function of equation 6.1-2. The other is spontaneous emission. Here the initial condition of equation 6.1-2 is that at t = 0, the flux resulting from spontaneous emission is zero. The complete result is obtained by a superposition of analyses.

6.1.3 Analysis for the Initial Condition of Photon Flux at t = 0.

The "round trip gain", in the "i"th wavelength slot, for a two segment device would be;

$$g_{rt}(\lambda_i) = r^2.\exp[\ 2(\ G_1(\lambda_i).L_1 + G_2(\lambda_i).L_2\ )\ ] \qquad (6.1.3\text{-}1)$$

Longer intervals are possible if a multiple of the round trip gain is used. In this case the gain after "m" round trips is;

$$g_{rt}(\lambda_i)^m = r^{2m}.\exp[\ 2.m.(\ G_1(\lambda_i).L_1 + G_2(\lambda_i).L_2\ )\ ] \qquad (6.1.3\text{-}2)$$

The observation, which has already been mentioned in the introduction to this chapter, that after a whole number (m) of "round trip times" the light will undergo "m" round trip gains and end up in the same position in the device travelling in the same direction. Also the round trip gain, in a particular wavelength slot is independent of position. Hence, after "m" round trip times, the photon flux will be;

$$P\left(z,m.t_{rt},\lambda_i\right) = P(z,0,\lambda_i)\ .\ g_{rt}(\lambda_i)^m + spon(\lambda_i) \qquad (6.1.3\text{-}3)$$

The analysis for the spontaneous emission "spon(λ_i)" adding to the total photon flux in equation 6.1.3-3 can be found in the next section.

6.1.4 Analysis for spontaneous emission.

This is particularly important in the inhomogeneously pumped laser because spontaneous emission and superluminescing are dominant before the device switches into the lasing state. The analysis here is for the resulting flux travelling in the positive z direction in the first segment. The same analysis can be applied to the reverse travelling flux in the first segment and to both directions in the second segment. There are three basic mechanisms which contribute to spontaneous emission during m round trip times, "$m.t_{rt}$". The first represents the initial build up of spontaneous emission throughout the device from $t = 0$. In this the flux emitted from a segment starts from zero at $t = 0$ and for the first segment grows to a maximum, and "steady-state" value, at $t = L_1/v$. The flux leaving this segment undergoes gain, or loss, as it circulates in the device to end up in the first segment travelling in the forward direction at $t=m.t_{rt}$. The second mechanism involves these "steady-state" fluxes leaving in the positive and negative travelling directions in both segments. These fluxes will also undergo gain, or loss, as appropriate. The amount of gain being dependent on the origin of the flux and of the path it must travel to end up travelling in the positive z-direction in the first segment. The third mechanism is simply the spatial distribution of the spontaneous emission generated in the segment at $t=m.t_{rt}$.

For these mechanisms we must apply the solution to the photon conservation equation given in 6.1.2-2. Wheras in section 6.1.3 an observation makes a complex analysis redundant, it is necessary to use this solution for calculating the amount of spontaneous emission added to the photon flux after the specified time interval. The analysis in this section applies directly to the contribution of

spontaneous emission to the forward travelling flux, after $m.t_{rt}$, in the first segment. The analysis can be easily applied to the forward travelling flux in the other segment and to the reverse travelling flux in both segments. To calculate the spontaneous emission term $spon(\lambda_i)$, in equation 6.1.3-3, it is necessary to find the arbitrary function $f((vt - z),\lambda_i)$, in equation 6.1.2-2. At time $t = 0$, the spontaneous emission is zero throughout the device. This is used as an initial condition in equation 6.1.2-2 to evaluate $f(-z,\lambda_i)$. Thus we obtain;

$$[\ \exp(G_1(\lambda_i).vt) - 1\ ]\ .\ \frac{\delta.S_1(\lambda_i)}{G_1(\lambda_i)} \qquad (6.1.4\text{-}1)$$

Care must be taken to ensure that the limits are known for when this equation is valid. As mentioned earlier there are three mechanisms through which spontaneous emission is added to the photon flux in this segment at the time, after the specified number of "round trips".

First there is the flux which originated in the first segment between;

$$Z_1 \geq vt \geq 0 \qquad (6.1.4\text{-}2)$$

which is;

$$spa_1(z,t,\lambda_i) = [\ \exp(G_1(\lambda_i).vt) - 1\ ].\frac{\delta.S_1(\lambda_i)}{G_1(\lambda_i)} \qquad (6.1.4\text{-}3)$$

where;
$Z_1 \geq z \geq vt \geq 0$

Using $spa_1(z,t,\lambda_i)$ as an initial condition for the complimentary function, equation 6.1.2-2 is used to calculate how this photon flux

propagates in the passive segment. The particular integral representing the source of spontaneous emission, in equation 6.1.2-2, may be neglected. This type of approach is valid as long as the spontaneous emission (particular integral) is considered separately as a source in the other mechanisms. It is a consequence of the superposition of solutions or in this case mechanisms.

We have at $z = Z_1$ the interface between the first and second segment;

$$spa_1(Z_1,t,\lambda_i) = [\ \exp(G_1(\lambda_i).vt) - 1\ ].\ \frac{\delta.S_1(\lambda_i)}{G_1(\lambda_i)}$$

$$= f((vt - Z_1),\lambda_i).\exp(G_2(\lambda_i).Z_1) \qquad (6.1.4\text{-}4)$$

Then;

$$f((vt - Z_1),\lambda_i) = \frac{\delta.S_1(\lambda_i)}{G_1(\lambda_i)}.[\ \exp\{G_1(\lambda_i).vt\} - 1\ ].\exp(-G_2(\lambda_i).Z_1) \qquad (6.1.4\text{-}5)$$

We wish to use a change of variable to obtain $f((vt - z),\lambda_i)$

$$vt' - Z_1 = vt - z \qquad (6.1.4\text{-}6)$$

$$vt' = vt - z + Z_1 \qquad (6.1.4\text{-}7)$$

$$f((vt - z),\lambda_i) = \frac{\delta.S_1(\lambda_i)}{G_1(\lambda_i)}.[\exp\{G_1(\lambda_i).(vt - z + Z_1)\} - 1].\exp(-G_2(\lambda_i).Z_1) \qquad (6.1.4\text{-}8)$$

Thus;

$$spa_1(z,t,\lambda_i) = f((vt - z),\lambda_i).\exp(G_2(\lambda_i).z)$$

$$= \frac{\delta.S_1(\lambda_i)}{G_1(\lambda_i)}.[\exp\{G_1(\lambda_i).(vt - z + Z_1)\} - 1].\exp\{G_2(\lambda_i).(z - Z_1)\} \qquad (6.1.4\text{-}9)$$

where $Z_2 \geq z \geq Z_1$

and

$$z \geq vt \geq z - Z_1$$

Using this method of analysis, it can be shown that after undergoing m round trips, at time $t = m.t_{rt}$;

$$spa_1\left(z, m.t_{rt}, \lambda_i\right) =$$

$$\frac{\delta.S_1(\lambda_i)}{G_1(\lambda_i)}.[\exp\{G_1(\lambda_i).(Z_1 - z)\} - 1].g_{rt}(\lambda_i)^m.\exp\{G_1(\lambda_i).(z - Z_1)\} \qquad (6.1.4\text{-}10)$$

$$0 \leq z \leq Z_1$$

The second mechanism where spontaneous emission contributes to the total flux after "m round trips" is a result of spontaneous emission which originated;

$$t \geq \frac{Z_1}{v} \qquad (6.1.4\text{-}11)$$

The significance of this limit is that the spontaneous emission emitted from the first segment, in the positive travelling direction, has reached its "steady-state" value and is constant, ie.;

$$\frac{\delta.S_1(\lambda_i)}{G_1(\lambda_i)}.[\exp(G_1(\lambda_i).Z_1) - 1] \qquad (6.1.4\text{-}12)$$

This continuous flux may undergo a series of m-1 "round trip gains" to a single "round trip gain";

$$[\, g_{rt}(\lambda_i)^{m-1} + g_{rt}(\lambda_i)^{m-2} + \ldots + g_{rt}(\lambda_i)^2 + g_{rt}(\lambda_i)\,]$$

$$.\exp\{G_1(\lambda_i).(z - Z_1)\}.\frac{\delta.S_1(\lambda_i)}{G_1(\lambda_i)}.[\exp(G_1(\lambda_i)Z_1) - 1] \qquad (6.1.4\text{-}13)$$

To simplify further the above equation and ones further on let;

$$f_1(\lambda_i) = \frac{\delta.S_1(\lambda_i)}{G_1(\lambda_i)}.[\ \exp(G_1(\lambda_i).Z_1) - 1\ ] \qquad (6.1.4\text{-}14)$$

where $f_1(\lambda_i)$ is the "steady-state" spontaneous emission out of the first segment. Similarly $f_2(\lambda_i)$ is the spontaneous emission out of the second segment. The analysis for the second mechanism is still incomplete since we have neglected the contribution of flux from the other segment and the contribution of spontaneous emission which originated as a flux in the reverse direction.

Contribution from light travelling in the positive z-direction, from segment 2 is;

$$[\ g_{rt}(\lambda_i)^{m-1} + g_{rt}(\lambda_i)^{m-2} + \ \ldots\ + g_{rt}(\lambda_i) + 1\ ] .f_2(\lambda_i).r^2.\exp\{\ G_2(\lambda_i).L_2 + G_1(\lambda_i).L_1\ \}.\exp(G_1(\lambda_i).z) \qquad (6.1.4\text{-}15)$$

Contribution from light travelling in the negative z-direction from segment 2 is;

$$[\ g_{rt}(\lambda_i)^{m-1} + g_{rt}(\lambda_i)^{m-2} + \ \ldots\ + g_{rt}(\lambda_i) + 1\ ] .f_2(\lambda_i).r.\exp\{\ G_1(\lambda_i).L_1\ \}.\exp(G_1(\lambda_i).z) \qquad (6.1.4\text{-}16)$$

Finally the contribution to spb_1 from the spontaneous emission originating in the negative z-direction in segment 1.

$$[\ g_{rt}(\lambda_i)^{m-1} + g_{rt}(\lambda_i)^{m-2} + \ \ldots\ + g_{rt}(\lambda_i) + 1\ ] .f_1(\lambda_i).r.\exp(G_1(\lambda_i).z) \qquad (6.1.4\text{-}17)$$

spb_1 is found by adding these contributions, and simplifying to give;

$$spb_1\left[z,m.t_{rt},\lambda_i\right] = \left(g_{rt}(\lambda_i)^{m-1} + g_{rt}(\lambda_i)^{m-2} + \ \ldots \ + g_{rt}(\lambda_i) + 1 \right)$$

$$.\left[\left[\left(f_1(\lambda_i).\exp\{G_2(\lambda_i).L_2\} + f_2(\lambda_i) \right).r.\exp\{G_2(\lambda_i).L_2\} + f_2(\lambda_i) \right]\right.$$

$$\left.\left.\exp\{G_1(\lambda_i).L_1\} + f_1(\lambda_i) \right].r.\exp(G_1(\lambda_i).z)\right.$$

$$- g_{rt}(\lambda_i)^m.f_1(\lambda_i).\exp\{G_1(\lambda_i).(z - Z_1)\}$$

(6.1.4-18)

Finally the third contribution which spontaneous emission makes to the total flux in the first segment is due to the spatial distribution of spontaneous emission in the segment at the end of the time interval which will be according to;

$$spc_1\left[z,m.t_{rt},\lambda_i\right] = \left(\exp(G_1(\lambda_i).z) - 1 \right).\frac{\delta.S_1(\lambda_i)}{G_1(\lambda_i)} \qquad (6.1.4\text{-}19)$$

We are now in a position to sum up all the contributions due to the different mechanisms spontaneous emission at the end of the time interval where;

$$sp_1 = spa_1 + spb_1 + spc_1 \qquad (6.1.4\text{-}20)$$

$$sp_1[z,m.t_{rt},\lambda_i] = (g_{rt}(\lambda_i)^{m-1} + g_{rt}(\lambda_i)^{m-2} + \ldots + g_{rt}(\lambda_i) + 1)$$

$$.\Big[\Big[(f_1(\lambda_i).\exp\{G_2(\lambda_i).L_2\} + f_2(\lambda_i)).r.\exp\{G_2(\lambda_i).L_2\} + f_2(\lambda_i) \Big]$$

$$.\exp\{G_1(\lambda_i).L_1\} + f_1(\lambda_i) \Big].r.\exp(G_1(\lambda_i).z)$$

$$- g_{rt}(\lambda_i)^m.f_1\lambda_i).\exp\{G_1(\lambda_i).(z - Z_1)\}$$

$$+ [\ \exp(G_1(\lambda_i).z) - 1\ ].\frac{\delta.S_1(\lambda_i)}{G_1(\lambda_i)}$$

$$+ g_{rt}(\lambda_i)^m.\frac{\delta.S_1(\lambda_i)}{G_1(\lambda_i)}.[\exp\{G_1(\lambda_i).(Z_1 - z)\} - 1].\exp\{G_1(\lambda_i).(z - Z_1)\}$$

(6.1.4-21)

The bottom three lines can be further simplified to give;

$$\frac{\delta.S_1(\lambda_i)}{G_1(\lambda_i)}.[\ \exp(G_1(\lambda_i).z) - 1\ ].(1 - g_{rt}(\lambda_i)^m)$$

(6.1.4-22)

6.1.5 Complete solution for photon flux.

Thus at time $t = m.t_{rt}$ the complete solution for the total photon flux travelling in the positive z-direction in the first segment is;

$$P\left[z,m.t_{rt},\lambda_i\right] = P(z,0,\lambda_i).g_{rt}(\lambda_i)^m$$

$$+ \left(g_{rt}(\lambda)^{m-1} + g_{rt}(\lambda_i)^{m-2} + \ldots + g_{rt}(\lambda_i) + 1 \right)$$

$$.\Big[\Big[\left(f_1(\lambda_i).\exp\{G_2(\lambda_i).L_2\} + f_2(\lambda_i) \right).r.\exp\{G_2(\lambda_i).L_2\} + f_2(\lambda_i) \Big]$$

$$.\exp\{G_1(\lambda_i).L_1\} + f_1(\lambda_i) \Big].r.\exp(G_1(\lambda_i).z)$$

$$+ \frac{\delta.S_1(\lambda_i)}{G_1(\lambda_i)} . \left[\exp(G_1(\lambda_i).z) - 1 \right] . \left(1 - g_{rt}(\lambda_i)^m \right)$$

(6.1.5-1)

The above equation shows that, as a result of the assumptions made, the photon flux may be calculated after a whole number of "round trip times". It should be noted that only the average photon flux in a segment is necessary for the carrier conservation equation. Therefore the complete spatial variation is not required and the only points of interest would be at either facet to facilitate the calculation of light output. The average photon flux in the first segment, travelling in the positive z-direction is;

$$\bar{P}_1(t,\lambda_i) = \frac{1}{Z_1} \int_0^{Z_1} P(z,t,\lambda_i)\, dz \qquad (6.1.5\text{-}2)$$

Substituting equation 6.1.5-1 into the above equation gives an analytic expression for the average photon density.

$$\bar{P}_1\left[2.m.t_{rt},\lambda_i\right] = \bar{P}_1(0,\lambda_i).g_{rt}(\lambda_i)^m$$

$$+ \left(g_{rt}(\lambda_i)^{m-1} + g_{rt}(\lambda_i)^{m-2} + \ldots + g_{rt}(\lambda_i) + 1 \right)$$

$$.\left[\left[\left(f_1(\lambda_i).\exp\{G_2(\lambda_i).L_2\} + f_2(\lambda_i) \right).r.\exp\{G_2(\lambda_i).L_2\} + f_2(\lambda_i) \right]\right.$$

$$\left.\left.\exp\{G_1(\lambda_i).L_1\} + f_1(\lambda_i) \right].r.\frac{\{\exp(G_1(\lambda_i).z) - 1\}}{G_1(\lambda_i).L_1}\right.$$

$$+ \frac{\delta.S_1(\lambda_i)}{G_1(\lambda_i)} \cdot \left[\frac{\{\exp(G_1(\lambda_i).z) - 1\}}{G_1(\lambda_i).L_1} - 1 \right] . \left(1 - g_{rt}(\lambda_i)^m \right)$$

(6.1.5-3)

6.2 Modelling Procedure.

The transient response must either start from a zero condition ie. P = 0, Q = 0, n = 0 or a steady-state solution. In the case of the transient model starting from a steady-state solution, this can be thought of as the device having been pre-biased before a step change or pulse in current or, a step change or pulse in optical injection.

6.2.1 Electrically Triggered Switching.

A step change of current in segment 1 is used to initiate switching. The solution to the carrier conservation equation, equation 6.1.1-7, uses the initial steady-state values of flux and the new level of injection to calculate the new carrier density in each segment after m round trip times "$m.t_{rt}$". From this, the corresponding gain and spontaneous emission are found for each of the wavelength slots in both segments. Using this information, the new round trip gains are calculated for each wavelength slot and consequently the new values of flux are calculated using, equation

6.1.5-3, for time $t = m.t_{rt}$. The light output from the facets are calculated using equation 6.1.5-1. These "new" values of flux are then placed in equation 6.1.1-7 to calculate the carrier density in each segment at time $t = 2.m.t_{rt}$. Again the new fluxes in the device are calculated using the values of carrier density and the process continues.

6.2.2 Optically Triggered Switching.

External optical injection of light at either, or both facets, is accomplished by considering the facet as a segment boundary. Continuity of flux across this boundary is assumed in the normal way, and the light entering the device through the front facet would be;

$$P_0(\lambda_i) \cdot (1 - r) \qquad (6.2.2\text{-}1)$$

where r is the reflectivity of the facets, and for the injection of light through the rear facet into the passive segment;

$$Q_3(\lambda_i) \cdot (1 - r) \qquad (6.2.2\text{-}2)$$

Depending upon the wavelength of the injected light, the light is either absorbed and the segment becomes optically pumped, or the light undergoes amplification in the active segment and then absorbed in the passive segment. The net effect is that the cavity loss is reduced.

6.3 Results for Electrically Triggered Switching.

v	=	0.67×10^{8} m S^{-1}
Γ	=	0.75
f_{cc}	=	10^{-21} m^{2}
B_r	=	10^{-16} m^{3} S^{-1}
P_0	=	4×10^{23} m^{-3}
δ	=	10^{-4}
d	=	0.3μm

Table 6.3-1

Table 6.3-1 details the electrical and optical parameters used in the analysis. In all the results presented, the time interval was set to a single round trip time (ie. m = 1), to ensure maximum temporal resolution. For the case of electrically induced switching, 31 wavelength slots were used covering the range 780nm to 840nm.

First the steady-state I-L characteristics are first obtained using the model of chapter 5. Figure 6.3-1 show the I-L characteristics for the three geometries stated, these being a laser, a bistable laser with a short passive segment and a laser with an appreciable length of passive segment. In the case of the bistable laser, the steady-state I-L characteristics must be used to determine where to pre-bias the device so to be midway between the "on" and "off" states. This is necessary for the device to act as a memory element, ie. to have two states for the same current.

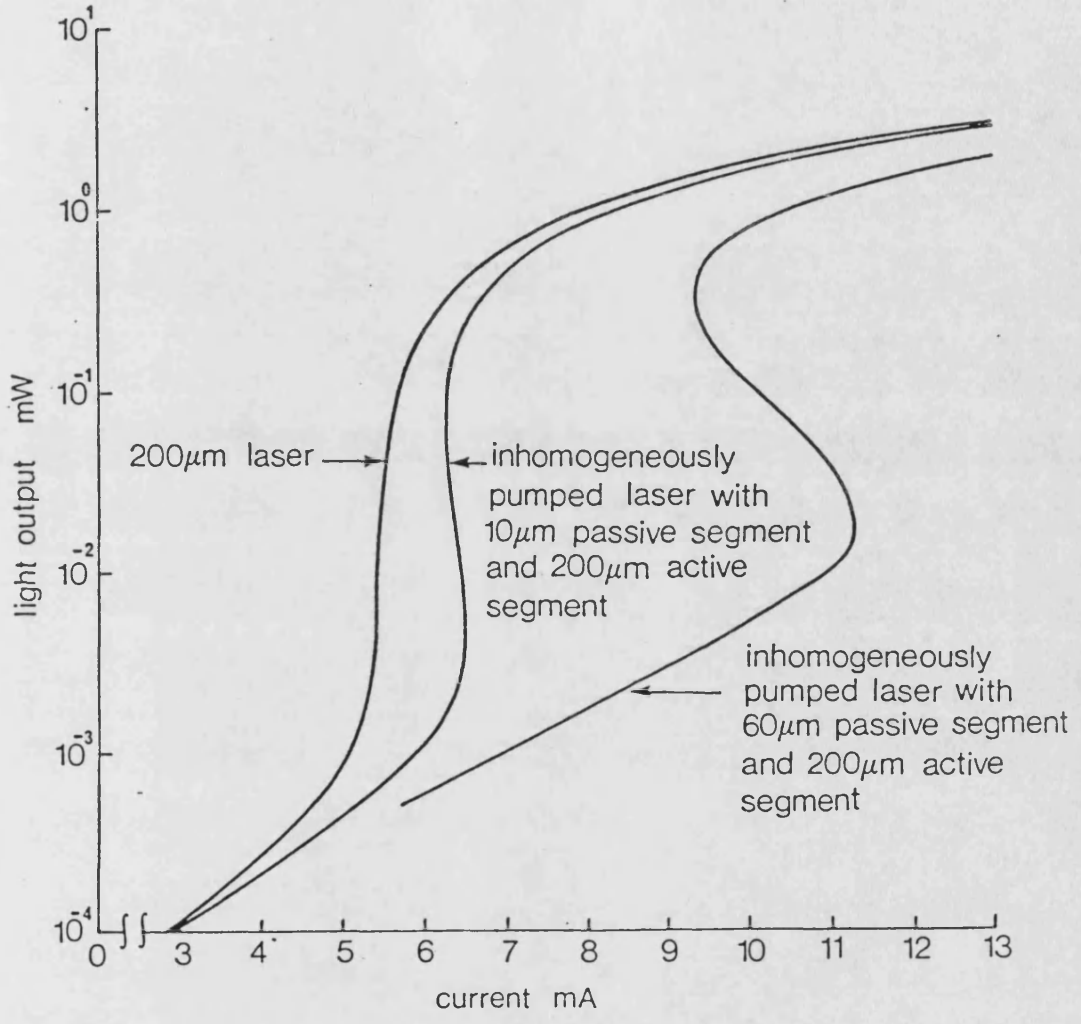

Figure 6.3-1 The static I-L characteristics of: a) 200μm long laser, b) two segment device with a 200μm pumped segment and a 10μm passive segment, c) two segment device with a 200μm pumped segment and a 60μm passive segment.

6.3.1 Transient Response of a Laser.

Figure 6.3-1a shows the static I-L characteristic of the 200μm long laser. The device has been pre-biased at a current of 2.82mA to give an optical output of 10^{-4}mW at each facet. Figure 6.3.1-1 shows the light output transient to a step change in electrode current to 7.96mA (corresponding to a steady-state light output power of 1mW at each facet). The results show the damped oscillatory response of the device and the sharpening of the spectrum as the device begins to lase.

6.3.2 Transient Response of a Laser with Short Passive Segment.

This device has the same length pumped segment as above but now has a short, 10μm passive segment. The model ignores the effect of diffusion of carriers from the active segment into the passive segment and also current spreading. These effects are likely to produce a sizeable error due to the relative short length of passive segment. However the model gives an insight to the dynamic behaviour of such a device or a laser with passive segments segments created through possibly ageing or faulty manufacture. The static I-L characteristics of this device is shown in figure 6.3-1b. The device is pre-biased at 2.91mA corresponding with an optical output of 10^{-4}mW at the front facet. The transient behaviour of the device to a step in current to 8.34mA, corresponding to a light output of 1mW at the front facet, is shown in figure 6.3.2-1. One striking feature is the initial transient which is rather different to the laser transient of figure 6.3.1-1. The spectral peak, during this initial transient, is slightly different from the steady-state lasing wavelength. As the device begins to lase, the strong stimulated recombination depletes the gain in the pumped segment and this gives

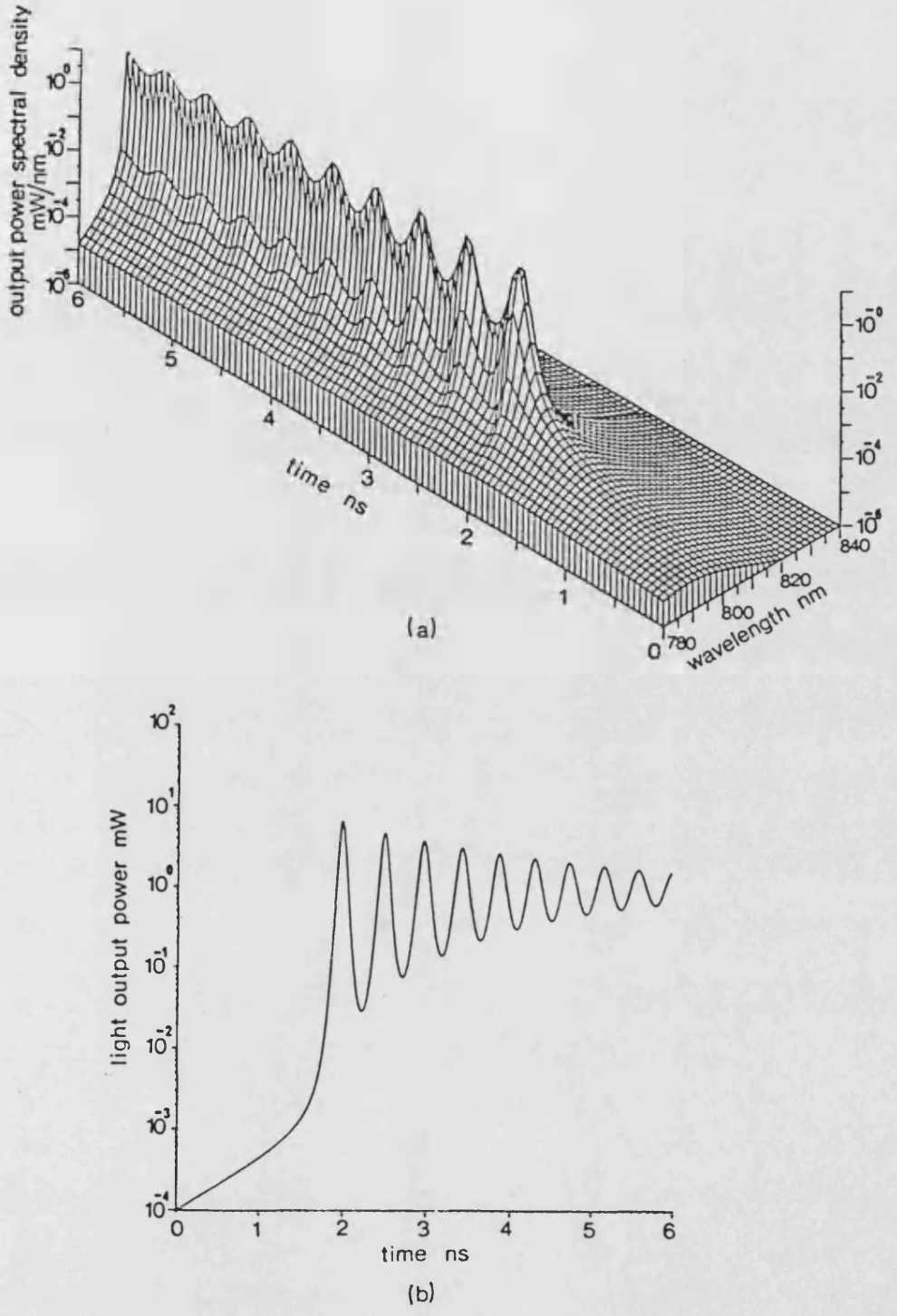

Figure 6.3.1-1 Optical transient from the front facet of the laser after being electrically switched into the "on-state" from the "off-state" pre-bias current of 2.82mA to a new current of 7.96mA, showing the transient change in the emitted sapectum.

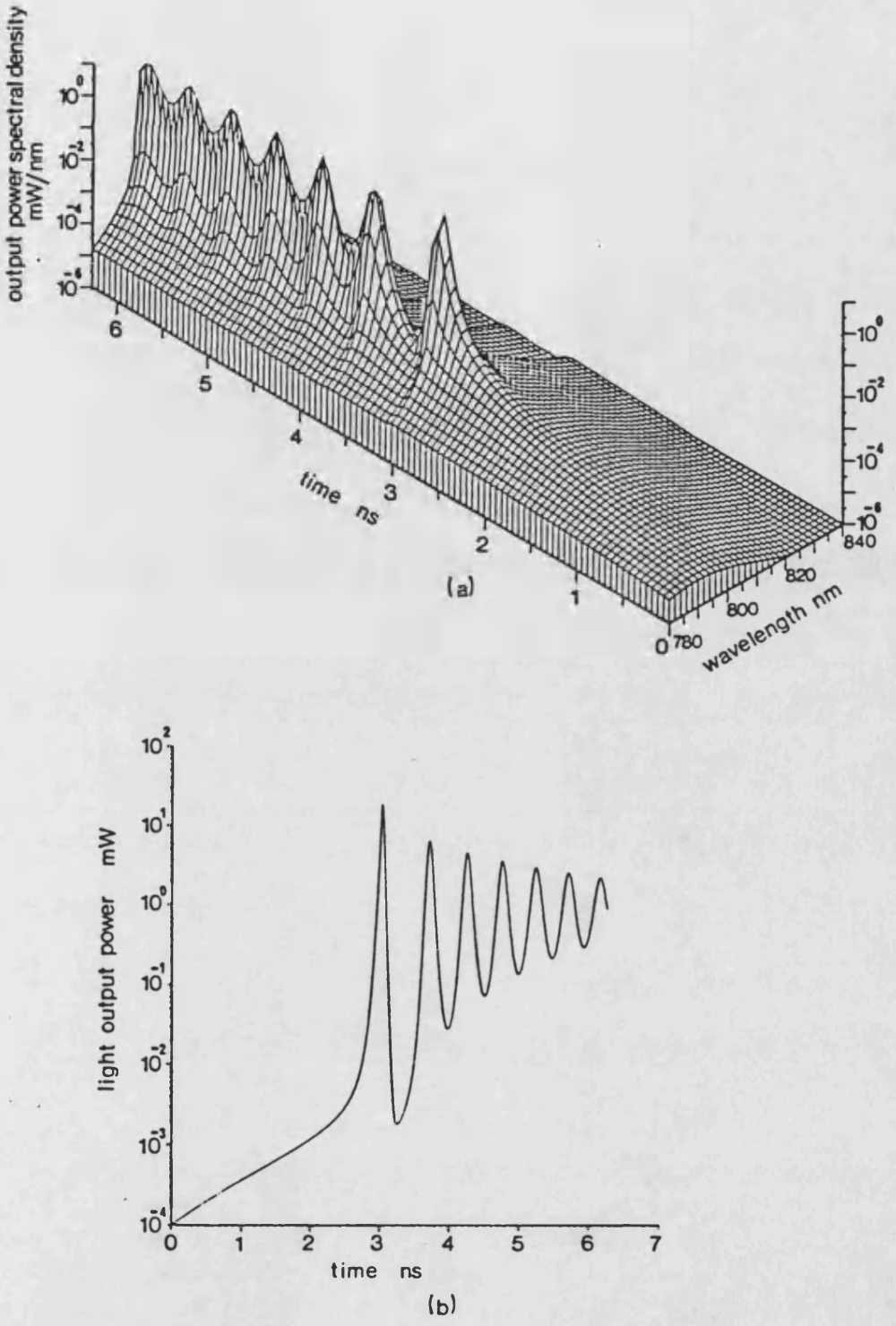

Figure 6.3.2-1 Optical transient from the front facet of the two segment device, with 10μm passive segment after a step change in current from a pre-bias current of 2.91mA to a new current of 8.34mA current step, showing the transient change in the spectrum.

rise to the large drop in total light output after the initial peak. Then there follows the usual damped oscillatory response towards the steady-state. It should be noted that the response is more oscillatory than the response from a laser.

6.3.3 Inhomogeneously Pumped Laser with 60μm Passive Segment.

The steady-state I-L characteristics of the device are shown in figure 6.3-1c. For the initial condition, prior to the step change in current, the device is biased at 10.3mA, midway between the upper and lower threshold currents, to give 6.3×10^{-3} mW light output at the front facet. Figures 6.3.3-1 to 6.3.3-4 show the switching transient behaviour to different values of step changes in currents. In each case figure b shows the transient of the total light output from the front facet.

The transient is similar to that obtained for a laser with a short passive segment, but the effects have become exaggerated. The major difference of a device with a long passive segment is that the device, below threshold, behaves similar to a superluminescing diode (SLED), emitting light of a relatively short wavelength. This wavelength of light will of course be greatly attenuated in the passive segment and as a result the initial lasing frequency can be seen to peak at a much longer wavelength than this peak of superluminescence. For this geometry the corresponding difference in the peaks of the maxima, in wavelength, is approximately 25nm. There is also a slight shift in wavelength, from the initial lasing wavelength, as the lasing wavelength settles to the steady-state value. For this device it can be seen to span four wavelength slots which is equivalent to 8nm.

Most apparent is the sharp "turn off", of the device, after the

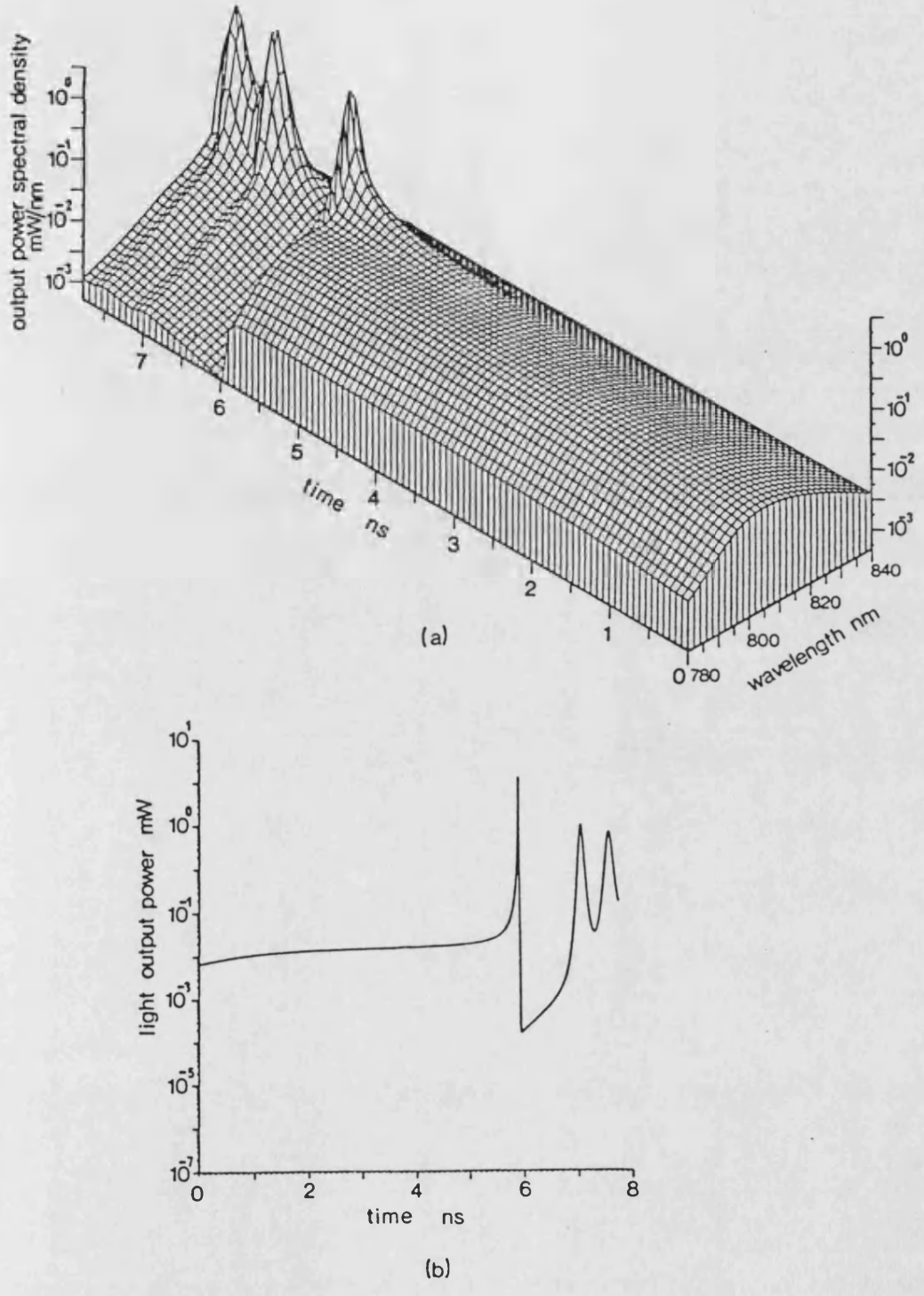

Figure 6.3.3-1 Optical transient from the front facet of the pre-biased two segment device, with 60μm passive segment after being electrically switched into the "on-state" from an "off-state" pre-bias current of 10.3mA to a new current of 12mA.

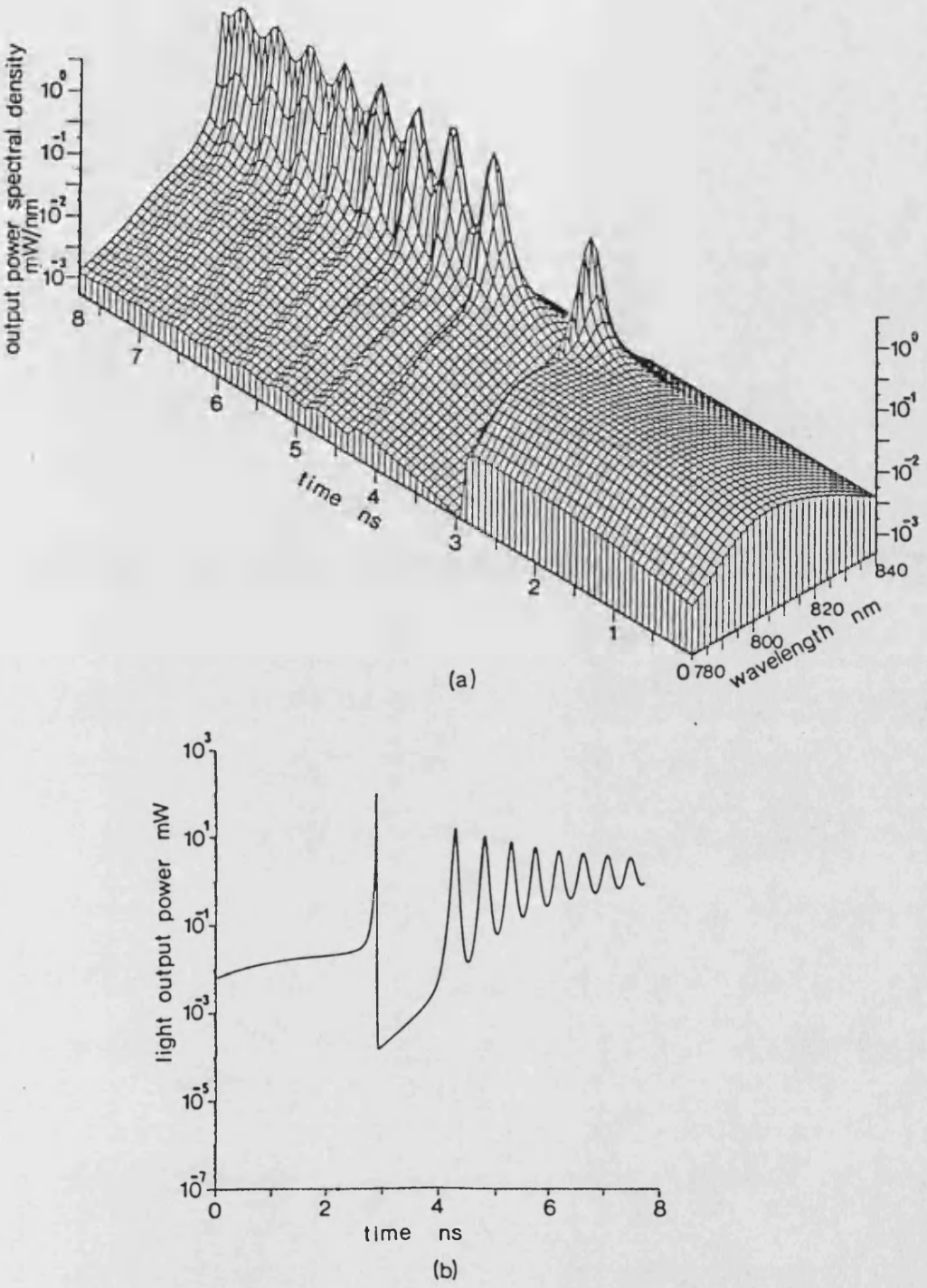

Figure 6.3.3-2 Optical transient from the front facet of the pre-biased two segment device, with 60μm passive segment after being electrically switched into the "on-state" from an "off-state" pre-bias current of 10.3mA to a new current of 13mA.

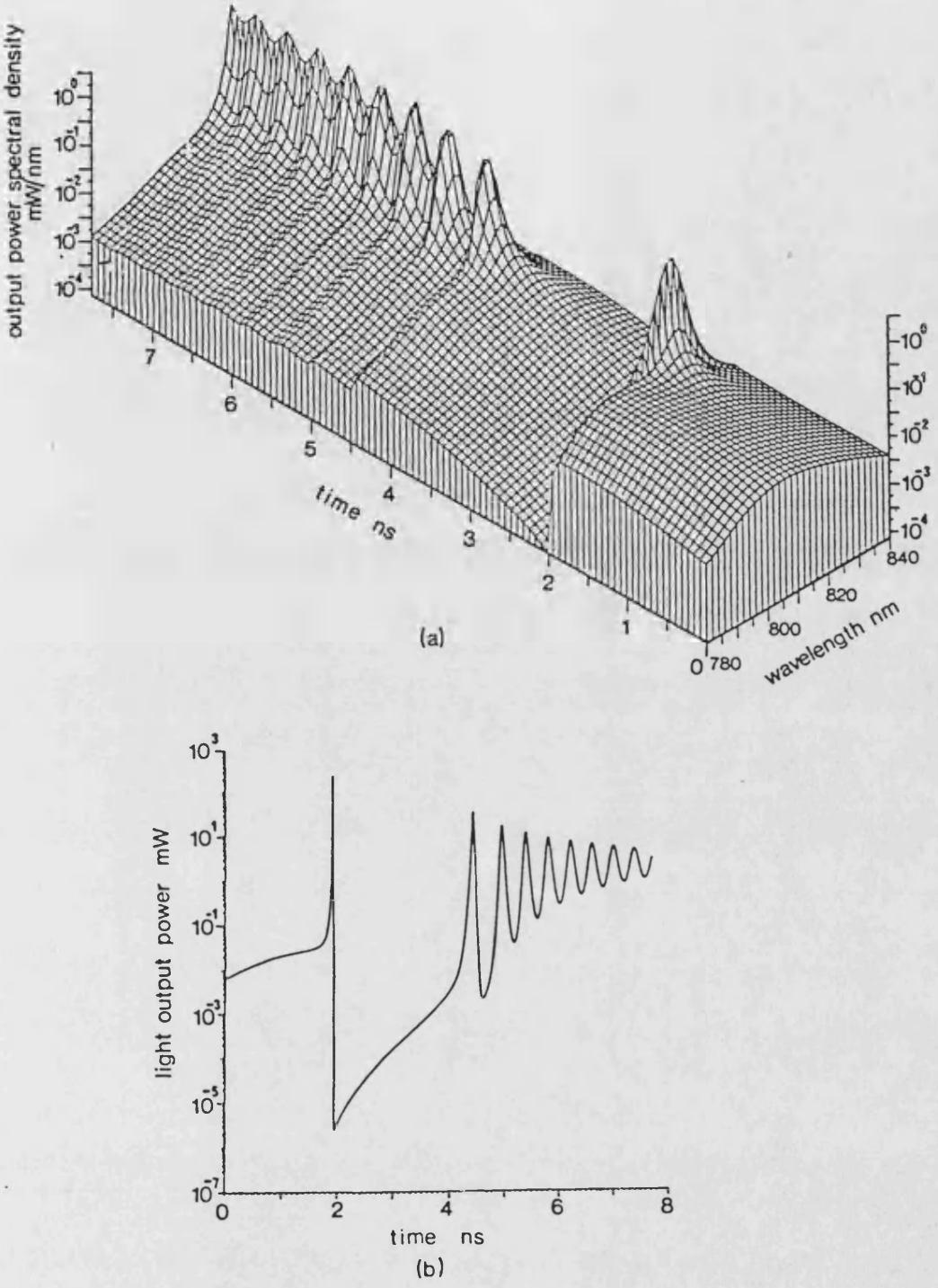

Figure 6.3.3-3 Optical transient from the front facet of the pre-biased two segment device, with 60μm passive segment after being electrically switched into the "on-state" from an "off-state" pre-bias current of 10.3mA to a new current of 14mA.

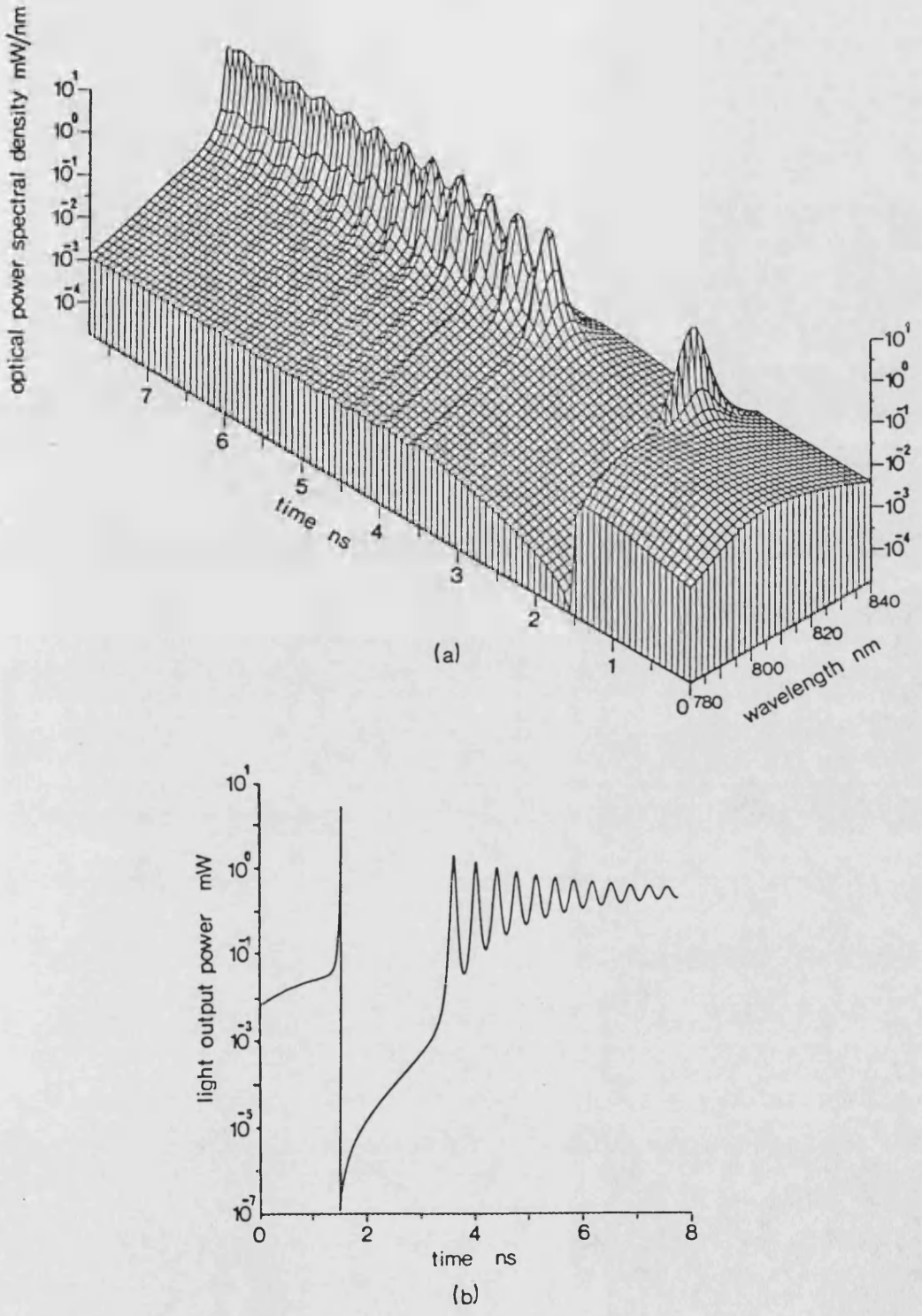

Figure 6.3.3-4 Optical transient from the front facet of the pre-biased two segment device, with 60μm passive segment after being electrically switched into the "on-state" from an "off-state" pre-bias current of 10.3mA to a new current of 15mA.

initial transient lasing peak. This is more pronounced than for the device with the shorter passive region, and has a longer recovery time. This may be explained as follows. The initial lasing peak can be seen to growing fast to a very high amplitude. This has two consequences. First, the passive segment is being optically pumped at wavelengths where the optical loss, at this (transient) lasing wavelength, is becoming less. The carrier lifetime of the passive segment is rather long so this segment can be thought of as a reservoir of carriers. Once this segment becomes optically pumped to transparency it is likely to stay in this state for a relatively long time. At the same time the increase in light level within the resonator increases the rate of stimulated emission in the pumped segment, which leads to its carrier density being depleted. The excess of light in the resonator results in the continuing depletion of carriers in the pumped segment even though the gain may have dropped (transiently) below that normally required to sustain lasing. The net effect of this is that the overall gain within the device falls by such an extent that there is a sudden loss of light leaving the resonator. The light decreases to a level where no lasing is visible in the spectral output.

It should be noted that as a result of the depletion of carriers in the pumped segment, and the resulting shift in gain curves, the light output due to superluminescence decreases around the initial peak in the transient. The spontaneous emission from the pumped segment then falls to a particularly low value, indicative of the fall in carrier density in this segment. Remembering that the passive segment is still moderately transparent to light at lasing wavelengths, the carrier density in the pumped segment increases through the injection of carriers, and that lasing is possible once

again. However, there is now less loss to overcome in the passive segment, and so a much reduced carrier density in the pumped segment is required to maintain a resonator "round trip gain" close to unity. This is illustrated by the spontaneous emission staying at such a low level.

As the step change in current is increased, it is seen that: a) the initial delay before the device starts lasing decreases, as expected; b) the depth of the "turn off" in light output increases quite markedly; c) the recovery time back to the subsequent stable, but underdamped lasing condition initially increases, but at higher step currents reduces.

6.4 Results for Optically Induced Switching.

This illustrated for the case of a device with a 200μm pumped segment and a 60μm long passive segment. The static light input-output characteristics are shown in figures 6.4-1 for injected light of several wavelengths. These are generated from the model outlined in chapter 5 using the optical and electrical parameters in table 6.3-1. For the case of electrically induced switching 31 wavelength slots were used but here 151 slots are used over the same range, 780 to 840nm. In figure (a) is for injection into the pumped segment, and (b) is for injection into the passive segment through the rear facet. In both cases the device is electrically pre-biased by a current of 9.27mA, which is below the lower (ie. OFF state) threshold current. The three wavelengths chosen represent; i) a wavelength shorter than the superluminescing wavelength; ii) the peak superluminescing wavelength and, iii) the lasing wavelength. The model used to obtain these static results are outlined in chapter five.

To achieve the transient response, the device is both

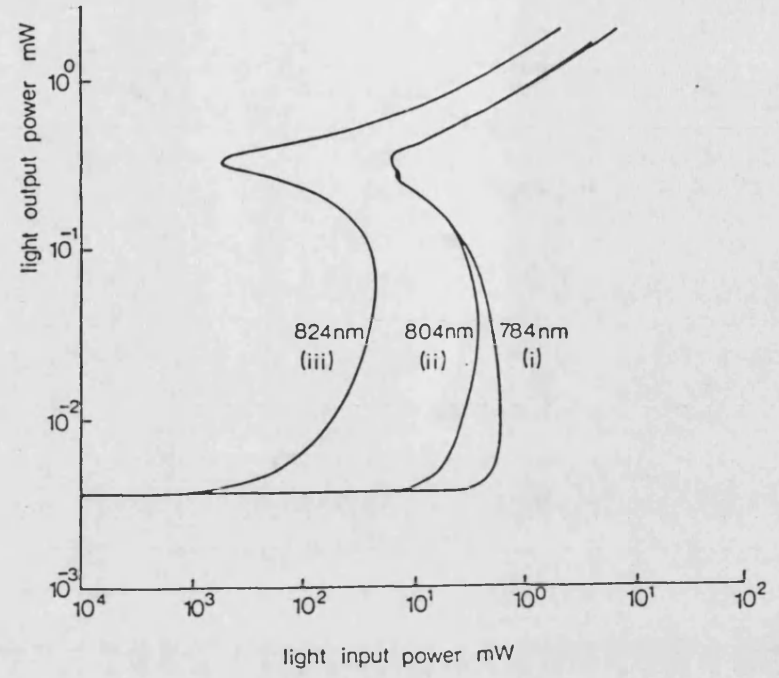

(a)

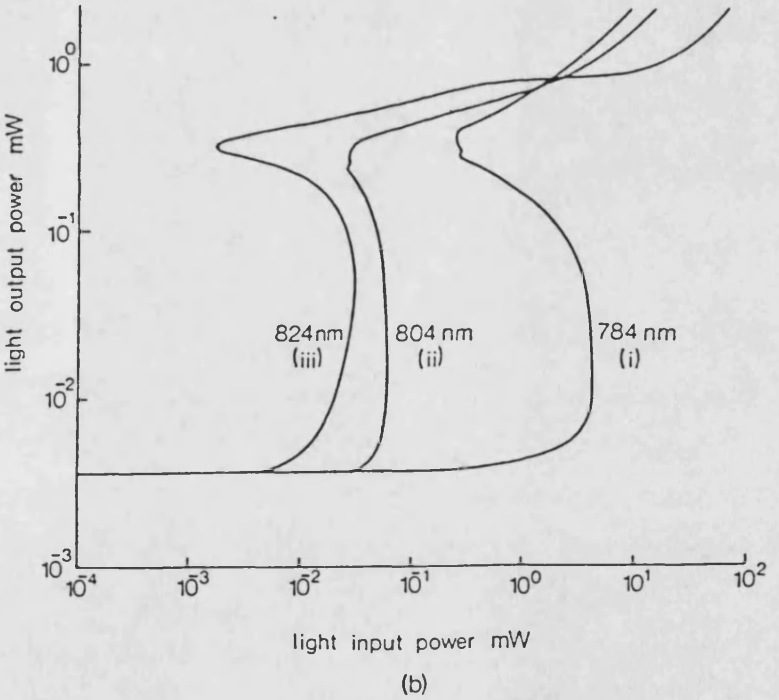

(b)

Figure 6.4-1 Optical input-output characteristics of a two segment laser with a 200μm pumped segment and a 60μm passive segment, electrically pre-biased by a current of 9.27mA for three wavelengths, injected; a) into the pumped segment throught the front facet and; b) into the passive segment through the rear facet.

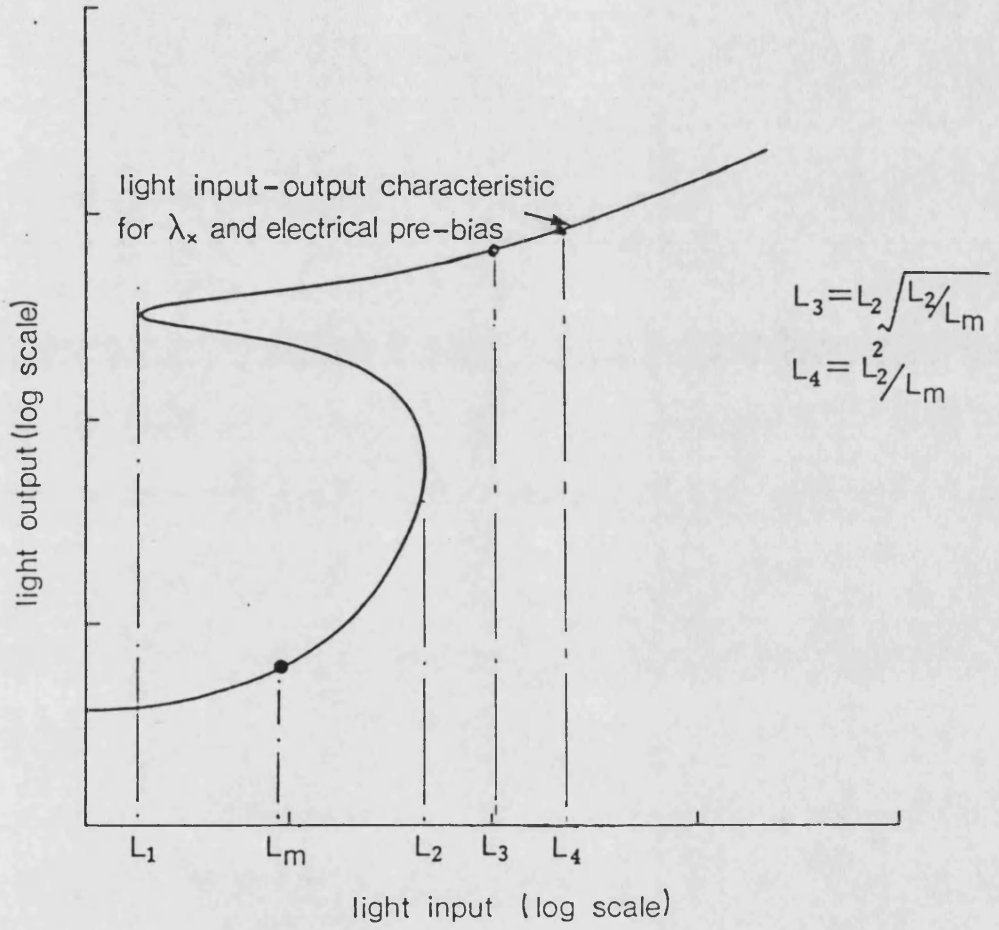

Figure 6.4-2 Diagram illustrating how the optical pre-bias level L_m and how the two levels of step changes of optical injection to L_3 and L_4 are chosen for each wavelength into both facets. This is in addition to an electrical pre-bias.

electrically and optically 'pre-biased' at the appropriate wavelength, as shown in figure 6.4-2. L_m represents the optical pre-bias level, and is chosen to be the geometric mean between the upper and lower threshold values of light input. This is because of the very wide range of light input level between the upper and lower thresholds.

Transient changes in the total light output from the front facet of the device have been obtained for the following cases of optical injection: a) at the lasing and superluminescing and short wavelengths into the front facet for two different levels of optical injection; and b) at the superluminescing and short wavelengths into the front facet, also for two different power levels. The two power levels used to initiate switching are marked on figure 6.4-2, and are determined by the following expressions;

$$L_3 = L_2 \cdot (L_2/L_m)^{0.5} \qquad (6.4\text{-}1)$$

$$L_3 = L_2 \cdot (L_2/L_m) \qquad (6.4\text{-}2)$$

6.4.1 Light at Lasing Wavelength Injected into the Passive Segment.

The transient for this condition is shown in figure 6.4.1-1. At this wavelength, much of the light is transmitted through the device, and appears at the front facet within a half round trip time. The switch on transient then follows. The response is well damped, more so for the lower level of injection. A feature of both input levels is the very long switch on time. These particular results should be treated with caution however, because the analysis excludes the existence of longitudinal modes in the device. In practice the response would be a combination of absorptive and dispersive bistability [9, 10]. Such problems do not exist for optical injection at other wavelengths where the round trip gain for such would be far

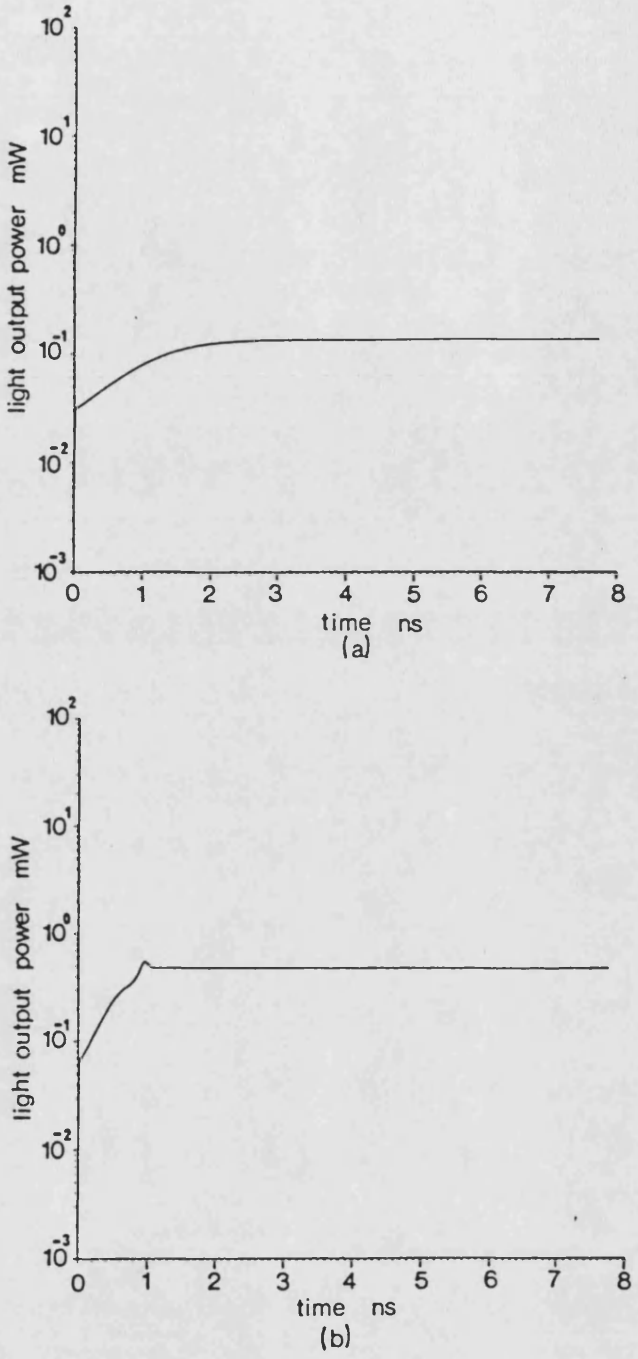

Figure 6.4.1-1 Transient response of the total light output from the front facet of a two sement laser with a 20 μm pumped segment and a 60μm passive segment, electrically pre-biased by a current of 9.27mA and optically with light of 824nM wavelength at a power of 8.96μW into the rear facet due to an increase in the optical injection power to a) 100μW and b) 224μW.

below unity.

6.4.2 Light at the Peak Superluminescence Wavelength into the Passive Segment.

These transients are shown figure 6.4.2-1 for bath optical injection levels. These show the normal underdamped response. The turn on time is shorter than the previous example. However, this is strongly dependent upon the injection level. The transients are similar to those obtained for a step change in current, shown in figures 6.3.3-1 to 6.3.3-4. This is not surprising since the optical injection at this wavelength is largely absorbed in the passive segment.

6.4.3 Light at the Peak Superluminescence Wavelength into the Pumped Segment.

These transients are shown in figure 6.4.3-1. A feature of the transient is the self-sustained pulsations for the lower of the two injection levels, but become damped at the higher injection level.

6.4.4 Light at a Short Wavelength Injected into the Pumped Segment.

These transients, shown in figure 6.4.4-1, are similar to figure 6.4.2-1. Here, light is strongly absorbed in the pumped segment, and hence this increased the gain to allow lasing.

6.5 Conclusion.

The transient response of the device to either electrically triggered switching is very similar, and optical triggering does not induce a faster response. The reason for this is that the effect of the optical injection is simply to optically pump the device to a higher gain, which is precisely the same effect as electrically

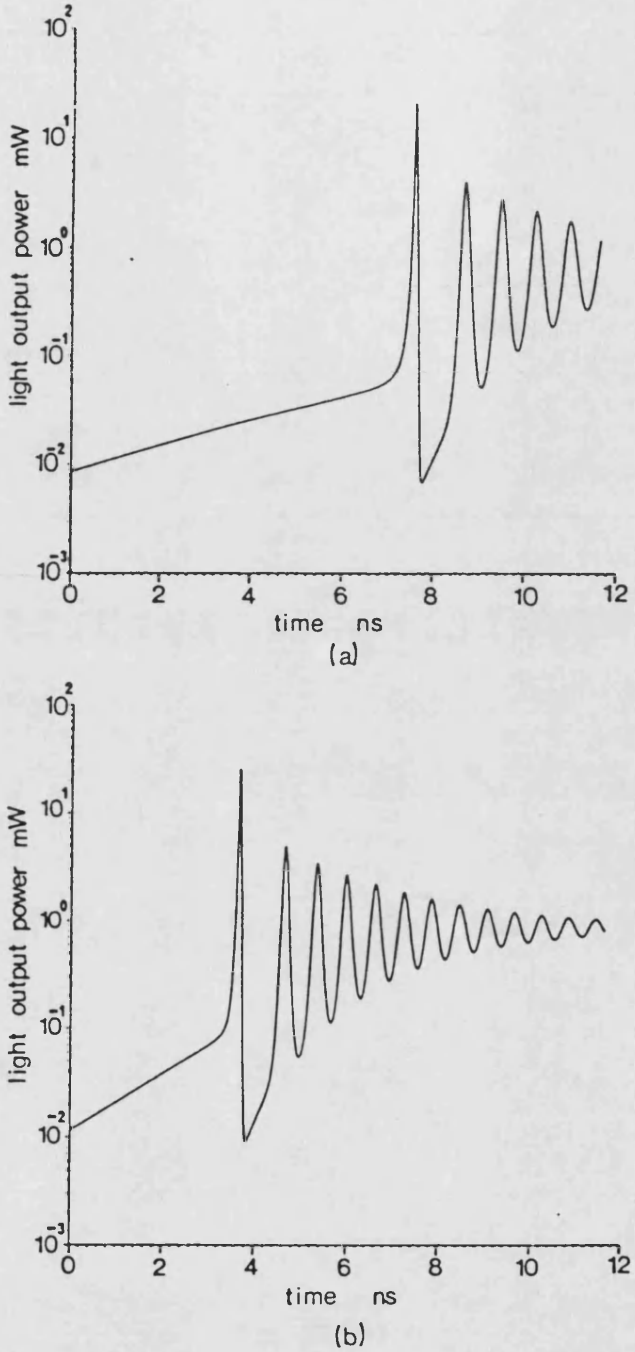

Figure 6.4.2-1 Transient response of the total light output from the front facet of a two sement laser with a 200μm pumped segment and a 60μm passive segment, electrically pre-biased by a current of 9.27mA and optically with light of 804nM wavelength at a power of 157μW into the rear facet due to an increase in the optical injection power to a) 634μW and b) 1.01mW.

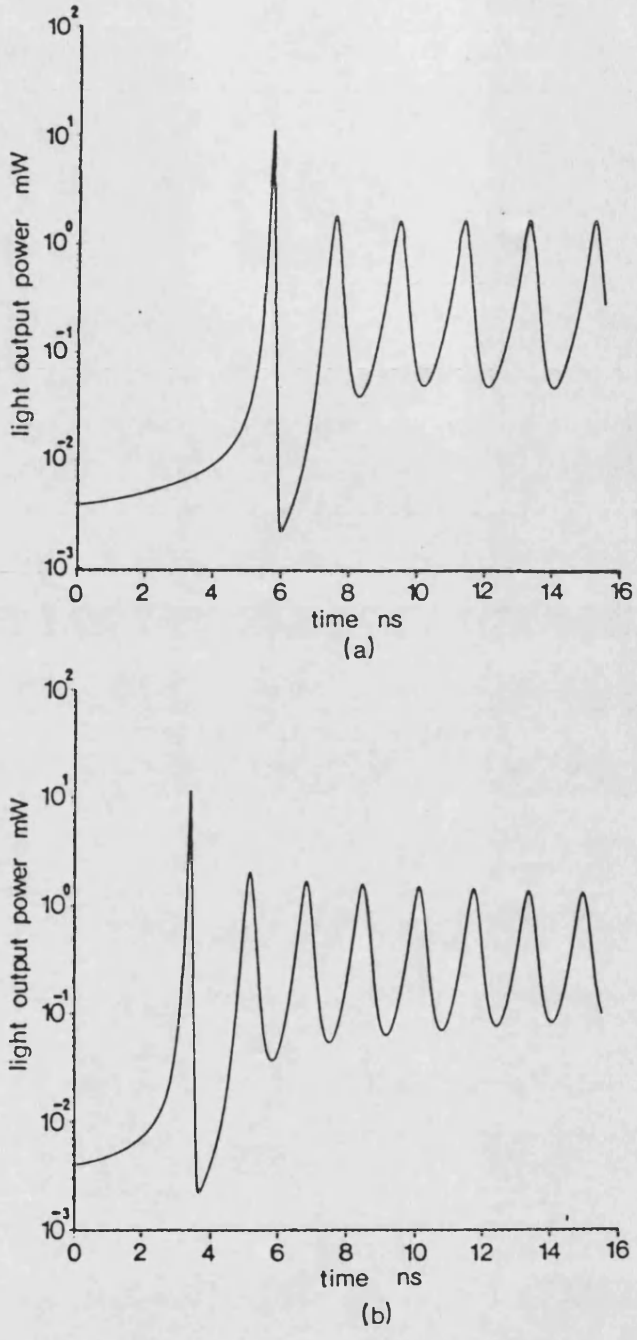

Figure 6.4.3-1 Transient response of the total light output from the front facet of a two sement laser with a 200μm pumped segment and a 60μm passive segment, electrically pre-biased by a current of 9.27mA and optically with light of 804nM wavelength at a power of 37.7μW into the front facet due to an increase in the optical injection power to a) 73.5μW and b) 91.6μW.

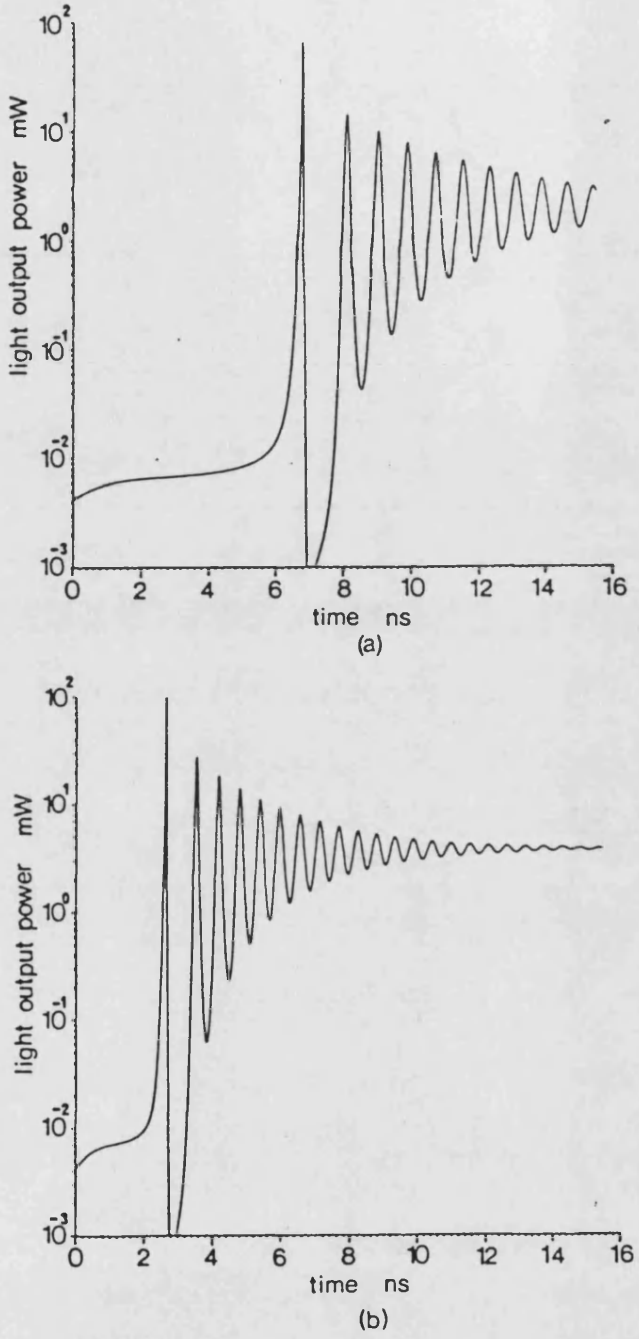

Figure 6.4.4-1 Transient response of the total light output from the front facet of a two sement laser with a 200μm pumped segment and a 60μm passive segment, electrically pre-biased by a current of 9.27mA and optically with light of 784nM wavelength at a power of 1.02mW into the front facet due to an increase in the optical injection power to a) 8.99mW and b) 18.6mW.

induced switching. It should be noted that increasing the length of the passive segment generally reduces the damping of the transient.

The observation of self-sustained oscillations, due to optical injection of light at the superluminescing wavelength, is of interest, and the dependence of this on the input injection level illustrates the non-linearity of the original problem. The self-sustained oscillations occur because of two competing mechanisms. Light at the superluminescing wavelength is amplified by the gain in the pumped segment, depleting the carriers slightly in this segment. The light is then completely absorbed in the passive segment, pumping the passive segment. The overall effect of optical injection at the superluminescing wavelength, into the front facet, is that there is a redistribution of carriers from the pumped segment to the passive segment where the carrier lifetime is much longer. Thus the total number of carriers in the passive segment is raised in a greater proportion than the total number of carriers depleted in the pumped segment. Lasing is now possible as the round trip gain is increased at the lasing wavelength. The light in the cavity builds up, thereby depleting the carriers in the region of gain. The superluminescence is not now amplified to the same level, and is insufficient to pump the passive segment. Consequently, the round trip gain at the lasing wavelength falls, and the light output with it. The gain in the pumped segment now increases and the above process is repeated. The results show that the self-pulsations stop if the injection level is raised. In this case, before lasing takes place, there is already a significant depletion of carriers in the pumped segment, through the amplification of superluminescing, such that when the device lases the carrier density, in the pumped segment, will change a lesser amount.

For light of shorter wavelength, this is purely absorbed in the appropriate segment, and there are no longer two wavelengths competing for gain.

References.

1) N. G. Basov; "O-1 Dynamics of injection lasers"; IEEE J. Quantum Electronics; Vol. QE-4; No. 11; 1968; p855-64.

2) T. L. Paoli. "Saturable absorption effects in the self-pulsing (AlGa)As junction laser"; Applied Physics Letters; Vol. 34; No. 10; 1979; p652-655.

3) D. Renner and J. E. Carrol. "Transients in injection lasers - phase-plane analysis and effects on absorbing sections"; Solid-State and Electron. Devices; Vol. 3; No. 6; 1979; p 224-32.

4) Ch. Harder, K. Y. Lau and A Yariv. "Bistability and Pulsations in Semiconductor Lasers with Inhomogeneous Current Injection"; IEEE Journal of Quantum Electronics; Vol. QE-18; No. 9; 1982; p 1351-61.

5) H. Kawaguchi. "Optical bistable-switching operation in semiconductor lasers with inhomogeneous excitation"; IEE Proc.; Vol. 129; No. 4; 1982; pl41-8.

6) H. Kawaguchi. "Optical bistability and chaos in a semiconductor laser with a saturable absorber"; Applied Physics Letters; Vol. 45; No. 12; 1984; p 1264-6.

7) M. Kuznetsov. "Theory of bistability in two-segment diode lasers"; Optics Letters; Vol. 10; No. 8; p 399-401.

8) Y. L. Wong and J. E. Carrol. "Short Optical Pulses from Injection Lasers investigated by Single-Mode Travelling-Wave Rate Equations"; Institute of Physics conference on; Semiconductor Injection Lasers and their Application. (SILA); 1984; Paper 10.

9) M. J. Adams, H. J. Westlake, M. J. O'Mahony and I. D. Henning. "A comparison of active and passive optical bistability in semiconductors"; IEEE Journal of Quantum Electronics; Vol. QE-21; No. 9; 1985; pl498-504.

10) M. J. Adams, J. V. Collins and I. D. Henning. "Analysis of semiconductor laser optical amplifiers"; IEE Procedings; Vol. 123; p58-63.

Chapter 7.

Conclusion.

7 Introduction.

The aim of the thesis has been to investigate absorptive bistability. Most of the work has centered on the analysis and modelling of absorptive bistability. The models include both the static characteristics and transient response of such a device and also optical injection induced bistability. Suggestions are given at the end of this chapter concerning further work on the subject of absorptive bistability.

7.1 Conclusions.

Chapter two introduces the concept of modes and guiding action in waveguides. Included is the confinement of optical energy to the waveguide which is particularly relevant in semiconductor lasers. Only the portion of optical energy which is confined to the active region will undergo gain. The slab waveguide is treated in detail and the importance of the EDC method is stressed due to its simplicity and more so for its accuracy. It gives good results for a variety of applications where a two dimensional waveguide problem can be reduced into two, one dimensional slab waveguide problems for which a more analytic approach may be possible. Gain guiding is significant in double heterostructure lasers which do not have lateral index guiding. Gain guiding of an homogeneously pumped laser confines much of the light under the pumped stripe along the length of the device. However, in an inhomogeneously pumped device without lateral index guiding, any optical pumping of a passive segment will defocus the light emerging from the pumped segment going into the passive segment. This gives rise to a high loss from the resonant cavity which would substantially reduce the efficiency of the device to the

extent that hysteresis may not be present at all in the I-L characteristics. The mechanisms are discussed in greater detail in chapter three where it is shown that the buried heterostructure (B-H), whose active region can be compared to a rectangular waveguide, would be a more appropriate structure for an absorptively bistable laser. Chapter three also contains the basic theory of the mechanisms involved in absorption and emission processes, and includes an overview of the calculation of gain and spontaneous emission.

Most of the original work in this thesis is found in chapters four, five and six. Chapter four paves the way by illustrating a more appropriate method for analysing absorptive bistability. The alternative approach uses a solution of the photon conservation equation. The analysis does not include the wavelength dependence of gain and spontaneous emission and this is usually referred to as a single wavelength model. The validity of some assumptions, which would greatly simplify the analysis of absorptive bistability, is discussed and it is found that the assumption of a uniform carrier density within a segment appears to be extremely good. However, one of the more significant findings is that the photon flux cannot be assumed uniform throughout the device. It must also be pointed out that the assumption of a uniform photon flux within the device gives rise to the concept of a photon lifetime. Photon lifetime represents the loss of light from the resonator and is is shown to be very sensitive on the spatial distribution of photon flux which is dependent on the level of injection and light output.

Chapter five examines the effect of geometry on the hysteresis in the I-L characteristics of an inhomogeneously pumped laser. The analysis is much the same as in chapter four but included is the

effect of the wavelength dependence of gain and spontaneous emission. Once again it has been found that the commonly used assumption of a uniform carrier density in each segment of the device is a reasonable one and causes very little error. This is when compared to solutions in which a more accurate carrier density profile is calculated. Although it is commonly assumed that by increasing the length of the passive segment the hysteresis will increase, it has been found that there is an upper bound to this, any further increase in the length of the passive segment actually reduces the hysteresis. This result is a possible explanation to the experimental result of a device by Harder, Lau and Yariv [9]. For their dynamically stable split stripe laser, with only one segment of the device is pumped and with the relatively long passive segment left open circuit, no hysteresis was observed.

The models of chapter six used alternative techniques to predict the transient characteristics of lasers with passive segments. The transient responses were rather oscillatory for step changes in both electrical and optical injection. For optical injection at the lasing frequency, the response was rather slow and overdamped (ie. with no overshoot). The validity of optical injection at the lasing wavelength is open to discussion since the models outlined in this thesis do not take into account longitudinal modes in the laser cavity. For the case of injection at the superluminescing wavelength, and shorter wavelengths, the round trip gain would be sufficiently low that longitudinal modes, at this wavelength, would not be evident. When light at the peak wavelength of the superluminescing spectrum is injected into the pumped segment, the transient behaviour is of particular interest. The device appears to be unstable, giving pulsations, and the oscillations may be damped by increasing the

level of injection.

7.2 Suggestions for further work.

As mentioned above the models outlined in chapter six ignore the effect of longitudinal modes. For static I-L characteristics this is acceptable where the wavelength slots are closely spaced. It may be assumed that the wavelength slot around the lasing peak is the approximate envelope of the round-trip gain of the device and slot is sufficiently wide to accommodate a number of longitudinal modes. If the transient characteristic of such a laser are now considered, the wavelength of the longitudinal modes are dependent on carrier density. Since the carrier density changes dramatically during a switch-on transient, the wavelength of the longitudinal mode will change in sympathy. The result of this on the transient behaviour is difficult to ascertain, the effect would be that gain would, at times, be diluted by an amount governed by the cavity detuning. Also during the transient it is possible for the lasing wavelength to "hop" from one mode to another. If these effects are the subject of further study then the concept of absorptive bistability combined with dispersive bistability can be explored.